Application of vibration-based damage detection techniques to civil infrastructure: Incorporating uncertainty quantification

Setonam Komla Dzvukamanja

A thesis submitted to the Department of Civil Engineering, University of Cape Town, in partial fulfillment of the requirements for the degree of Master of Science in Civil Engineering
Supervised by Associate Prof. Pilate Moyo and Prof. Mark Alexander

May 2008

Declaration

I declare that this dissertation is my own unaided work. It is being submitted for the degree of Master of Science in Civil Engineering at the University of Cape Town. It has not been submitted before for any degree or examination in any other university.

_____

_____ day of _____2008

Abstract

Literature was reviewed with an aim to identify research needs in vibration based damage detection techniques and the quantification of the uncertainty in these techniques. It was discovered that the literature lacked examples of the explicit propagation of measurement uncertainty through damage detection algorithms. Instrumentation errors and variable environmental and operational conditions were identified as sources of uncertainties. It was established that in order to ensure reliability of the damage detection techniques and to assess their robustness, a damage detection framework which, accounting for sources of error in the measurements, propagates the uncertainty through the algorithms of the damage detection techniques. Standard methods of uncertainty quantification and propagation were reviewed and summarized, thus identifying the tools available for developing the desired framework for the inclusion of uncertainty quantification in damage detection techniques.

Frameworks for the application of non-model-based vibration-based damage detection techniques, incorporating uncertainties, were developed. The frameworks consisted of data collection, feature extraction, feature discrimination and damage diagnosis with a quantitative measure of confidence in the diagnosis. The adopted feature extraction technique consisted of an algorithm that compared the residual errors of an ARX model fitted to a reference dynamic system with the residual errors of the same model fitted to a potentially damaged dynamic system. The damage-sensitive feature was chosen as the ratio between the standard deviation of the residual errors for the ARX model applied to the reference data and the standard deviation of the residual errors when the same model is fitted to data from an unknown structural state. Two feature discrimination techniques were investigated, namely a probability density approach and an outlier analysis approach. These feature discrimination techniques were statistical models that involved Monte Carlo simulations for uncertainty quantification.

The frameworks for the application of non-model-based vibration-based damage detection techniques, incorporating uncertainties, were tested using experimental data. The test structures were steel-reinforced concrete beams. Damage was gradually introduced into the beams by the accelerated corrosion of their steel reinforcement.

Vibration tests were conducted on the beams at various degrees of corrosion and different core temperatures of the beams. The results of the application of the proposed damage detection frameworks to the test data revealed a high correlation between the degree of corrosion and the probability that the structure was damaged. The chosen damage-sensitive feature proved to be insensitive to changes in the core temperature of the beams. It was concluded that the ARX damage detection technique was capable of detecting the damage brought about by corrosion of the longitudinal steel reinforcement in concrete beams. By including uncertainty quantification, the damage detection frameworks proposed in this thesis were able to output quantitative measures of the certainty in their diagnoses. The frameworks accounted for instrumentation errors and errors due to changes in temperature. They can however be generalised to account for other environmental and operational effects by developing a comprehensive reference database of the adopted damage sensitive features. Civil infrastructure suffers from subtle and complex forms of damage, such as the deterioration brought about by steel reinforcement corrosion in concrete structures and due to the problems brought about by uncontrollable environmental and operational conditions. The frameworks developed in this thesis for the detection of damage address these complexities and are therefore applicable to the structural health monitoring of civil infrastructure.

Acknowledgements

I thank Associate Prof. Pilate Moyo and Prof. Mark Alexander for their supervision and guidance. I also thank the civil engineering laboratory and workshop staff for their technical assistance.

I acknowledge the following for their financial support:

University of Cape Town Department of Civil Engineering

The National Research Foundation

The Cement and Concrete Institute

Murray & Roberts Marine

I thank my family for their moral, emotional and financial support.

Contents

List of Figures

Chapter 1

1 Introduction

Early detection of damage is essential for effective maintenance of civil infrastructure. In most cases the replacement costs far exceed the cost of maintenance over the useful life of infrastructure. In this regard, the field of structural health monitoring (SHM) has received great attention from researchers. In the broadest sense, SHM is defined as the process of implementing a damage detection strategy for aerospace, civil, and mechanical infrastructure (Sohn *et al.* 2001). The aim of structural health monitoring is to detect damage at its early stages so that repair work may be conducted as soon as is necessary, or preventative measures may be implemented to halt further deterioration. For this reason, damage detection algorithms form a crucial part of structural health monitoring methodologies. These algorithms form the tools in SHM methodologies for characterizing the structural state of infrastructure.

1.1 Background to damage detection in structural health monitoring

The characterization of structural condition can be said to consist of three main levels (Sohn *et al.* 2003, Fassois *et al.* 2006). The first level is damage detection. This concerns detecting a change in structural state. The output of this level is a statement saying either that a change has occurred, or that no change has occurred. The second level is damage identification. This concerns determining the particular type of damage or fault that has occurred, including identifying the location of the damage. The third level is damage estimation and concerns determining or estimating the magnitude and extent of the fault.

Of equal importance to the three levels of structural state characterization, described above, is the estimation of the remaining useful life of the structure (Sohn *et al.* 2001). This addition to the structural characterization procedure is often referred to as prognosis, and is particularly important when a fault has indeed been reported by the damage detection process. Remaining-useful-life estimations aid in making decisions pertaining

to the need for repair or replacement of infrastructure, and have implications to economic cost and human safety. For example, for countries with an increasing stock of aging infrastructure, the challenge lies in deciding whether or not the infrastructure has deteriorated to such an extent as to require replacement. If it is decided that repair work would suffice, estimations as to how long the infrastructure would maintain safety standards are essential.

Civil infrastructure is plagued with the common problem of chloride induced corrosion. This is significant because steel-reinforced concrete is the material of choice for the construction of civil infrastructure such as bridges. This form of deterioration, if unchecked, can significantly weaken structures and render them unsafe and unsightly (Figure 1.1). Unfortunately, steel reinforcement corrosion can go unnoticed until the effects are evident on the surface of the structure, and the structure has already been significantly weakened. The following section briefly describes the structural effects of steel reinforcement corrosion and highlights the difficulties associated with its detection.

Figure 1.1: The effects of steel reinforcement corrosion in a bridge pier

1.1.1 The structural effects of steel reinforcement corrosion

Chloride ions, or other aggressive substances, lower the PH of the concrete environment in the vicinity of the steel reinforcement. Conditions conducive to the electrochemical process of steel corrosion are created. As corrosion progresses, the chemical reactions associated with the process produce substances that are greater in volume than the steel that has been corroded away. For degrees of corrosion up to about 4 % of steel cross-section, this build up of corrosion products results in an increase in the bond at the steel-concrete interface, due to an increase in pressure (Almusallam *et al.* 1996). At greater degrees of corrosion, the internal stresses imposed on the concrete due to the increase in the volume of corrosion products eventually leads to cracks forming in the concrete and a significant loss of bond at the steel-concrete interface. Bond slippage reduces the effectiveness of steel reinforcement, since the tensile stresses in the concrete can no longer be transferred to the steel. The strength of the bond ensures that the concrete and steel act as a composite and any disruption of the bond will negatively affect the load-deflection characteristics of the structural element (De Vos Theron 1994). Severe cracking leads to spalling, where chunks of concrete separate from the structural element, exposing the steel reinforcement. Apart from the consequences of a weakened structure, there are obvious safety risks associated with masses of concrete falling from height. The bridge pier in Figure 1.1 has experienced severe steel reinforcement corrosion, leading to spalling. Figure 1.2 illustrates the mechanism by which structural elements are weakened by steel reinforcement corrosion. Clearly, it is essential to detect the onset of this process, so that measures can be taken to prevent such structural damage.

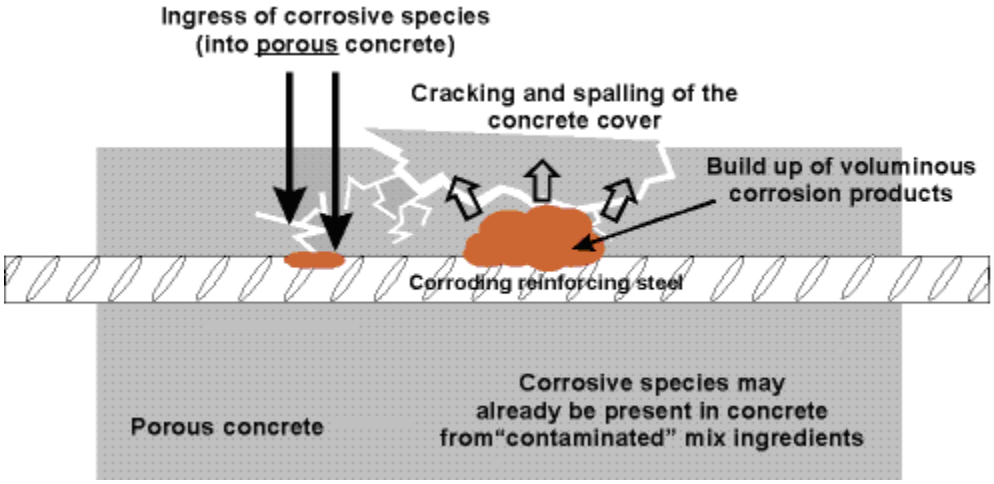

Figure 1.2: The mechanism by which steel reinforcement corrosion weakens reinforced concrete structures

1.1.2 Traditional methods of detecting steel reinforcement corrosion

The products of steel corrosion consist of iron oxides which have a reddish brown colour. Therefore, the occurrence of steel reinforcement corrosion often results in brown rust stains on the concrete surface. These stains present themselves before the effects of the corrosion have caused significant structural damage. In such cases, visual inspections are sufficient for the detection of the corrosion. Unfortunately, a common phenomenon, known as pitting corrosion, is an example of how steel reinforcement corrosion can go unnoticed until structural integrity is compromised. Pitting corrosion results when the penetration of the ions that initiate the corrosion process occurs in a localised region of the concrete, like at construction joints or in cracks, or if these substances were present in the constituents of the concrete mix (De Vos Theron 1994: Marshal 1990, Brown 1983). This can lead to a severe loss of steel cross-sectional area in a localised region of a structural element, invisible to the naked eye. Traditionally, visual inspections have been combined with other, less subjective, methods of detecting steel reinforcement corrosion. These methods include potential mapping (Elsener 2001), concrete resistivity measurements (Polder 2001), and coring for chloride profiles.

The method of potential mapping measures the potential difference between the steel reinforcement and a reference electrode and relates it to a probability that corrosion is taking place. The potential difference reading is taken at intervals over the structure and a

contour map of corrosion potential can be developed. Table 1 was obtained empirically and it gives the probability of the occurrence of corrosion associated with potential difference readings (Ha-won Song *et al.* 2007).

Table 1: Probability of corrosion occuring

Potential difference (V) (between steel and $CuSO_4$ electrode)	Probability of corrosion
> -0.20	< 5 %
-0.20 to -0.35	50 %
< -0.35	> 95 %

The process of corrosion potential mapping over a whole structure is tedious and time consuming.

The method of concrete resistivity measurements is based on the assumption that the concrete's resistivity is proportional to the corrosion rate (Ha-won Song *et al.* 2007). Like the method of corrosion potential measurement, it involves using electrodes to measure the resistivity of the concrete at intervals over the structure and developing a contour map indicating areas where corrosion is probable. Resistivity measurements, as well as being time consuming, can be inaccurate as they are affected by factors such as the dimensions of the structural element under investigation and inhomogeneities such as layers of concrete with different properties.

The method of chloride profiles is a destructive method that involves the removal of cores from the structure. The material at different depths of the core is ground to a powder and tested by titration to measure the amount of chloride ions present. The profile of chloride content with depth can then be obtained and, based on this, the likelihood of the occurrence of corrosion can be deduced. Apart from the negative impact on the aesthetics of the structure, coring methods on their own often tend to be too localised for practical purposes. Furthermore, the durability of the concrete is compromised because new paths for the ingress of harmful substances are opened.

1.2 Vibration-based damage detection

As mentioned in the previous section, traditional techniques for detection of deterioration include visual inspections and destructive methods such as coring, as well as various mapping techniques. Unfortunately, these techniques tend to be either subjective, time consuming or too localized. Visual inspections are susceptible to human subjectivity and by the time damage is visible to the naked eye, as is the case with pitting steel reinforcement corrosion, deterioration may be at an advanced stage. Mapping techniques are extremely tedious and time consuming. Detection techniques that require coring tend to be inadequate as they only detect damage in localized areas of the structure under investigation. However, these traditional methods of corrosion damage detection cannot be discounted and may compliment other, more global, techniques of damage detection.

More recently, damage detection techniques based on the vibration response of a structure have been investigated for the purpose of structural health monitoring. The fundamental principle upon which vibration-based methods are founded is that changes (faults) in a structure cause discrepancies in its vibration response (Fassois *et al.* 2006). The raw data obtained from vibration tests on a structure is in the form of vibration signals such as that shown in Figure 1.3. Vibration signals are time histories of the displacement, acceleration or strain of a point on the structure. They are measured using sensors such as accelerometers and strain gauges, and recorded using data acquisition hardware. Important characteristics of the vibration signal, including moment statistics of the amplitudes and natural frequencies of vibration, may be extracted for analysis of the vibration response of the structure.

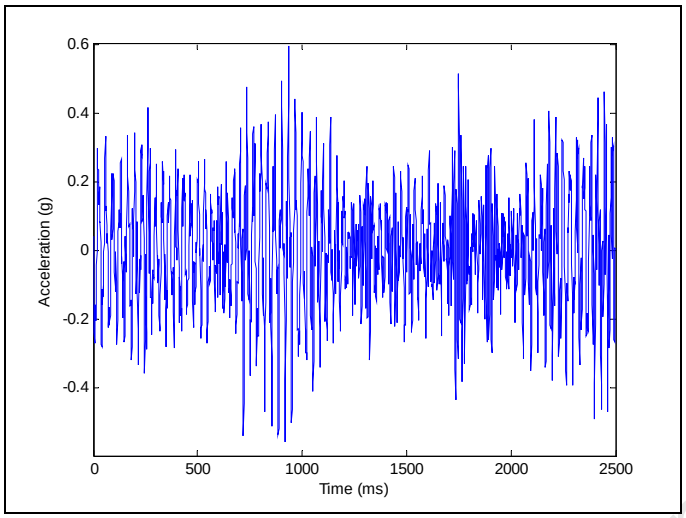

Figure 1.3: A vibration signal

Vibration-based damage detection techniques have been successfully applied to mechanical and aerospace structures (Fugate *et al.* 2001). The challenge lies in their application to civil infrastructure. Characteristics of typical civil infrastructure, including uncontrollable environmental conditions such as temperature, precipitation and wind, and non-linearities due to complex composite materials such as reinforced concrete, lead to the challenge of successfully applying vibration-based damage detection techniques to them. The appeal of these techniques lies in their non-destructive and non-disruptive nature, and their potential for global system monitoring (Fugate *et al.* 2001). In other words, these techniques, if successfully applied, to a bridge for example, could allow for automatic detection of damage anywhere in the bridge without closures for inspection and without the removal of physical samples from the bridge. Furthermore, in cases where the vibration-based damage detection technique requires only data from ambient vibrations (vibrations caused by normal operation), and where wireless data transmission is possible, minimal equipment is required on site. Only sensors such as accelerometers or strain gauges are required, and these may be imbedded in the structure.

In this study, vibration based damage detection techniques are divided into two main categories. These are model-based and non-model-based techniques. Model-based damage detection techniques involve the development of an analytical model of the test structure. This is typically a finite element model. Figure 1.4 represents a visualization of a finite element model of a grandstand at the Athlone Stadium in Cape Town.

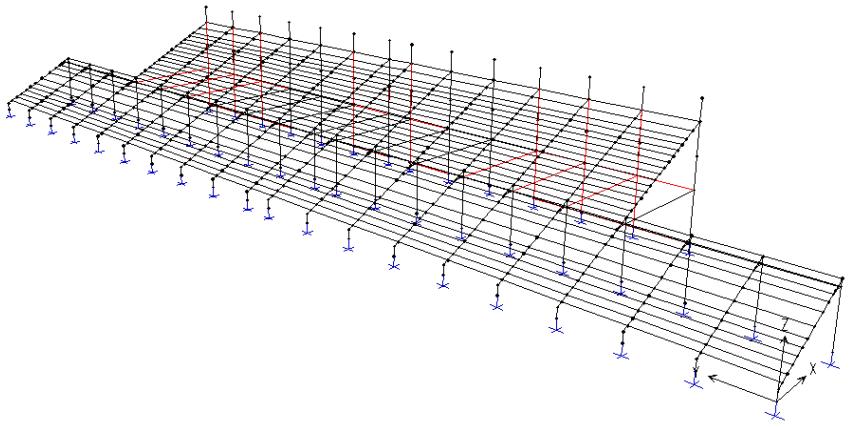

Figure 1.4: A finite element model of a grandstand at the Athlone Stadium

Damage is detected by updating the analytical model so that the vibration response from the actual structure matches the response from the model (Cattarius *et al.* 1996). Changes in the vibration response that are indicative of the presence of damage include changes in stiffness, which may result in changes in the natural frequencies of the structure and a resulting change in the structure's mode shapes. The basis of this damage detection approach is that every natural frequency of a structure is associated with a mode of vibration which results in the structure assuming a certain basic shape as it vibrates. Figure 1.5 shows the mode shapes of part of a bridge deck at different natural frequencies of vibration. The scale is exaggerated for visualization purposes. The drawback of model-based damage detection techniques is that there are always errors involved in any analytical representation of a physical system. It has also been noted that natural frequencies are not sensitive to small amounts of damage (Cattarius *et al.* 1996: Resos *et al.* 1990, Dong *et al.* 1994).

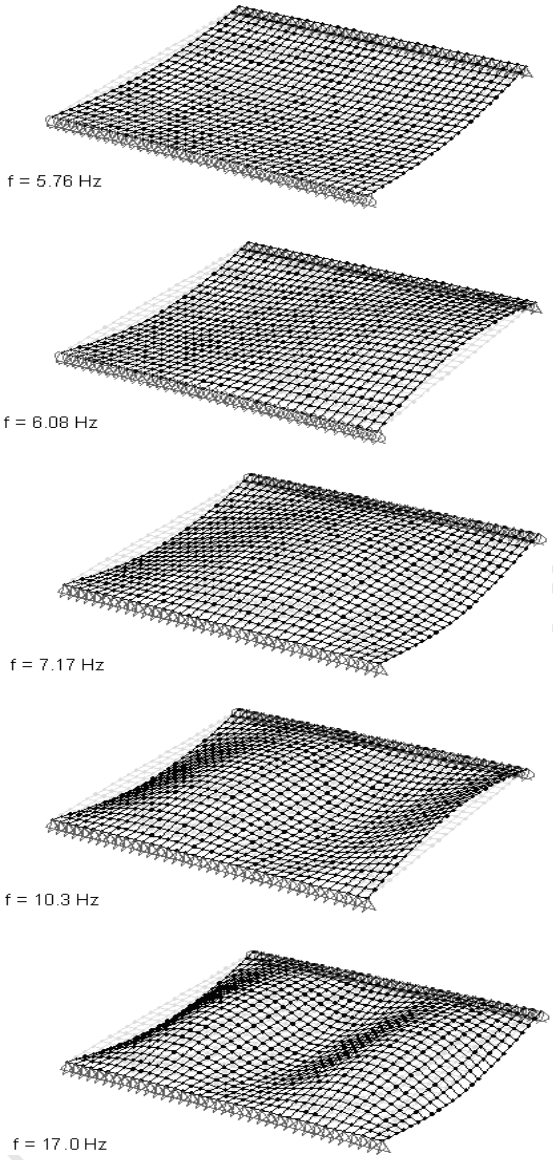

Figure 1.5: Mode shapes of part of a bridge deck

As their name implies, non-model-based damage detection techniques do not employ analytical models of the test structure, thus avoiding the problem of modeling errors. These techniques use only experimental data, and damage is detected by direct comparison of the data from the structure in its reference or undamaged state and the data from the structure in its potentially damaged state. For example, Cattarius *et al.* (1996) successfully employed what they called a beat method to the problem of damage detection in a cantilever beam. By subtracting the time response of the damaged state from the time response of the undamaged state, they observed a beating phenomenon

which was attributed to a small phase shift as a result of a subtle change in natural frequency (Figure 1.6). They showed that the time response was able to detect material damage in cases that produced very small changes in the frequency response.

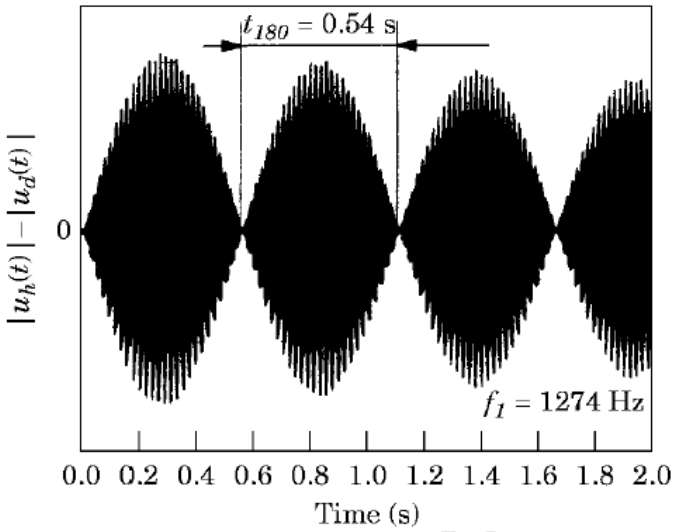

Figure 1.6: The beating phenomenon, indicating a phase shift in a new signal, *ud(t)*, relative to a reference signal, *ud(t)* (Cattarius *et al.* 1996)

The comparison between the damaged and undamaged state may also be achieved by manipulating vibration data to identify and extract features of the vibration data that change with the introduction of damage to the structure. For example, it has been shown (Sohn *et al.* 2001, Lu *et al.* 2004, Nair *et al.* 2005) that when the vibration response of the structure is modeled using a time series model, such as an auto-regressive (AR) model, the coefficients of this model are damage-sensitive features. An example of an AR model is shown in Equation 1.1.

$$x_t = \sum_{j=1}^{p} \alpha_j x_{t-j} + e_x(t) \qquad 1.1$$

where x_t is the measured vibration response at time t, a_j are auto-regressive coefficients, p is the order of the model, j is the lag and $e_{x(t)}$ is the random residual error at time t.

1.3 Pattern recognition

Lately, researchers have proposed that the damage detection problem requires a statistical pattern recognition approach (Park *et al.* 2004, Sohn *et al.* 2003, Taha *et al.* 2005). The reason is that statistical pattern recognition provides a more robust framework for detecting changes in structural condition than methods that strictly analyze changes in system parameters such as dynamic modal parameters. In brief, the aim of statistical pattern recognition is to detect damage using features in the vibration data which change with the introduction of damage to the structure. These methods are also characterized by statistical rigour in the formation of the algorithms for diagnosis of the structure. Statistical methods are employed to define what changes are significant enough to represent damage. Sohn *et al.* (2001) describe the statistical pattern recognition paradigm for damage detection as a four-part process consisting of the following:

1. *Operational evaluation*: The operational and environmental conditions under which the system is to be monitored are identified. Operational evaluation begins to set limitations on what will be monitored and how to perform the monitoring as well as tailoring the monitoring to unique aspects of the system and unique features of the damage that is to be detected (Fugate *et al.* 2001). This involves defining "damage" for the particular structural health monitoring case.
2. *Data acquisition and cleansing*: This includes decisions as to the type, location and number of sensors to be used, as well as the amount of data to be captured. The data is normalized and accepted or rejected according to some predefined criteria. Data may also be re-sampled at a lower rate (decimated) and filtered to remove undesirable frequencies to avoid phenomena such as aliasing.
3. *Feature extraction and data reduction*: Damage-sensitive features, characteristics of the data that change due to the presence of damage, are identified in the response data. Due to the large volumes of data collected for the purpose of monitoring, it is necessary to reduce the data to small dimensional *feature vectors*. A feature vector is a row or column vector in which each element is a damage-sensitive feature.

4. *Statistical model development for feature discrimination*: Algorithms are developed to diagnose the structure and to determine the extent of damage present. Detecting a change in damage-sensitive features is insufficient for confident diagnosis of a structure. Statistical rigour is required to ascertain whether the changes in the damage-sensitive features are in fact due to damage, thereby reducing the risk of false-positive and false-negative indications of damage. This step often includes the determination of thresholds for the detected changes.

Literature contains many examples of steps 1 to 3, with the most emphasis being on feature extraction and data reduction. For example, Nair *et al.* (2005) modeled the vibration time-history using an auto-regressive model (AR) and showed that the mean of the coefficients of the model were damage-sensitive features. Lu *et al.* (2004) derived a novel ARX model (auto-regressive model with exogenous inputs) from the general dynamic equation governing a vibrating system and identified the variance of the residual errors of this model as the damage-sensitive feature when applied to vibration data from multiple degree of freedom structural systems. Yan *et al.* (2005) applied a principal component analysis (PCA) to the natural frequencies of a wooden bridge model and concluded that the statistics of the residual error of the PCA prediction model provided an indication of damage. Sohn *et al.* (2001) investigated the use of the bispectrum (third-order power spectrum) to detect the onset of non-linearities associated with damage.

1.4 The purpose of the study

Few researchers have devoted their attention to the effect of measurement errors on the outputs of the damage detection algorithms and explicitly quantify the uncertainty in the final diagnosis. Typical uncertainties associated with vibration-based damage detection techniques include instrumentation errors and errors due to changing environmental and operational conditions. Instrumentation errors include sensor resolution errors and quantization errors in the data acquisition card. Changing environmental and operational conditions may change the performance of the instrumentation and/or the behaviour of the structure under investigation. These errors, if ignored, could lead to false-negative or

false-positive detections of damage. Quantification of the uncertainty in diagnoses would strengthen step 4 of the statistical pattern recognition methodology, namely statistical model development for feature discrimination. A quantitative level of confidence in the diagnosis of a structure would allow for objective decisions as to what action to take.

In summary, with regard to the purpose of the research, the following must be kept in mind. SHM is essential for early detection of damage and the onset of deterioration in infrastructure. Vibration-based damage detection techniques for SHM are desirable for their non-destructive nature, their potential for global system monitoring and their potential for full automation. More specifically, non-model-based vibration-based damage detection techniques are preferred to model-based techniques due to the difficulty and computational expense of accurately modelling complex structures and their support conditions (Owen *et al.* 2004). However, vibration-based damage detection techniques require further research and development for their application to civil infrastructure, due to the more subtle and complex forms of damage, such as the deterioration brought about by steel reinforcement corrosion in concrete structures and due to the problems brought about by uncontrollable environmental and operational conditions. These present cross-cutting issues, as the need for the detection of subtle damage leads to problems associated with the sensitivity of the damage detection techniques to uncertainties and variable environmental and operational conditions. In order to confirm whether or not environmental and operational conditions and measurement errors influence the results of damage detection algorithms, it would be desirable to quantify or eliminate (if possible) the uncertainties that result from these effects and propagate them through the damage detection algorithms to determine the uncertainty in the final results. A framework is required that makes the damage detection techniques robust in the presence of instrumentation errors and changing environmental and operational conditions.

Given the research needs presented above, the aim of the research is to investigate the application of non-model-based vibration-based damage detection techniques to the detection of steel reinforcement corrosion damage in concrete structures, and to develop a framework that quantifies the uncertainty in the damage detection techniques in the

presence of changing environmental and operational conditions. Since, ultimately, the damage detection techniques are intended for real structures in the field and not only laboratory models, the framework must be practical.

With regard to the scope of the study, this thesis will be limited to damage detection. Damage identification, damage magnitude estimation and prognosis are beyond the scope of the thesis.

1.5 Plan of development

The following approach will be adopted. A review of non-model-based vibration-based damage detection techniques will first be presented. Then, the errors involved in vibration testing will be described. Next, a review of general uncertainty propagation and quantification techniques will be presented. Useful concepts and ideas can then be drawn from these uncertainty propagation and quantification techniques and applied to frameworks for damage detection in the presence of uncertainty. A selection of possible frameworks will then be presented and tested on simulated data. Thereafter, laboratory experiments to validate these damage detection frameworks, incorporating uncertainty quantification, will be described in detail. The results will then be discussed and conclusions drawn.

Chapter 2

2 Non-Model-Based Feature Extraction Techniques

As stated in Chapter 1, damage detection, when implemented with a statistical pattern recognition approach, consists of four steps. These are: (1) operational evaluation, (2) data acquisition and cleansing, (3) feature extraction and data reduction, and (4) statistical model development for feature discrimination. All vibration-based damage detection techniques adopt the first three steps of this approach in one form or the other. What qualifies a damage detection technique as a *statistical pattern recognition* technique is the inclusion of the last step, namely statistical model development for damage discrimination. It is convenient, at this stage, to highlight a point that often lacks clarity in the literature. The differences in damage detection techniques, and consequently the names assigned to them, lie in the methods they use to extract damage-sensitive features from the vibration data. The statistical models used to actually discriminate between the damaged and undamaged states of the structure are not peculiar to particular damage detection techniques, but may be applicable to all. Therefore, since complete damage detection consists of all four steps listed above, the term *feature extraction technique* will refer to the completion of the first three steps and *damage detection technique* will be reserved for algorithms employing all four steps of the statistical pattern recognition methodology. In this chapter, damage detection approaches are categorized based on the methods of feature extraction. Statistical model development for feature discrimination will be discussed in Chapter 4. Furthermore, the term “damage detection technique” is, henceforth, reserved for algorithms that include all four steps of the damage detection process.

2.1 Time-series based feature extraction techniques

Vibration data is collected by recording the acceleration, strain or displacement of the structure at instances in time using sensors such as accelerometers and strain gauges. This forms a time signature (or vibration signal) such as the one shown in Figure 1.3.

Time-series-based damage detection techniques consist of modeling the vibration signal as a time-series model. These techniques work on the premise that a recognizable change in a damage-sensitive feature of the time series model will occur as the structure is damaged. Researchers have employed different time-series models. The most important of these, for the purposes of feature extraction for damage detection are the *Auto-Regressive Moving Average models with exogenous inputs* (ARMAX). This is a very general class of model which can be separated into three main parts; the auto-regressive part, the moving average part, and the exogenous part. The form of ARMAX models will be described briefly before their application to feature extraction is explained.

An auto-regressive model (AR) is a mathematical expression that relates the response data at one instance in time to the response at previous instances in time. equation 1.1 is the general form of an AR model, and this is repeated below.

$$x_t = \sum_{j=1}^{p} \alpha_j x_{t-j} + \varepsilon_{x(t)} \qquad 2.1$$

where x_t is the response at time t, α_j are AR coefficients, p is the order of the model (the number of AR coefficients), j is the lag and $\varepsilon_{x(t)}$ is the random residual error at time t, often referred to as the noise component to the signal.

A moving average model (MA) is a model in which the response is regressed on past samples of unknown random inputs (i.e. noise). Moving average models thus take the following form.

$$x_t = \sum_{j=1}^{r} \gamma_j \varepsilon_{t-j} + \varepsilon_{x(t)} \qquad 2.2$$

Here γ_k are the MA coefficients and r is the order (the number of MA coefficients).

The exogenous part of the model (which introduces the X in ARMAX) refers to a regression of the response on past, known, measurable inputs (i.e. exogenous inputs). This is expressed as follows.

$$x_t = \sum_{j=1}^{q} \beta_j u_{t-j} + \varepsilon_{x(t)} \tag{2.3}$$

Here β_j are the exogenous coefficients, u_t is the exogenous input at time t, and q is the order.

A complete ARMAX model thus takes the form

$$x_t = \sum_{j=1}^{p} \alpha_j x_{t-j} + \sum_{j=1}^{q} \beta_j u_{t-j} + \sum_{j=1}^{r} \gamma_j \varepsilon_{x(t-j)} + \varepsilon_{x(t)} \tag{2.4}$$

This form of time-series model implies that the response at a particular point in time is as a result of four different input sources. These input sources are the four terms on the right hand side of equation 2.4. In other words, the response is due to a weighted average of past responses, past measurable inputs, past noise, and the noise present at the instant of sampling. When exogenous inputs are not included in the modelling of the vibration response (i.e. when all β_k are taken to be zero) an auto-regressive moving average model (ARMA) is formed.

$$x_t = \sum_{j=1}^{p} \alpha_j x_{t-j} + \sum_{j-1}^{r} \gamma_j \varepsilon_{x(t-j)} + \varepsilon_{x(t)} \tag{2.5}$$

When the response is not regressed on past samples of noise (i.e. when all MA coefficients γ_k are taken to be zero) an auto-regressive model with exogenous inputs (ARX) is formed:

$$x_t = \sum_{j=1}^{p} \alpha_j x_{t-j} + \sum_{j=1}^{q} \beta_j u_{t-j} + \varepsilon_{x(t)} \tag{2.6}$$

Equations 2.1 to 2.6 all represent possible models for the vibration (or dynamic) system under investigation. Using the standard block diagram for input-output systems, this system can be represented as follows (Worden *et al.* 2001):

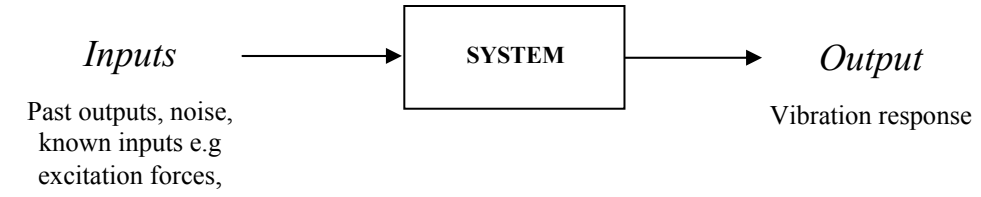

Figure 2.1: A block diagram representation of a vibration system

If the dynamic system represents the vibration behaviour of a structure in its reference (or undamaged) state, then damage, or any other changes to the structure, will change the nature of the dynamic system. It is logical, therefore, for the purpose of damage detection, to determine the governing system for the vibration behaviour of the structure and observe any changes in this system. The problem of modelling the governing system is not trivial and is known as *system identification*. Engineering knowledge of the system under investigation greatly simplifies the system identification problem, as the form of the equation that models the vibration response of the structure can be deduced (Worden *et al.* 2001). For example, it can be shown that the dynamic equation for a simply supported beam (a single degree-of-freedom system) is an ARX(2,1), i.e. an ARX with two AR coefficients and one exogenous input coefficient. The proof, as given by Worden and Tomlinson (2001) is presented here. Consider the general linear single degree-of-freedom system. Newton's equation of motion for the response of the structure at the instant t is

$$m\ddot{x}_t + c\dot{x}_t + kx_t = u_t \qquad 2.7$$

where u_t is the excitation, x_t is the response, $\dot{x}_t$ and $\ddot{x}_t$ are its 1st and 2nd derivatives respectively, m is the mass, c is the damping coefficient and k is the stiffness. Considering the response at a sequence of discrete times t separated by the sampling interval Δt, the derivatives $\dot{x}_t$ and $\ddot{x}_t$ can be approximated as follows:

$$\dot{x}_t \approx \frac{x_t - x_{t-\Delta t}}{\Delta t} \tag{2.8}$$

$$\ddot{x}_t \approx \frac{x_{t+\Delta t} - 2x_t + x_{t-\Delta t}}{\Delta t^2} \tag{2.9}$$

Substituting these into equation 2.7 yields

$$m\left(\frac{x_{t+\Delta t} - 2x_t + x_{t-\Delta t}}{\Delta t^2}\right) + c\left(\frac{x_t - x_{t-\Delta t}}{\Delta t}\right) + kx_t = u_t \tag{2.10}$$

Multiplying both sides of the equation by $\frac{\Delta t^2}{m}$, grouping like terms and then making $x_{t+\Delta}$ the subject of the equation yields

$$x_{t+\Delta t} = \left(2 - \frac{c\Delta t}{m} - \frac{k\Delta t^2}{m}\right)x_t + \left(c\frac{\Delta t}{m} - 1\right)x_{t-\Delta t} + \frac{\Delta t^2}{m}u_t \tag{2.11}$$

Regressing by one sampling interval of time yields

$$x_t = \left(2 - \frac{c\Delta t}{m} - \frac{k\Delta t^2}{m}\right)x_{t-\Delta t} + \left(c\frac{\Delta t}{m} - 1\right)x_{t-2\Delta t} + \frac{\Delta t^2}{m}u_{t-\Delta t} \tag{2.12}$$

Taking the index j to represent an integer number of sampling intervals, and, for convenience, representing the response at time $t\text{-}j\Delta t$ as $x_{t\text{-}j}$ yields

$$x_t = \left(2 - \frac{c\Delta t}{m} - \frac{k\Delta t^2}{m}\right)x_{t-1} + \left(c\frac{\Delta t}{m} - 1\right)x_{t-2} + \frac{\Delta t^2}{m}u_{t-1} \tag{2.13}$$

or $$x_t = \sum_{j=1}^{2} \alpha_j x_{t-j} + \sum_{j=1}^{1} \beta_j u_{t-j} \tag{2.14}$$

where $\alpha_1 = \left(2 - \frac{c\Delta t}{m} - \frac{k\Delta t^2}{m}\right)$, $\alpha_2 = \left(c\frac{\Delta t}{m} - 1\right)$ and $\beta_1 = \frac{\Delta t^2}{m}$ are constant coefficients.

This is clearly an ARX(2,1). This result is proof that if the vibration response of a structure is modelled as an ARMAX-type time-series, the coefficients of the model are closely related to the dynamic parameters of the structure, namely damping coefficients,

mass and stiffness. It is these parameters that change as a result of structural damage. However, it is not necessary, from a statistical pattern recognition point of view, to determine the values of the parameters *c*, *k* and *m*, as only the *effects* of changes in these parameters are required for the detection of damage. These changes are reflected in the coefficients of the time-series model. Therefore, the coefficients of the time-series model serve as damage-sensitive features.

Furthermore, since the residual error is the difference between the response predicted by the time-series model and the measured response, the statistics of the residual error are related to the goodness of fit of the model. The model represents the dynamic system of the structure and its goodness of fit should not change as long as the dynamic system remains unchanged. Damage to the structure would cause changes in the dynamic system and therefore the fit of the model. This would result in changes in the variance of the residual error. If a time-series model representing the vibration behaviour of the structure in its reference state is estimated, then the variance of the residual errors between the reference model and the measured response of the structure in an unknown structural state serves as a damage-sensitive feature.

Several methods exist for the estimation of the model coefficients, and they can be found in literature such as Box *et al.* (1994). The most common method is the simple least-squares method which computes the set of coefficients that minimises the square of the residual error. Mathematical analysis software packages such as Matlab™ have built-in functions for this purpose.

Examples of the use of time-series feature extraction techniques can be found in literature by Nair *et al.* (2005), Sohn *et al.* (2001) and Lu *et al.* (2004). Nair *et al.* (2005) modeled the vibration time-history using an ARMA and showed that that the first AR coefficient normalized by the square root of the sum of the squares of the first three AR coefficients was a damage-sensitive feature (*d*). i.e:

$$d = \frac{\alpha_1}{\sqrt{\alpha^2{}_1 + \alpha_2{}^2 + \alpha_3{}^2}} \qquad 2.15$$

where α_i is the ith AR coefficient of the time series model.

The authors tested the technique on a physical model of a steel storey building. The technique was shown to be sensitive to mechanical damage such as the removal of braces from the physical model. Lu *et al.* (2004) derived a novel ARX model (autoregressive model with exogenous inputs) from the general dynamic equation governing a vibrating system and identified the variance of the residual errors of this model as the damage-sensitive feature when applied to the vibration data from multiple degree-of-freedom structural systems. However, the technique was applied only to simulated data.

2.2 Spectral techniques for feature extraction

The term *spectral* refers to representations of the vibration response of a structure in the frequency domain. In contrast, the time-series model approach described in the previous section represents the vibration response of the structure in the time domain. Frequency domain representations of the dynamic system of a structure include frequency response functions (FRF), transmissibility functions and the bispectrum. The selection of frequency domain representations presented here is by no means exhaustive. A vast number of spectral techniques have been employed for feature extraction (Park 2005, Worden 1999, Sohn *et al.* 2001, Johnson 2002) and only a few common ones are described here.

2.2.1 Frequency response function (FRF)

The FRF of a system subjected to harmonic excitation is the ratio of the amplitude of the input (u) to the amplitude of the response (x), for a given frequency (ω) of the harmonic excitation. The harmonic excitation can be expressed as

$$u_t = U\cos\omega t \qquad 2.16$$

where U is the amplitude of the excitation. The response will also be harmonic with the same frequency, but lagging the input in phase by φ radians. i.e.

$$x_t = X\cos(\omega t - \varphi) \qquad 2.17$$

Where X is the amplitude of the response

The response of a dynamic system is governed by Newton's equation of motion (equation 2.7). By substituting Equations 2.16 and 2.17 into the equation of motion and rearranging, it can be shown (Worden *et al.* 2001) that the FRF for a single degree of freedom forced vibrating system is given by

$$|H(\omega)| = \frac{X}{U} = \frac{1}{\sqrt{\left(-m\omega^2 + k\right)^2 + c^2\omega^2}} \qquad 2.18$$

The value of $H(\omega)$ is clearly governed by the dynamic system parameters: stiffness, damping and mass. An alternative representation of the FRF is obtained by applying the Discrete Fourier Transform (DFT) to the time domain response signal. An efficient algorithm for computing the DFT is the Fast Fourier Transform (FFT). The FRF, as computed using Fourier analysis, is a complex function and takes the form

$$H(\omega) = \frac{1}{k - m\omega^2 + \mathrm{i}c\omega} \qquad 2.19$$

The plot of a typical FRF for a SDOF vibrating system is shown in Figure 2.2. The FRF is a maximum when the excitation frequency coincides with the resonant frequency ω_r.

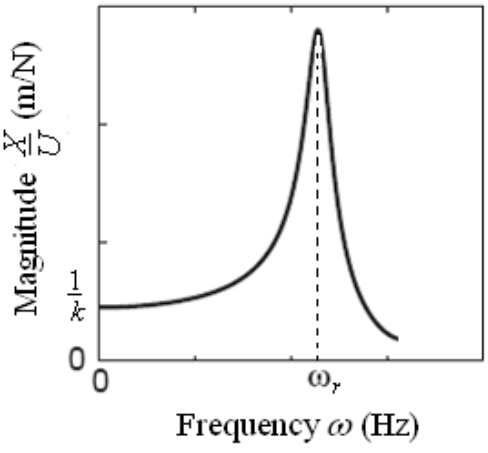

Figure 2.2: The FRF of a SDOF system

The physical interpretation of the FRF is the proportional change in the amplitude of the signal as it passes through the system $u_t \rightarrow x_t$ (Worden *et al.* 2001). Any changes in the system, such as damage, will cause distortions in the relationship between the input and the response. Therefore, the variable $\frac{X}{U}$ serves as a damage-sensitive feature. $\frac{X}{U}$ can be sampled at several frequencies to provide a large data set of damage-sensitive features. The FRF tends to be most sensitive to damage for excitation frequencies in the vicinity of resonant frequencies (Worden *et al.* 1999).

2.2.2 Transmissibility

Motion transmissibility is the ratio between the amplitude of the response at one location on a structure and the amplitude of the response at another location on the structure, due to the same excitation. Physically, it describes the relative motion of different parts of the structure. The transmissibility, T_{ij}, between two points, i and j, on a linear structure is constant, for a constant excitation frequency, and will not change unless the structure is subjected to changes such as damage. As an extreme example, the formation of a plastic hinge between two points on a structure will change the relative motion of the two points, and therefore the transmissibility between them will also change. Therefore, the transmissibility between pairs of points on a structure serves as a damage-sensitive feature. As with the FRF, transmissibility is most sensitive to damage for excitation frequencies in the vicinity of resonant frequencies. An advantage of the use of transmissibility as damage-sensitive features is their sensitivity to localised damage. The approach is useful when a particular form of damage is expected and a particular part of the structure is to be monitored. The transmissibility between two points i and j is given by

$$T_{ij(p)} = \frac{X_{ip}}{X_{jp}} = \frac{X_{ip} / U_p}{X_{jp} / U_p} = \frac{H(\omega)_{ip}}{H(\omega)_{jp}} \qquad 2.20$$

where *p* denotes the location of the excitation force. Computing the transmissibility using the response measured from two adjacent sensors in an array will detect changes in structural condition in the proximity of those sensors.

2.3 Time-frequency-based feature extraction techniques

As mentioned in the previous section, the frequency content of the dynamic response is an important feature for damage detection, and can be obtained from the FRF. However, vibration response signals are not always stationary, meaning that the frequency may change over time. For example, cracked concrete beams may exhibit non-stationary vibration response due to stiffness degradation. Unfortunately, the FRF does not capture temporal changes in frequency content. In other words, the FRF and other FFT-based representations of the dynamic response of a structure provide no information about *when* in time a particular frequency band occurred (Basu 2005). Figure 2.3 highlights this point. The two signals have the same FRF representation, even though their frequency bands occur at different times.

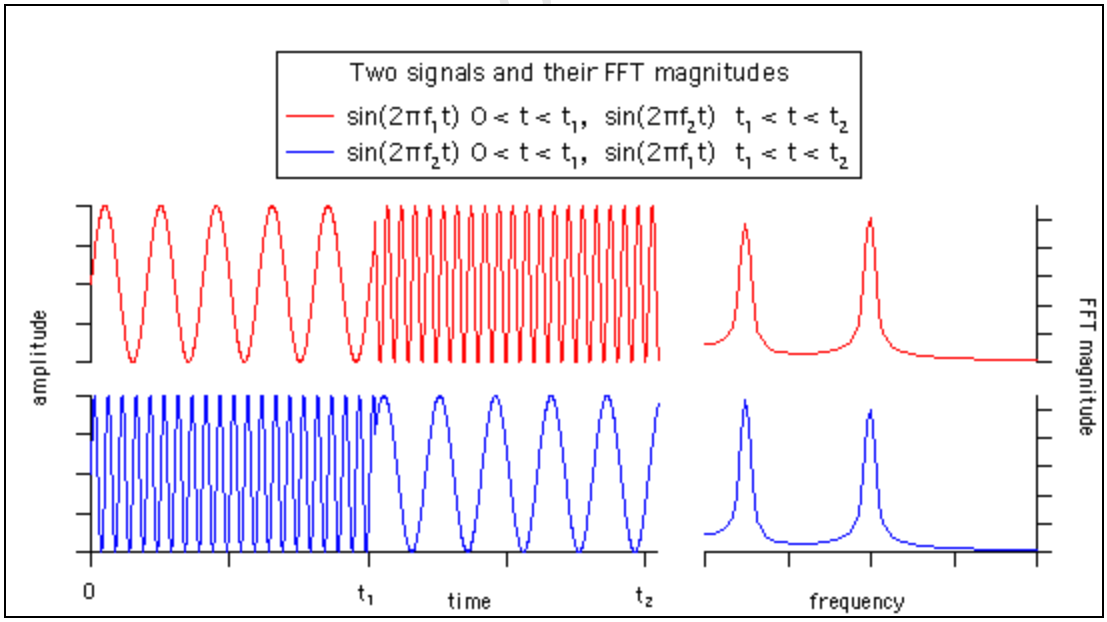

Figure 2.3: The inability of the Fourier transform to depict the time-varying spectral properties of non-stationary signals (www.wavemetrics.com). These two very different signals have the same FFT.

Given that the time-varying properties of a vibration signal may contain valuable information about its structural state, the deficiencies of frequency domain analysis in

this regard, have raised interest in *time-frequency* analysis. Time-frequency techniques for analysis of vibration signals aim to determine the frequency content of a signal, as well as the intervals of time over which the frequency bands occur. When used for feature extraction, these techniques benefit from both the temporal and the spectral characteristics of the vibration response. Methods of time-frequency analysis include wavelet analysis, the Wigner Transform and the Short-Time Fourier Transform (sonogram).

2.3.1 Wavelet transform

The wavelet transform is a representation of a signal by breaking it up into many sub-signals. The sub-signals are a set of functions that are generated by translations and dilations of a main function. The sub-signals are called wavelets and the main signal is referred to as the mother wavelet or basis function. Fourier analysis consists of the breaking up of a signal into sine waves of various frequencies and phases, whereas wavelet analysis is the breaking up of a signal into shifted and scaled versions of a mother wavelet (Kim *et al.* 2003). The continuous wavelet transform of a signal is given by

$$W(a,b) = \frac{1}{\sqrt{a}} \int x(t) \psi^* \left(\frac{t-b}{a} \right) dt \qquad 2.21$$

where $\psi(t)$ is the basis function and $\psi^*(t)$ is its complex conjugate , b is the shift of the basis function and a is the dilation or contraction of the basis function along the time axis. W(a,b) is the wavelet coefficient, and it measures the similarity between the signal $x(t)$ and each wavelet function. The basis function for a wavelet of order N takes the form

$$\psi(n) = \sum_{j=0}^{N-1} (-1)^j c_j (2n + j - N + 1) \qquad 2.22$$

where c_j is a coefficient. There are two main rules for the selection of the basis function (Kim *et al.* 2003). The first rule states that the basis function must be wavy in appearance, i.e. having equal area above and below the time axis. Stated mathematically

$$\int_{-\infty}^{\infty} \psi(t)dt = 0 \qquad 2.23$$

The second rule states that the basis function must have most of its energy confined within a finite duration. Stated mathematically

$$\int_{-\infty}^{\infty} |\psi(t)|^2 dt < \infty \qquad 2.24$$

The dominant frequency components of the signal create wavelet coefficients with prominent amplitudes (Yan *et al.* 2005). Thus, $W(a,b)$ contributes to the signal $x(t)$ in the neighbourhood of $t = b$ and in the frequency band corresponding to the dilation factor a (Basu 2005). Structural damage changes the modal parameters of a system, resulting in changes in the wavelet coefficients. The power of wavelet analysis, for the purpose of pattern recognition, lies in its ability, through the wavelet coefficients, to zoom into localized parts of the vibration signal and observe for changes. Therefore, the wavelet coefficients serve as damage-sensitive features.

2.4 Matrix decomposition-based feature extraction techniques – Principal components analysis

Matrix decomposition is a process that uses linear algebra to reduce the dimension of multivariate data. It is a useful statistical technique that can be used to identify patterns in data of restrictively high dimensions. These dimension reducing properties are desirable, given that a vast amount of features can be extracted from vibration data. Matrix decomposition techniques project the data onto a set of orthogonal axes that represent the greater part of the variability of the original data set. Principal components analysis (PCA) is a common matrix decomposition technique which can simplify the identification of patterns in data by reducing the dimensions of the data set. Data containing the most variation can be separated from the data with the least variation. This expresses data sets in such a way as to highlight their similarities and differences. In short, the principal components of a data set are the eigenvectors of their covariance matrix. The use of PCA in the feature extraction process is illustrated using an example (Smith 2002).

Given the two-dimensional variable (*a*,*b*), each data point can be represented as a point in space (Figure 2.4). The eigenvectors of the covariance matrix of this data set are two perpendicular lines, one of which, the first principal component, lies parallel to the direction of the most variability (Figure 2.5). Projecting the data onto either of the two principal components yields a new set of one-dimensional data, whose single axis is the principal component. In our example, projecting the data onto the first principal component results in Figure 2.6. In so doing, all the variability in the direction of the second principal component has been discarded. The resulting data now contains only the most significant variability.

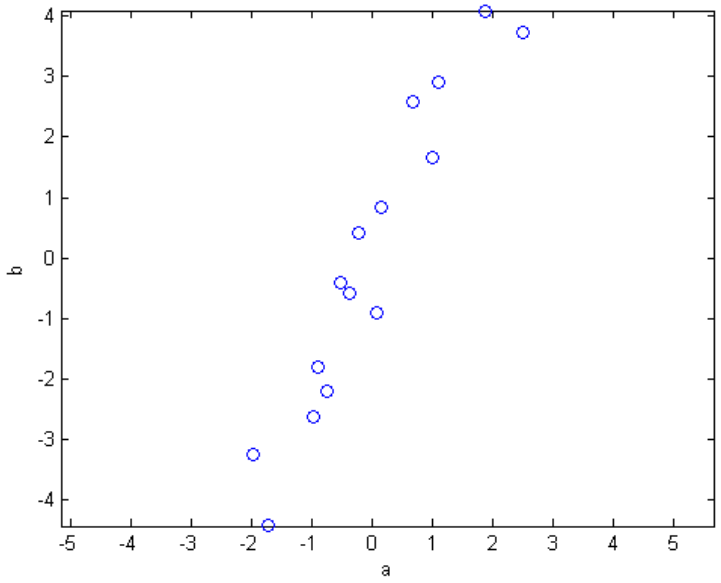

Figure 2.4: A plot of a hypothetical multivariate data set (a,b)

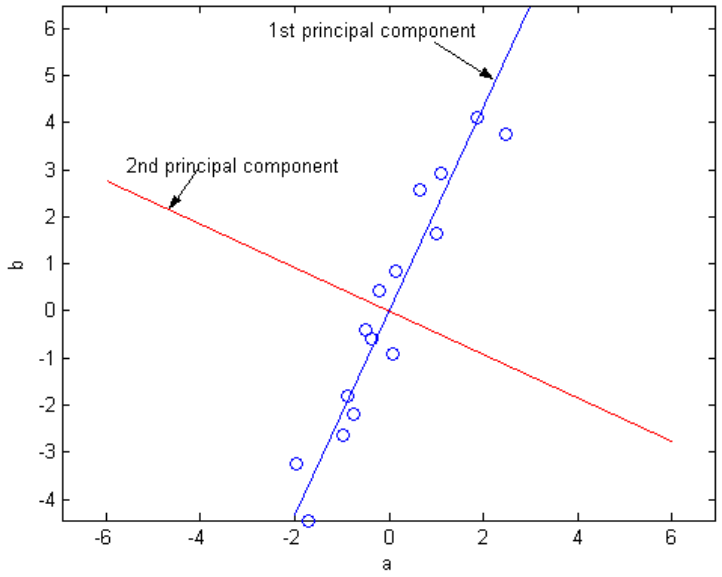

Figure 2.5: The directions of the first two principal components

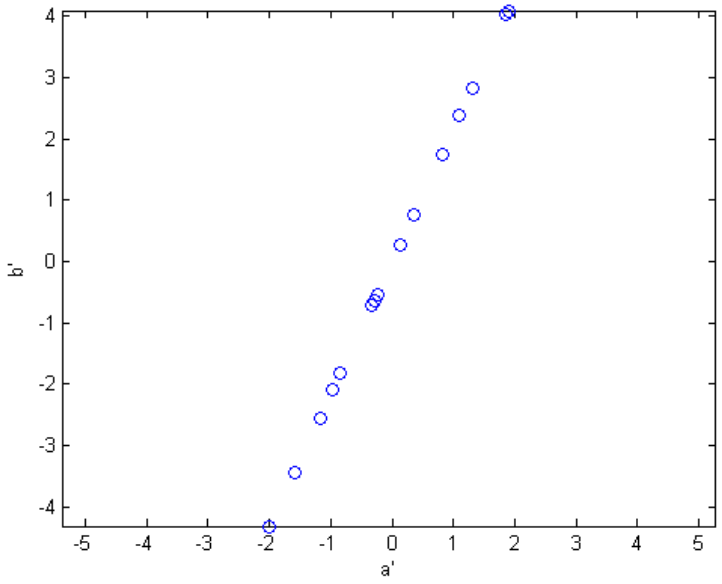

Figure 2.6: Projecting the data onto the 1st principal component reduces the data to 1 dimension if the principal component is taken as a new axis. Variability in the direction of the second principal component is neglected.

Thus, having extracted several damage-sensitive features using different feature extraction techniques, PCA can be used to identify the most salient features and to discard the rest.

2.5 Summary

The following constitute the main points of the chapter:

- A damage-sensitive feature is a characteristic of the measured data that changes due to the introduction of damage in a structure. Multiple damage-sensitive features may be combined to form a feature vector.
- Feature extraction is the reduction of data to feature vectors.
- Feature extraction is typically the third step in the damage detection process when implemented with a statistical pattern recognition approach. Feature extraction follows operational evaluation and data acquisition in the statistical pattern recognition approach to vibration-based damage detection.
- Feature extraction is not in itself a damage detection technique, but requires the next step in the statistical pattern recognition approach, namely feature discrimination, to diagnose the structure as either damaged or undamaged. Feature extraction merely identifies symptoms of damage, while feature discrimination provides the diagnosis.
- Non-model-based feature extraction techniques can be categorized into time-series-based techniques, spectral techniques, time-frequency-based techniques and matrix-decomposition-based techniques.

Chapter 3

3 Uncertainty

The issue of uncertainty in structural health monitoring remains one of the greatest challenges in the research community. The problem lies in identifying the correct approach to delivering objective results in which a degree of confidence is achieved. In the case of damage detection, confident diagnoses of structural state are required. The attainment of this goal is complicated by the fact that error is inherent in all measured data. Error can be defined as a deviation from some target or "true" value. The presence of error leads to uncertainty as to the true value of a quantity of interest such as a damage-sensitive feature, or some computed damage indicator. Typical sources of error in measurements include deviations due to varying environmental conditions and errors in measurement instrumentation. These errors propagate through calculation algorithms and models, introducing uncertainty to the results obtained. Without knowledge of the uncertainty involved in a damage detection technique, it is impossible to guarantee that the results obtained are valid, making diagnosis of a structure difficult and somewhat subjective. This leads to the question of how to quantify something seemingly as *qualitative* as uncertainty. A logical step towards solving this problem is to identify and classify all sources of uncertainty. The method of uncertainty quantification chosen will then depend on the classes of uncertainty under investigation.

3.1 Types or classes of uncertainty

Two general classes of uncertainty can be identified. These are aleatory uncertainty and epistemic uncertainty. In short, aleatory uncertainty can be defined as variability and epistemic uncertainty can be defined as ignorance (Ferson *et al.* 1996). Increasing knowledge will reduce epistemic uncertainty whereas aleatory uncertainty is an irreducible scatter of a variable (Donders *et al.* 2005). Further clarification is provided below.

3.1.1 Aleatory uncertainty

The word aleatory is derived from the Latin word for dice and it means "depending on chance" (Oxford 1996). Aleatory uncertainty describes those uncertainties that are random in nature and can be characterized by probability distributions. It describes the inherent variability associated with a physical system or environment (Oberkampf 2005). For this reason, aleatory uncertainty is also referred to as irreducible uncertainty or stochastic uncertainty. For example, the variability in the measured lengths of a structural member in a bridge, or the variability of the compressive strength of a number of concrete samples from the same batch all constitute aleatory uncertainty.

3.1.2 Epistemic uncertainty

The word epistemic is derived from the Greek word for knowledge and it means "relating to the philosophy of knowledge" (Oxford 1996). Epistemic uncertainty describes those uncertainties that stem from a lack of knowledge of quantities or processes of a system (Oberkampf 2005). Typical examples of epistemic uncertainty include lack of understanding or lack of data describing physical phenomena and lack of knowledge of support conditions of a structure. This type of uncertainty often arises in the development of models describing or governing physical systems. Parameter uncertainties with variability are basically aleatory uncertainties, but they may be treated as epistemic uncertainties when insufficient data is available to describe the distribution of the data (Bae 2004). Epistemic uncertainty is also referred to as model-form uncertainty, subjective uncertainty or reducible uncertainty (Oberkampf 2005). The bias, or systematic error in a measurement is an example of epistemic uncertainty, if the true value of the measurement is not known.

3.2 Sources of uncertainty in typical vibration tests

Uncertainty analysis in damage detection procedures involves identifying and quantifying error from all possible sources, then accounting for the effect of this error in the final outputs of the algorithms. In developing an error model for vibration data, the following possible sources of error have been identified.

3.2.1 Instrumentation errors

Errors result from the inherent imperfection in instruments such as computers, signal conditioners, sensors, and cables. These are explained below in more detail.

Quantization errors in the data acquisition card: Analogue-to-Digital Converters (ADCs) transform an analogue voltage to a binary number (a series of 1's and 0's), and then eventually to a digital number (base 10) for reading on a meter, monitor, or chart. The number of binary digits (bits) that represent the digital number determines the ADC resolution. However, the digital number is only an approximation of the true value of the analogue voltage at a particular instant because the voltage can only be represented (digitally) in discrete steps. How closely the digital number approximates the analogue value also depends on the ADC resolution.

Errors inherent in the sensors: Casing mounted transducers, such as velocity coils or accelerometers are subject to signal error sources in the form of cross axis vibrations. Improper mountings will exacerbate these errors. In addition, random errors such as electrical line noise are introduced while the signal is transmitted through connecting cables.

Sensor resolution errors: Sensor resolution error refers to the smallest value of the measurand that the sensor can detect. As a result of this error, values containing fractions smaller than the sensor resolution are rounded to the nearest value compatible with the sensor's measuring capabilities.

Sensor placement: some tests may require that a sensor be placed at a particular location on the structure. It is impossible to obtain exact sensor placement and errors occur.

3.2.2 Errors due to changing environmental and operational conditions

Environmental conditions such as temperature, pressure, and humidity or operational conditions such as wind, precipitation, and loads due to traffic may fluctuate during a test session, or they may be different from test session to test session. This can lead to random

fluctuations in instrument accuracy. Furthermore, changing environmental and operational conditions may have an effect on the test structure itself. This is particularly problematic when vibration data is collected for the purposes of damage detection. For example, after rain, the amount of water on a structure may influence its vibration response. It becomes unclear whether changes in the vibration response are due to damage in the structure or changing environmental conditions.

3.2.3 Miscellaneous errors

Aliasing: This occurs when the sampling rate is less than twice the highest frequency component in the continuous signal being recorded. Figure 3.1 shows how aliasing can result from not sampling at a rate that characterizes the signal sufficiently.

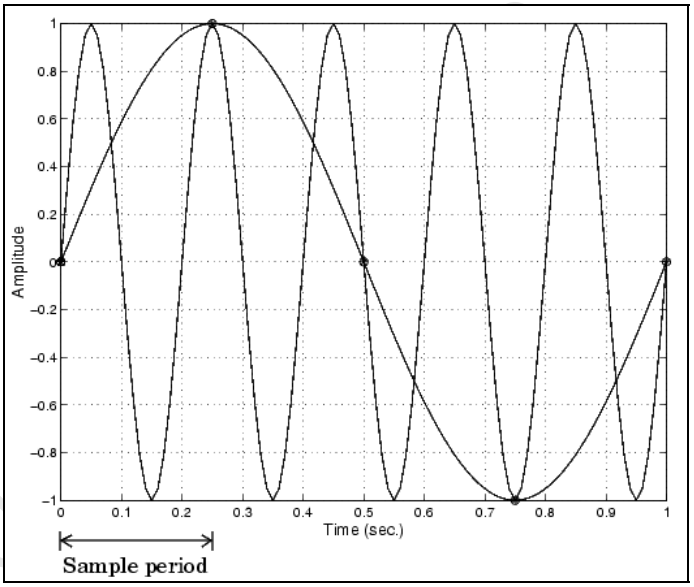

Figure 3.1: The danger of aliasing. A 1Hz sine wave cannot be distinguished from a 5Hz sine wave if the sampling interval is less than 10Hz. (The Mathworks)

Human error: Manual methods of excitation such as drop hammers introduce variability into vibration tests. Drop hammers must come into flush contact with a surface for accurate measurement of the resulting input force. Human fallibility prevents consistency in this regard.

3.3 Uncertainty Quantification and Propagation Techniques

Uncertainty *quantification* can be defined as the process of assigning a quantitative measure of the degree of confidence that the reported value of a variable represents its "true" value. For quantitative data, an interval on which the true value must lie is often used to indicate the uncertainty in a variable. An accompanying measure of the confidence that the variable lies on that interval may also be reported.

Uncertainty *propagation* is the process of quantifying the uncertainty in a variable that results from a model-based calculation or a combination of measurements. It involves determining how the uncertainty in the input variables leads to uncertainty in the output. For example, given a set of uncertain inputs, $\mathbf{X}=[x_1, x_2 \ldots x_n]$ where each input may follow a different probability distribution, calculations involving these inputs will result in an uncertain output *y*. i.e:

$$y = f(\mathbf{X}) \qquad 3.1$$

where *f* represents a function used to model the physical quantity *y*. The main aim of uncertainty propagation is to quantify the uncertainty in the output and therefore, as described above, it aims to determine one, or both, of two things:

- The range of values that the "true" value of the output *y* can assume: This is often termed "the interval on which the true value of *y* exists".
- The probability distribution of the output *y*: This can be either in the form of a cumulative distribution function (CDF) or in a probability density function (PDF). Having determined the distribution of the output, it can be said, with a quantitative level of confidence (a probability, or a possibility), that the true value of *y* lies on a particular interval. In other words, "confidence intervals" for the output can be calculated.

The most common approaches to uncertainty quantification and propagation revolve around probability theory. The classical definition of probability is the ratio of the number of favourable cases of an event to the number of possible cases. Another

definition adopts the frequentist approach and defines probability as the limits of frequencies of observed events. While probability theory is suited for dealing with random variability, epistemic uncertainty should not be modelled in a probabilistic manner because there is not enough information available. Assigning a probability density function to epistemic variables changes the problem definition in a subjective way (Donders *et al.* 2005). For example, in the case of total ignorance about a variable, one is not capable of identifying all possible events, and therefore it does not make sense that the measure of uncertainty attributed to the events should depend on the number of alternative events (Dubois *et al.* 1988). Possibility theory deals with epistemic uncertainty by interpreting uncertainty in terms of more or less possible events, and more or less certain events. It provides a framework that describes the uncertainty of an event both by the degree of possibility of the event itself and by the degree of possibility of the contrary event (Dubois *et al.* 1988).

Some authors have proposed approaches to dealing with specific uncertainties associated with non-model-based damage detection techniques. For example, Taha *et al.* (2005) proposed a fuzzy pattern-recognition approach to quantify the uncertainty due to ambiguous levels of damage. They pointed out that damage cannot be classified as a random process because the frequency of occurrence of a healthy state in a database is not constant from one set of observations to another. Therefore they used fuzzy sets to depict the progressive nature of damage. Some authors have identified damage detection algorithms that are *insensitive* to changing operational and environmental conditions. Vanlanduit *et al.* (2004) showed that a singular value decomposition of features extracted from the vibration data from aluminium beams was able to detect damage under changing operational conditions. They also explained that, in general, techniques employing matrix decomposition (e.g. singular value decompositions and principal component analysis) of damage-sensitive features are insensitive to changing operational conditions because effects such as environmental conditions influence the structure on a global level, whereas damage causes a localized effect such as a local reduction in stiffness near the location of the damage. This results in features from the damaged structure being outliers with respect to features from the undamaged structure (Vanlanduit *et al.* 2004: Worden *et al.* 2000, Kullaa *et al.* 2002). Peeters *et al.* (2001) proposed performing a correlation

between the measured vibration characteristics and the corresponding environmental conditions in order to parameterize the reference state of the structure to reflect the different environmental and operational conditions. Yan *et al.* (2005) point out that the method proposed by Peeters *et al.* (2001) lacks practicality due to problems surrounding measurement of environmental conditions for large or complex structures. However, each damage detection problem is different and the approach adopted may be more applicable to one structure than to another. In cases where the measurement of environmental conditions is not practical, an alternative approach must be developed.

Some uncertainty quantification and propagation techniques are described here. The choice of the technique to adopt depends on the nature of the problem and the resources available to the analyst (Morgan *et al.* 2004). Since the approach to damage detection adopted in this study is non-model-based, the uncertainty quantification and propagation techniques described here are based on probability theory. Probability theory also has the advantage of being less complex than possibility-based approaches such as Dempster-Shafer theory and fuzzy arithmetic.

There is a dearth of information on the performance of damage detection techniques in the presence of uncertainty. Ideally, the diagnosis from the application of a damage detection algorithm should be accompanied by a measure of certainty in the diagnosis, given the errors involved in the computations of the algorithm. The remainder of this document aims to review and summarise uncertainty quantification and propagation techniques. This will identify tools available for the development of a framework for incorporating uncertainty quantification in damage detection techniques.

3.3.1 Uncertainty propagation based on interval-based computations

The aim of interval based computations for uncertainty propagation is to determine the range of *mathematically* possible values that the output of a calculation model or algorithm can assume. Manufacturers of measuring instruments provide an upper bound on the error associated with measurements taken by instruments. Consider a measurement x. The manufacturer of the measuring instrument may state that the upper bound on the measurement error is Δx. This means that the true value of x, call it z, lies on the interval [x-Δx , x+Δx]. This interval can be expressed as $[x_L , x_U]$. Therefore

$$x_L = x - \Delta x \tag{3.2}$$

$$x_U = x + \Delta x \tag{3.3}$$

$$z : [x_L , x_U] \tag{3.4}$$

Suppose the measurement is required as an input in a mathematical model

$$y = f(x) \tag{3.5}$$

If no probabilistic information for the measurement error Δx is provided, the maximum and minimum values of the input x are combined so as to determine the resulting interval $[y_L , y_U]$ on which the output y is expected to lie. The arithmetic required to achieve this is described below with the aid of some examples.

Given two uncertain variables a and b whose true values lie on the intervals $[a_L , a_U]$ and $[b_L , b_U]$ respectively, the following interval arithmetic holds true (Berleant *et al.* 2005)

$$[a_L , a_U] + [b_L , b_U] = [a_L + b_L , a_U + b_U] \tag{3.6}$$

$$[a_L, a_U] - [b_L, b_U] = [a_L - b_U, a_U - b_L] \quad 3.7$$

$$[a_L, a_U] \times [b_L, b_U] = [\min(a_L \cdot b_L, a_L \cdot b_U, a_U \cdot b_U, a_U \cdot b_L), \max(a_L \cdot b_L, a_L \cdot b_U, a_U \cdot b_U, a_U \cdot b_L)] \quad 3.8$$

So, for the function y = $f(a,b)$, the relevant interval computations form the program

$$[y_L, y_U] = f([a_L, a_U], [b_L, b_U]) \quad 3.9$$

The main drawback of interval based computations is that they rapidly become computationally expensive with increasing complexity of the model through which the uncertainty is being propagated. For polynomial functions, the problem of computing the exact range for the output is computationally impractical (Berleant *et al.* 2005).

3.3.2 Analytical methods of uncertainty propagation

These uncertainty propagation techniques generally require a closed form solution for the model through which the uncertainty is to be propagated.

3.3.2.1 Uncertainty propagation based on the method of moments (the perturbation method)

The aim of the perturbation method is to estimate the parameters of the probability distribution of the output of a model-based on the known uncertainties of the input variables. The probability distribution of the output is assumed to be Gaussian, and therefore the required parameters are the mean and variance. The perturbation method is derived from the sensitivity of the output variable to the inputs.

A measure of how each input contributes to the uncertainty of the output variable can be termed a measure of uncertainty importance (Morgan *et al.* 2005). One example of a measure of uncertainty importance is sensitivity. Sensitivity, in this case, is the change induced in the output by a unit change in the input. Graphically, this is simply the gradient of the response surface in the plane formed by the input and the output. The response surface is the surface formed by plotting the input-output relationship. A single input will result in a response curve. Given an uncertain input *x*, and a functional model

$$y = f(x) \tag{3.10}$$

the sensitivity of output y to input x is denoted $U_s(x, y)$. So, for a model involving n inputs, the sensitivity of the output to the i^{th} input is given by

$$U_s(x_i, y) = \frac{\partial y}{\partial x_i} \quad (i = 1, 2, \ldots, n) \tag{3.11}$$

This is evaluated at the point on the curve corresponding to the nominal values of the inputs (i.e. the best guess or measured values for the inputs).

If the degree of uncertainty in each input x_i can be expressed as its standard deviation σ_{x_i} (i.e. if the probability distribution of the inputs can be assumed to be Gaussian) then a measure of uncertainty importance, which also takes into account the degree of uncertainty in each input, is found by multiplying the sensitivity by the standard deviation of the input. Termed the Gaussian approximation, this is expressed as follows (Morgan *et al.* 2005).

$$U_G(x_i, y) = \left[\frac{\partial y}{\partial x_i}\right]\sigma_{x_i} \quad (i = 1, 2, \ldots, n) \tag{3.12}$$

The value $U_G(x_i, y)$ is the contribution of the input, x_i, to the total uncertainty in the output σ_y. This can be used to estimate the variance in the output as follows:

$$\sigma_y \approx U_G(x_i, y) = \left[\frac{\partial y}{\partial x_i}\right]\sigma_{x_i} \quad (i = 1, 2, \ldots, n) \tag{3.13}$$

$$\mathrm{var}(y) = \sigma_y^{\,2} \tag{3.14}$$

$$\therefore \text{var}(y) \approx \sum_{i=1}^{n}\left[\frac{\partial \text{y}}{\partial x_i}\right]^2 \sigma_{x_i}{}^2 \qquad 3.15$$

This approximation follows more generally from the Taylor series expansion for expressing deviations of an output from its nominal value as a function of deviations of the inputs from their respective nominal values. If the nominal values of the inputs are x_i^o and the resulting nominal output is y^o then (Morgan *et al.* 2005: Korn *et al.* 1968)

$$y\text{-}y^o = \sum_{i=1}^{\text{n}}(x_i - x_i{}^0)\left[\frac{\partial y}{\partial x_i}\right] + \frac{1}{2!}\sum_{i=1}^{n}\sum_{j=1}^{n}(x_i - x_i{}^0)(x_j - x_j{}^0)\left[\frac{\partial^2 y}{\partial x_i \partial x_j}\right] + \ldots \qquad 3.16$$

Higher order terms of this expansion approach zero if the deviations are small. It may even be sufficient in some cases to use only the first term. Furthermore, the variance of a set of variables is equivalent to the expectation of the square of their deviations from their nominal values. So that

$$\text{var}(y) = \text{E}\left[(y - y^0)^2\right] \qquad 3.17$$

$$\therefore \text{var}(y) \approx \text{E}\left[\left(\sum_{i=1}^{n}(x_i\text{-}x_i{}^0)\left[\frac{\partial y}{\partial x_i}\right]\right)^2\right] \qquad 3.18$$

and because $\text{E}[(x_i - x_i{}^o)(x_j - x_j{}^o)]$ is equivalent to the covariance:

$\text{covar}(x_i, x_j) = \text{covar}(x_j, \text{x}_\text{i})$,

the expression simplifies to:

$$\text{var}(y) \approx \sum_{i=1}^{n}\text{var}(x_i)\left[\frac{\partial y}{\partial x_i}\right]^2 + 2\sum_{i=1}^{n}\sum_{j=\text{i}+1}^{n}\text{covar}(x_i, x_j)\left[\frac{\partial y}{\partial x_i}\frac{\partial y}{\partial x_j}\right] \qquad 3.19$$

For independent inputs, $\text{covar}(x_i, \text{x}_\text{j}) = 0$ and the expression reduces to the Gaussian approximation in equation 3.15

The mean of the output distribution can be estimated by

$$\mu_y \approx y^0 + \sum_{i=1}^{n} \frac{\partial y}{\partial x_i}(\mu_x - x_i^0) \qquad 3.20$$

The partial derivatives of the model can be approximated as follows (Morgan *et al.* 2005)

$$\frac{\partial y}{\partial x_i} \approx \frac{f(x_i^0 + \Delta x_i) - f(x_i^0)}{\Delta x_i} \qquad 3.21$$

where Δx_i is a small perturbation in x_i.

The perturbation method of uncertainty propagation is useful if a closed form mathematical expression exists to model the output and if the model has a smooth, continuous response surface (Berleant *et al.* 2005). For simple models, it provides a relatively straightforward method of uncertainty propagation. Based on the assumed Gaussian distribution, confidence intervals can be determined for the output.

So far the method has assumed that the inputs x_i are normally distributed. Nevertheless, this incurs no loss in generality since random variables may be transformed into uncorrelated Gaussian variables exactly using the Rosenblatt transformation, or approximately using the Nataf transformation (Fonsesca *et al.* 2005: Worden *et al.* 2005, Melchers 1999).

The major drawbacks of the method are that it loses accuracy when the uncertainties are large or if the response surface of the model is not continuous (Morgan *et al.* 2005). Furthermore it assumes that the output is normally distributed. Many situations in reality result in non-Gaussian outputs.

Applicability of the perturbation method to structural health monitoring depends on the mathematical complexity of the damage detection algorithms involved. The method may be useful if the damage detection algorithms can be broken up into one or more closed form equations.

3.3.2.2 Uncertainty propagation using the first order reliability method

The aim of the first order reliability method is to obtain the probability distribution of the output of a mathematical model, given that the joint probability distribution of the uncertain inputs to the model is known. Continuing with the adopted notation, the uncertainty propagation problem is set in the following scenario; the model $y = f(\mathbf{X})$ is to be computed, where $\mathbf{X} = [x_1,...,x_n]$ are the uncertain inputs to the model and y is the uncertain output. The cumulative distribution function (CDF), $F(y_o)$, is to be estimated, where:

$$F(y_0) = P(y < y_0) \tag{3.22}$$

for all y_0 in the domain of y. This CDF is computed as follows:

$$F(y_0) = \int ... \int_{f(\mathbf{X})<y_0} p(x_1,...,x_n)dx_1,...,dx_n \tag{3.23}$$

where $p(x_1,...,x_n)$ is the joint probability density function of the input variables. For example, in the case of two input variables

$$F(y_0) = \int_{f(\mathbf{X})<y_o} \int_{f(\mathbf{X})<y_0} p(x_1,x_2)dx_1dx_2 \tag{3.24}$$

The geometric representation of these integral expression for $F(y_o)$ is the volume under the joint distribution function bounded by the limit surface $q(\mathbf{X}) = 0$, where

$$q(\mathbf{X}) = f(\mathbf{X}) - y_o \tag{3.25}$$

(Worden *et al.* 2005). Returning to the more general case of n input variables, for most practical cases solving the integral analytically is almost impossible, firstly, because of the complexity of the joint probability density function and, secondly, because of the complexity of the limit surface $q(\mathbf{X})$. The first order reliability method contains two steps that aim to solve this problem (Worden *et al.* 2005, Melchers 1999).

To simplify the integrand, the joint probability density function is replaced by a joint independent Gaussian distribution. This is achieved by using a nonlinear transformation to transform the input vector $\mathbf{X} = [x_1,...,x_n]$ to a vector of independent Gaussian variables $\mathbf{V} = [v_1,,v_n]$. Either the Rosenblatt transform or the Nataf transform may be used (Fonsesca *et al.* 2005, Worden *et al.* 2005, Melchers 1999). The required integral then becomes

$$F(y_0) = \int ... \int_{g(\mathbf{V})<0} p(v_1,...,v_n) dv_1,...,dv_n \qquad 3.26$$

where $q(\mathbf{V}) = f(\mathbf{V}) - y_0$

The advantage of the variables **V** being independent comes from the fact that the joint distribution of independent random variables is simply the product of the individual probability distribution functions of the random variables (Nathabandu *et al.* 1998). i.e.

$$p(v_1,...,v_n) = p(v_1)p(v_2)...p(v_n) \qquad 3.27$$

thus simplifying the integrand in equation 3.26

In order to simplify the domain of the integral in equation 3.26, the limit surface $q(\mathbf{V})$ is approximated by a hyperplane $h(\mathbf{V})$ using a first order Taylor approximation about the point on the true limit surface which is closest to the origin (Worden *et al.* 2005). The distance between this point and the origin is of importance and is assigned the symbol β. The required integral then becomes

$$F(y_0) = \int ... \int_{h(\mathbf{V})<0} p(v_1) p(v_2)...p(v_n) dv_1 dv_2 ..., dv_n \qquad 3.28$$

where $q(\mathbf{V})$ has been transformed to the plain

$$h(V) = a_1 v_1 + ... + a_n v_n + a_o = 0 \qquad 3.29$$

using a Taylor approximation. The solution to this integral is simply $\Phi(-\beta)$, where Φ is the standard normal cumulative distribution function (Worden *et al.* 2005, Melchers 1999).

3.3.3 Uncertainty propagation based on the Monte Carlo method

The most widely used of the numerical sampling techniques for uncertainty propagation is the method of Monte Carlo simulations. This involves generating random samples of the input variables based on their known probability distributions. The calculation through which the uncertainty is being propagated is conducted for each set of inputs to provide a corresponding output. The process is conducted several times, generating several realizations of the inputs and several corresponding outputs. If a sufficient number of outputs is generated in this way, the probability distribution of the output can be estimated. Increasing the number of numerical simulations (i.e. increasing the number of outcomes of the output) increases the accuracy of the estimated probability distribution. The Monte Carlo method for uncertainty propagation can be summarised as follows:

Given a model $y = f(\mathbf{X})$, where the inputs $\mathbf{X} = [x_1, ..., x_2]$ are a set of random variables, the probability distribution p(y) can be estimated if the individual probability distributions $p(x_i)$ and the joint probability distribution $p(\mathbf{X})$ are known. This is achieved by generating n possible outcomes of the inputs $\mathbf{X}$ based on their individual and joint probability distributions, and thus generating n possible outcomes of the output y. According to the Central Limit Theorem, the probability distribution of the numerically generated outputs will approach $p(y)$ for large n. A simple example is described below (Regan *et al.* 2006).

Given two uncertain inputs x_1 and x_2 with known cumulative distribution functions F_1 and F_2 respectively, the values U_1 and U_2 are the probabilities of not exceeding a particular value of x_1 and x_2 respectively. Therefore:

$$F_1(x_1) = U_1 \qquad 3.30$$

$$F_2(x_2) = U_2 \qquad 3.31$$

In other words, $F_1^{-1}(U_1)$ is the value which is not exceeded by the random variable x_1, $100U_1$ % of the time. Similarly, $F_2^{-1}(U_2)$ is the value which is not exceeded by the random variable x_2, $100U_2$ % of the time. This is explained graphically in Figure 3.2.

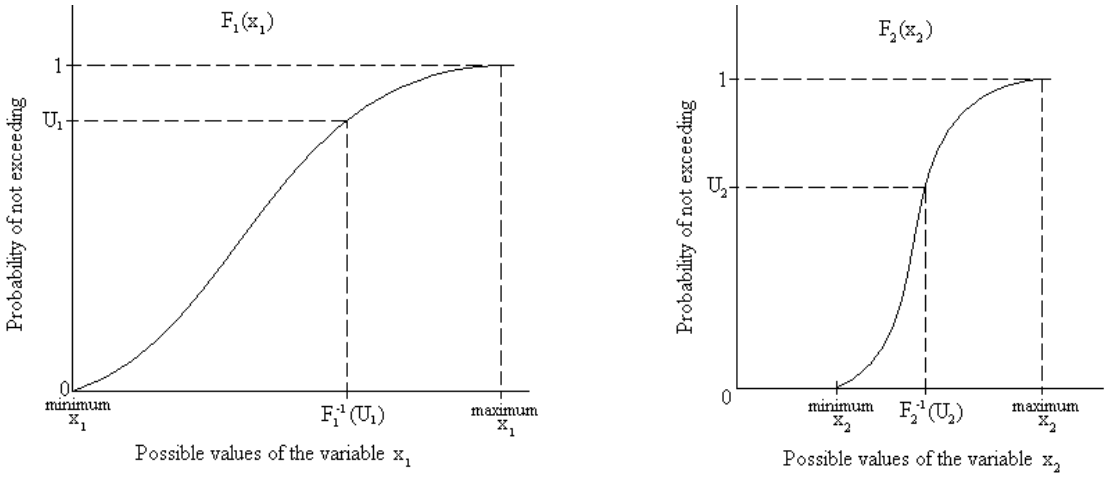

Figure 3.2: Hypothetical examples of the cumulative distribution functions of two variables x_1 and x_2.

For the calculation:

$$y = f(\mathbf{X}) = f(x_1, x_2) \tag{3.32}$$

the probability distribution of y is determined by randomly generating several pairs of the uncertain inputs x_1 and x_2 then conducting the calculation in equation 3.32. In other words, a single simulation involves generating the pair $\left(F_1^{-1}(U_1), F_2^{-1}(U_2)\right)$ and then performing the calculation:

$$y = f\left(F_1^{-1}(U_1), F_2^{-1}(U_2)\right) \tag{3.33}$$

There are certain constraints to the use of Monte Carlo simulations for uncertainty propagation (Regan *et al.* 2006). In the description above, the random inputs **X** are assumed to be independent. If the dependency of the inputs **X** is known, the sampling method must be adjusted to ensure that each set of inputs **X** generated always exhibits the same dependency.

Two simple scenarios for the dependency of the uncertain inputs are; if they are perfectly positively correlated or if they are perfectly negatively correlated. Perfect positive correlation is the case where the correlation coefficient is 1 and if one variable is large relative to its full range then the other variable will also be large relative to its full range. Perfect negative correlation is the case where the correlation coefficient is -1 and if one variable is large relative to its full range the other variable will be small relative to its full range (Regan *et al.* 2006). If x_1 and x_2 are perfectly positively correlated, then the pairs of the uncertain inputs must always be generated such that $U_1=U_2$. Similarly, if x_1 and x_2 are perfectly negatively correlated, then the pairs of uncertain inputs must always be generated such that $U_1=1-U_2$. Other degrees of correlations between the inputs can also be accommodated by Monte Carlo simulations.

On the other hand, if the dependency of the random inputs **X** is unknown, then the simulations may produce misleading results for the probability distribution of the uncertain output *y*.

3.3.4 The maximum likelihood method

The maximum likelihood method is not, in itself, an uncertainty propagation technique. The method is used to determine the most likely parameters, $\boldsymbol{\theta}$, of a probability distribution given a set of measured data from a population of a random variable. For a multivariate normal distribution, $\boldsymbol{\theta}=[\boldsymbol{\mu},\boldsymbol{\Sigma}]$, where $\boldsymbol{\mu}$ is the mean vector and $\boldsymbol{\Sigma}$ is the covariance matrix. For example, given a set of measurements of the uncertain inputs $\mathbf{X}=[\boldsymbol{x}_1,...,\boldsymbol{x}_n]$ where $\boldsymbol{x_i}$ is a column of *m* measurements of the input variable x_i, the likelihood of the measurement $L(\boldsymbol{\theta}_x)$ is determined as follows (Fonseca *et al.* 2005).

$$L(\boldsymbol{\theta}_x) = p(x_1,...,x_n|\boldsymbol{\theta}_x) \qquad 3.34$$

where *p* denotes a probability density function. The maximum likelihood estimator for $\boldsymbol{\theta}_x$ is the value of $\boldsymbol{\theta}_x=[\boldsymbol{\mu}_x,\boldsymbol{\Sigma}_x]$ for which $L(\theta_x)$ attains a maximum. Conventional uncertainty propagation techniques such as the Monte Carlo method can then be used to determine

the probability distribution of an output based on the probability distribution of the inputs.

Fonseca *et al.* (2005) employ the maximum likelihood method for what they termed *uncertainty identification*. Uncertainty identification was described as the inverse uncertainty propagation problem where, given a set of direct measurements of a response, the probability distributions of the parameters governing the response was sought. In other words uncertainty propagation was required for the inverse model,

$$\mathbf{X} = f^{-1}(y) \tag{3.35}$$

In this way, the probability distributions of parameters of interest, such as the stiffness of a structure, can be determined. This is particularly useful in the case of model-based damage detection techniques. The probability distributions of the input parameters can also be used for uncertainty propagation in cases where the output cannot be measured directly. However, the problem is far from trivial. Fonseca *et al.* (2005) pointed out that applying the conventional uncertainty propagation techniques directly to equation 3.35 is in most cases impossible because the function *f* may not be invertible. Instead, they proposed the following approach.

For a set of *n* independent measurements of the uncertain responses $\mathbf{Y} = [\boldsymbol{y}_1,...,\boldsymbol{y}_n]$, where $\boldsymbol{y}_i$ is a column of *m* measurements of the response y_i, the measurement likelihood is determined as follows.

$$L(\boldsymbol{\theta}_x) = p(y_1,...y_n \,|\, \boldsymbol{\theta}_x) = \prod_{i=1}^{n} p(y_i \,|\, \boldsymbol{\theta}_x) \tag{3.36}$$

This is an iterative process whereby a value of $\boldsymbol{\theta}_x$ is chosen and $p(y_i \,|\, \boldsymbol{\theta}_x)$ is estimated using conventional uncertainty propagation techniques like FORM and the perturbation method. The maximum likelihood estimator is the value of $\boldsymbol{\theta}_x$ that maximises $L(\boldsymbol{\theta}_x)$.

The drawback of the maximum likelihood method, when applied to uncertainty quantification and propagation is the fact that a particular parametric family of probability distributions (e.g. normal distribution, Weibull distribution etc) to which the variable belongs must be assumed. This lack of generality results in inaccuracies in cases where the probability distribution of the variable is in fact non-parametric.

3.4 Applicability of uncertainty quantification and propagation techniques to the damage detection techniques

Non-model-based damage detection techniques generally require fewer measured inputs for their algorithms than model-based techniques. Model-based damage detection techniques require the measurement or estimation of several parameters such as material properties, dimensions and masses. Non-model-based techniques, on the other hand, often only require the measurement of vibration signals, in which case the measurement uncertainty lies in the amplitudes of the samples. Each sampled point on the vibration signal could be considered as an uncertain variable. However, for interval-based computations and analytical methods such as the perturbation method and the first order reliability method, this leads to an impractical number of error terms. Interval based uncertainty propagation techniques suffer the added disadvantage of providing no information about the probability distribution of the output variable, only providing an interval on which the true value of the output variable is expected to occur. As a result, confidence intervals cannot be determined and there is insufficient information for risk assessment and objective decision making (Castrup 1992).

Numerical sampling methods such as the Monte Carlo method can provide relatively straightforward uncertainty propagation. Unlike analytical methods like the first order reliability method and the perturbation method, the Monte Carlo method can be used even when a closed-form mathematical model for the output is not available. The lack of closed form mathematical models is evident in many non-model-based damage detection techniques. For example, there is no closed form solution for the calculation of the coefficients of an autoregressive time-series model (Section 2.1). Monte Carlo

simulations are therefore an attractive option for the propagation of uncertainty through non-model-based vibration-based damage detection techniques.

In the next chapter, statistical models for feature discrimination will be developed incorporating Monte Carlo simulations for uncertainty quantification.

3.5 Summary

The following constitute the main points of the chapter:

- Error is inherent in all measurements and leads to uncertainty in the outputs of algorithms with measured inputs.
- Uncertainty can be categorized into aleatory (random) uncertainty and epistemic (reducible) uncertainty.
- Typical sources of uncertainty include instrumentation errors, errors due to changing environmental and operational conditions and miscellaneous errors such as the variability brought about by human operators on equipment.
- The presence of errors leads to uncertainty in the diagnoses of damage detection techniques in structural health monitoring. Uncertainty propagation techniques can be used to quantify the confidence in the outputs of a damage detection algorithm.
- Typical uncertainty propagation techniques include interval-based techniques, analytical techniques such as the method of moments and the first order reliability method, the Monte Carlo method and the maximum likelihood method.
- Numerical sampling methods such as the Monte Carlo method can provide relatively straightforward uncertainty propagation even in the absence of a closed-form mathematical model for the output of an algorithm. Of the uncertainty propagation techniques reviewed, the Monte Carlo method is therefore the most readily applicable technique to uncertainty quantification in non-model-based vibration-based damage detection algorithms.

Chapter 4

4 Statistical model development for feature discrimination

Damage detection using pattern recognition relies on the identification of statistical patterns or statistical variables that can be related to the state of damage of a structure. As mentioned in Chapter 1, such patterns or variables are referred to as damage-sensitive features. Any statistically significant changes in damage-sensitive features imply that a change has occurred in structural condition, and is likely to be caused by damage. Therefore, once damage-sensitive features have been identified for structural health monitoring, a structured decision making process must be conducted to objectively establish whether changes detected in the damage-sensitive features are significant enough to diagnose the structure as damaged. The process of recognizing these changes and assessing their statistical significance requires the development of statistical models. This process constitutes the fourth step of the statistical pattern recognition approach to damage detection (Section 1.3). The development of a statistical model that discriminates between structural states, based on the significance of the changes in damage-sensitive features, is what qualifies the use of the term "*statistical* pattern recognition".

These statistical models fall into two main categories, namely supervised learning and unsupervised learning. Unsupervised learning refers to statistical models that are applied to situations in which examples of data representing the damaged structure are not available. Supervised learning refers to statistical models that are applied to situations in which examples of data representing the damaged structure are available. Unsupervised learning models are limited to damage detection, but supervised learning models may also be capable of identification, estimation, and prognosis (Sohn *et al.* 2003). Since this study is limited to the first level of structural state characterization, namely damage detection, only unsupervised learning models will be considered here. Examples of such models include statistical process control, outlier analysis and probability density approaches.

Since the application of the damage detection techniques to civil infrastructure is being investigated, and in particular, their application to the detection of a form of damage as subtle as early-stage steel reinforcement corrosion, it is important that the uncertainties associated with vibration testing of civil infrastructure be considered in the damage detection algorithms. Due to the subtlety of the form of damage to be detected, there is a danger that changes in the damage-sensitive features due to the onset or advancement of damage will be masked by changes due to environmental and operational conditions as well as the effects of measurement uncertainty. Therefore the statistical models for feature discrimination have been combined with uncertainty quantification techniques, selected from those described in Chapter 3.3, to develop frameworks for the application of damage detection algorithms in the presence of uncertainties. A Monte Carlo based uncertainty quantification technique (Section 3.3.4) was adopted. The proposed framework for damage detection is summarized in Figure 4.1.

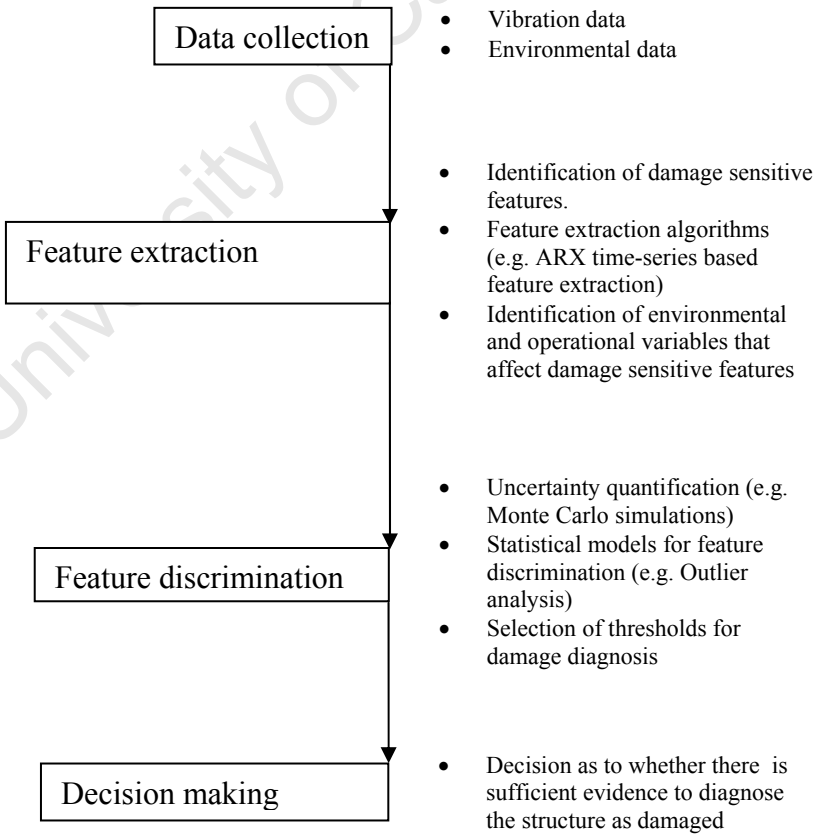

Figure 4.1: Damage detection framework

4.1 The choice of the threshold for damage discrimination

Adopting terminology from classical statistics, the aim of damage detection using statistical pattern recognition is to identify whether there is sufficient evidence to reject the hypothesis that a structure is undamaged. The hypothesis that the structure is undamaged is termed the null hypothesis (H_o). The alternative or research hypothesis (H_1) is the hypothesis that states that the structure is damaged. Applying this convention, the feature discrimination problem can be defined as:

$$\begin{aligned} H_o &: DSF_\zeta = D_t \\ H_1 &: DSF_\zeta > D_t \end{aligned} \qquad 4.1$$

where DSF_ζ is a damage-sensitive feature from a structure in an unknown structural state and D_t is a threshold value such that values of DSF_ζ above the threshold represent a damaged structure.

The significance level (p) of the threshold is the probability that the damage-sensitive feature from an undamaged structure would, by chance, exceed the threshold value, leading to the rejection of the null hypothesis. In other words, the significance level is equal to the probability of a false-positive diagnosis of damage. Therefore, increasing the significance level of the threshold increases the chances of false-positive diagnoses and, conversely, reducing the significance level of the threshold increases the chances of false-negative diagnoses. For this reason, the choice of threshold in a feature discrimination model is equally as important as the choice of damage-sensitive features to extract. Significance levels of the threshold must be chosen according to the relative consequences of either false-positive or false-negative diagnoses of damage (Keller *et al.* 2000). For example, if damage undetected could result in the loss of life, the engineer would rather err on the side of caution and choose a threshold with a high significance level. In other words, false-positive diagnoses would be preferred to false-negative diagnoses.

4.2 Feature discrimination based on probability densities

This framework for the application of non-model-based damage detection techniques is based on the following hypothesis. Given two damage states of a structure, a reference (known) state and a new (potentially damaged) state, the vibration data from the new state is directly comparable to the vibration data from the reference state, if data from both states were collected under similar environmental conditions. In such a case, effects of the environmental and operational conditions on damage-sensitive features need not be quantified. It can be assumed that any changes in the vibration data are as a result of a change in structural condition. Only probabilistic uncertainty due to instrumentation errors needs to be considered. Application of this approach requires the measurement of the environmental and operational conditions under which all data is collected. The framework can be cast symbolically as follows.

Given a combination of environmental and operational conditions, i, the vibration data collected from the reference state under conditions i is assigned $\mathbf{X}_o^i$ and the vibration data collected from the new state under conditions i is assigned $\mathbf{X}_\zeta^i$, then

$$\mathbf{X}_o^i \xleftrightarrow[\text{of features}]{\text{Direct comparison}} \mathbf{X}_\zeta^i$$

Before application of the damage detection algorithm, $g(\mathbf{X})$, to compute the damage indicator for the reference state and the damage indicator for the new state of the structure, Monte Carlo simulations, based on the probability distribution of the instrumentation errors, $f(\mathrm{e})$, must be conducted. In other words, if the errors in the reference signal are the vector $\boldsymbol{e}_o$ and the errors in the new signal are the vector $\boldsymbol{e}_\zeta$, then

$$\hat{\boldsymbol{X}}_o^i = \boldsymbol{X}_o^i - \boldsymbol{e}_o \tag{4.2}$$

$$\hat{\boldsymbol{X}}_\zeta^i = \boldsymbol{X}_\zeta^i - \boldsymbol{e}_\zeta \tag{4.3}$$

where $\hat{\boldsymbol{X}}_o^i$ and $\hat{\boldsymbol{X}}_\zeta^i$ are possible outcomes of the "true" reference data and the "true" new data respectively. In other words, the two vibration signals are corrected for measurement

errors. Randomly generating several possible pairs $(\boldsymbol{e}_o, \boldsymbol{e}_\zeta)$ leads to several possible pairs $(\hat{\boldsymbol{X}}_o^{\,i}, \hat{\boldsymbol{X}}_\zeta^{\,i})$. As a result, several possible pairs of damage-sensitive features (DSF_o, DSF_ζ) can be output from the damage detection algorithm where

$$g(\hat{\boldsymbol{X}}_o^{\,i}) = DSF_o \tag{4.4}$$

$$g(\hat{\boldsymbol{X}}_\zeta^{\,i}) = DSF_\zeta \tag{4.5}$$

If a sufficiently large number of DSF_o and DSF_ζ are generated, the sampled probability distributions $f_o(DSF_o)$ and $f_\zeta(DSF_\zeta)$ can be estimated. If a (100P) % confidence level is required, the lower and upper limits, *L* and *U*, can be computed by solving the following (Castrup 1992):

$$\int_{-\infty}^{L} f(DSF)\, d(DSF) = \frac{1-\mathrm{P}}{2} \tag{4.6}$$

$$\int_{U}^{\infty} f(DSF)\, d(DSF) = \frac{1-\mathrm{P}}{2} \tag{4.7}$$

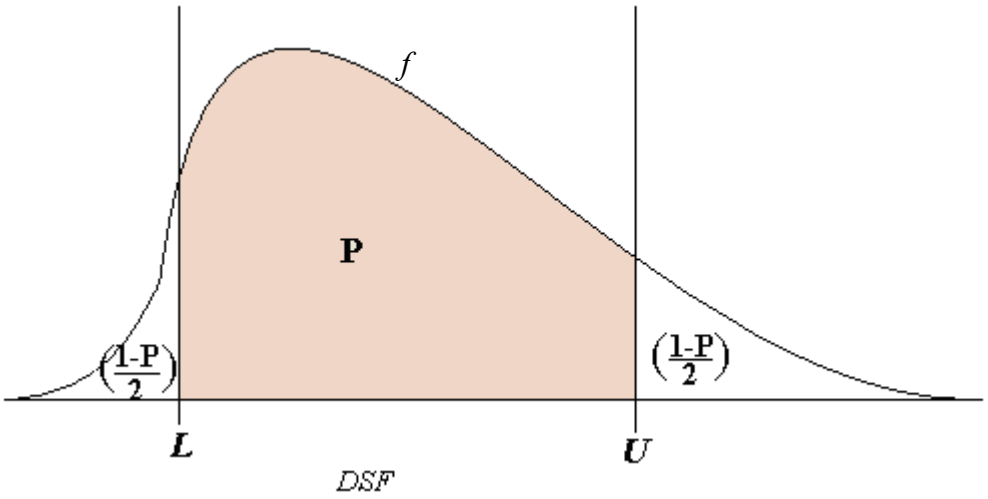

Figure 4.2: Calculation of confidence limits on the damage-sensitive features

It becomes possible to state, with a quantitative level of confidence, whether the new structural state is different from the reference structural state. For example, if a threshold

for the damage-sensitive features is set at some value, D_t, above which a feature is deemed to represent a damaged structure, the probability that $DSF_\zeta > D_t$ can be approximated to the probability that the structure is damaged. That is

$$\mathrm{P}_{\mathrm{damage}} = 100 \int_{D_t}^{\infty} f_\zeta(DSF_\zeta)\, dDSF_\zeta \ \% \qquad 4.8$$

A possible choice for an objective threshold is the (100-p) % upper one sided confidence interval on the damage-sensitive features of the reference data (Figure 4.3). The use of such a threshold implies that the probability of a damage-sensitive feature from an undamaged structure having a value greater than the threshold D_t is p %.

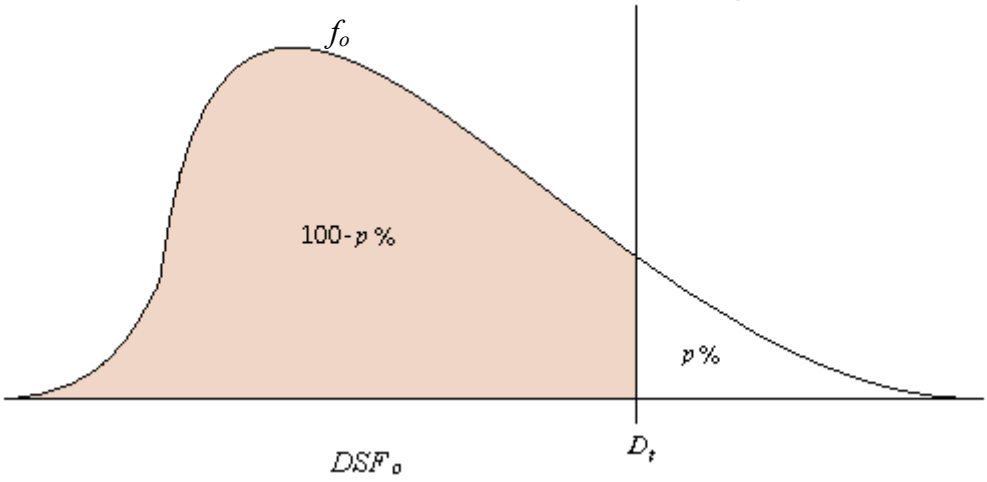

Figure 4.3: The p % threshold value for the damage-sensitive features

4.3 Feature discrimination based on outlier analysis

An outlier in a set of measurements can be described as a measurement that is conspicuous or inconsistent with other measurements. An outlier may arise due to gross measurement error or it may be a genuine observation that happens to be rare. It may also be that the outlying observation is not due to an erroneous measurement, but may have been generated by an alternative mechanism to the other data (Worden *et al.* 1999). The latter reasoning has been adopted for the purpose of feature discrimination in statistical pattern recognition. Damage to a structure changes the system that governs its vibration

response, resulting in the features measured from the damaged structure being outliers with respect to the features measured from the undamaged structure.

Intuitively, for one to identify an inconsistent observation, one must have identified the 'pattern' of observations that would constitute consistent or non-outlying measurements. This pattern of observations is the probability distribution of the set of non-outlying or homogenous observations. Thus, outliers are identified in relation to probability models (Barnett *et al.* 1994).

The application of outlier analysis to feature discrimination in non-model-based damage detection techniques is based on the following hypothesis. If, in the absence of environmental changes, the damage detection algorithm can clearly distinguish between different structural states, then the same algorithm must be able to distinguish between different structural states under changing environmental conditions, provided sufficient data exists describing the reference structural state under a sufficiently wide range of environmental conditions. Features from the new structural state would be outliers in the data set containing features from the reference data (Worden *et al.* 1999).

Worden *et al.* (1999) proposed that the concept of discordancy, from the statistical discipline of outlier analysis, be used to signal deviation from normal structural condition. A discordancy test is some measurement of the degree to which an object in a data set can be considered to be an outlier (Knorr *et al.* 2001). Based on an appropriate measure of discordancy, and an objective threshold value for this measure, feature vectors from an unknown structural condition can be deemed to be outliers with respect to a sample of feature vectors from the normal condition.

In cases where the damage detection technique extracts a single damage-sensitive feature, univariate outlier analysis can be used to determine whether the features of the new data are outliers with respect to the reference data set. The discordancy measure (a measure of how far the potential outlier lies from the other data points of the sample) is calculated as follows:

$$z_\zeta = \frac{\left| x_\zeta - \bar{x} \right|}{s} \tag{4.9}$$

where x_ζ is the potential outlier, $\bar{x}$ is the mean value of the data set containing features from the reference data collected over a range of environmental and operational conditions, and s is the sample standard deviation of the reference data set.

In cases where the damage detection technique extracts more than one damage-sensitive feature, multivariate outlier analysis, such as the Mahalanobis squared distance measure, can be used. Unlike the case of univariate data, each datum in a multivariate sample can be represented as a point in multidimensional space, and can be difficult to visualize (Barnett *et al.* 1994). The discordancy measure is therefore calculated as follows

$$d_\zeta = (\mathbf{F}_\zeta - \overline{\mathbf{F}})^T \mathbf{S}^{-1} (\mathbf{F}_\zeta - \overline{\mathbf{F}})^T \tag{4.10}$$

where $\overline{\mathbf{F}}$ is the vector whose elements are the mean of each type of damage-sensitive feature in the reference vibration data. $\mathbf{F}_\zeta$ is the potential outlier and is the vector of damage-sensitive features from the new data. $\mathbf{S}$ is the sample covariance matrix.

In this thesis a framework is proposed that extends the approach proposed by Worden *et al.* (1999) to address the complication of variable environmental and operational conditions as well as instrumentation errors. Implementation of the framework involves collecting vibration data from the test structure in its reference (undamaged) state under n combinations of environmental and operational conditions. n must be sufficiently large that nearly the full range of possible combinations of environmental and operational conditions is represented in the resulting database of reference vibration data. Each signal must be "corrected" for instrumentation errors by subtracting a vector whose elements follow the probability distribution of the instrumentation errors (Section 5.1). l such error vectors must be randomly generated, thereby generating, for each recorded signal, l possible outcomes of the error-corrected signal.

$$\mathbf{X}^i{}_o - \mathbf{e}^i{}_j = \hat{\mathbf{X}}^i{}_{oj} \tag{4.11}$$

where i denotes the combination of environmental and operational conditions. i =1, 2,..,n

j denotes a possible outcome of the instrumentation error vector. j = 1, 2 …, l

o denotes the reference or undamaged state of the structure

$\hat{\mathbf{X}}_{oj}^{i}$ are the resulting error-corrected signals

For each combination of environmental and operational conditions, m vibration signals must be collected in order to achieve an adequate sample size in the database of feature vectors. This can be achieved by collecting a long vibration signal at each test session, and then dividing the signal into m sub-signals. A feature vector can then be extracted from each sub-signal forming a database of n x l x m damage-sensitive features.

The decision as to whether an observation is an outlier relative to a set of data is dependent on some threshold for the measure of discordancy adopted for the investigation. The threshold discordancy measure is determined by computing the Mahalanobis distance of each feature vector in the reference database from the rest of the reference database. The p % threshold value is the value above which p % of the resulting discordancy measures lie. This implies that there is only a p % probability that the Mahalanobis distance between a feature vector from an undamaged structure and the feature vectors from the reference data set will exceed this threshold.

Data from the structure in its unknown (potentially damaged) state is collected under an unknown combination of environmental and operational conditions. The new data is processed in the same way as the reference data by correcting for instrumentation errors and subdividing the signal, then extracting damage-sensitive features. This results in a new data set containing l x m feature vectors.

The Mahalanobis distance measure is computed for each of the feature vectors in the new database relative to the reference database. The proportion of the discordancy measures from the new database that are greater than the threshold discordancy measure can be used as a quantitative indicator of damage. The framework is summarized in Figure 4.4.

Care must be taken as to the choice of discordancy measure for the outlier analysis. For example, the use of the Mahalanobis distance measure assumes that the distribution of the reference data is normal. For reference data that is not near normal, alternative tests for discordancy must be considered or the data must be transformed (Barnett 1994, Worden *et al.* 1999).

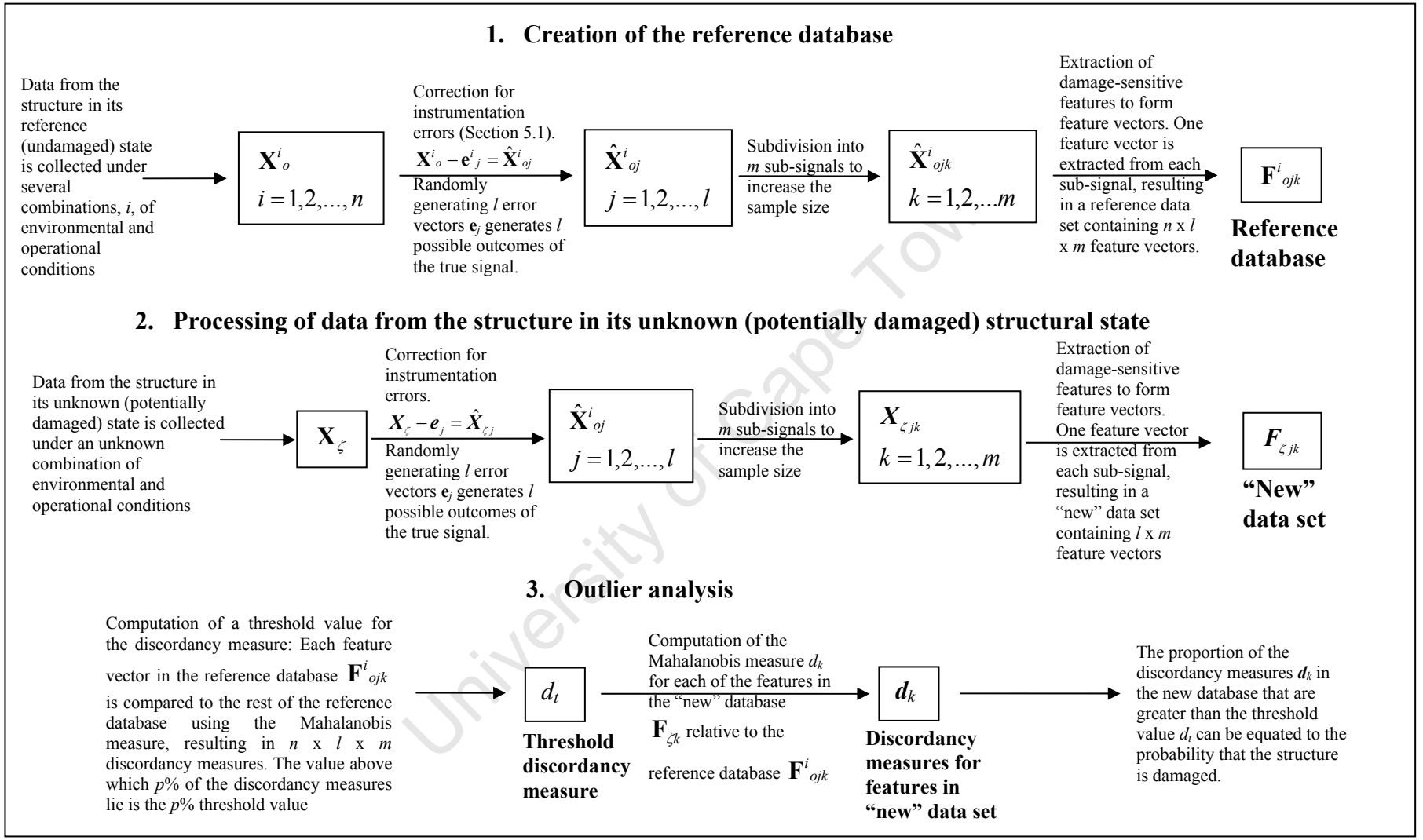

Figure 4.4: Summary of the outlier analysis framework for damage detection under changing environmental and operational conditions

4.4 Summary

The following constitute the main points of the chapter:

- The aim of damage detection using statistical pattern recognition is to identify whether there is sufficient evidence to reject the hypothesis that a structure is undamaged. Feature discrimination is a structured decision making process to objectively establish whether changes detected in the damage-sensitive features are significant enough to diagnose the structure as damaged.
- The threshold value in a statistical model for feature discrimination is a value chosen such that any damage-sensitive feature exceeding this threshold represents a damaged structure. The significance level (p) of the threshold is equal to the probability of a false-positive diagnosis of damage. Therefore, increasing the significance level of the threshold increases the chances of false-positive diagnoses and, conversely, reducing the significance level of the threshold increases the chances of false-negative diagnoses.
- Statistical models for feature discrimination fall into two main categories, namely supervised learning and unsupervised learning. Two unsupervised learning statistical models for feature discrimination, namely a probability density-based model and an outlier analysis-based model, were described in detail.
- Due to the subtlety of the form of damage to be detected, early-stage steel reinforcement corrosion, there is a danger that changes in the damage-sensitive features due to the onset or advancement of damage will be masked by measurement uncertainty resulting from changing environmental and operational conditions and instrumentation errors. Therefore, the statistical models for feature discrimination were combined with an uncertainty quantification technique. A Monte Carlo based uncertainty quantification technique was adopted. As a result, the output the damage detection technique would read (P being any number between zero and a hundred.): "Based on the chosen threshold, there is a P % probability that the structure is damaged."

Chapter 5

5 Experiments to test the damage detection techniques, incorporating uncertainty quantification

A time domain approach, using time series analysis, was selected to investigate the practicality of the damage detection approaches. The algorithm for feature extraction is first described before being applied to simulated data and then to experimental data. In each experiment, the frameworks developed in Chapter 4 for feature discrimination incorporating uncertainty quantification using Monte Carlo simulations are applied.

5.1 Accounting for instrumentation errors

Although the uncertainties involved in non-model-based damage detection are not limited to instrumentation errors, only errors due to instrumentation were considered in the analysis of the simulated data. The uncertainties due to environmental effects such as temperature were considered during the analysis of experimental data. As pointed out in Section 3.2, the sources of instrumentation errors involved in vibration testing are numerous. Therefore, an approach that grouped all the hardware and instrumentation into a single instrument "set" was adopted. The set constituted an accelerometer, connecting cables, signal conditioner, data acquisition card, and computer. By using this approach, it could then be assumed that all the errors resulting from hardware and instrumentation were manifested in the amplitudes of the vibration signals as shown in Figure 5.1.

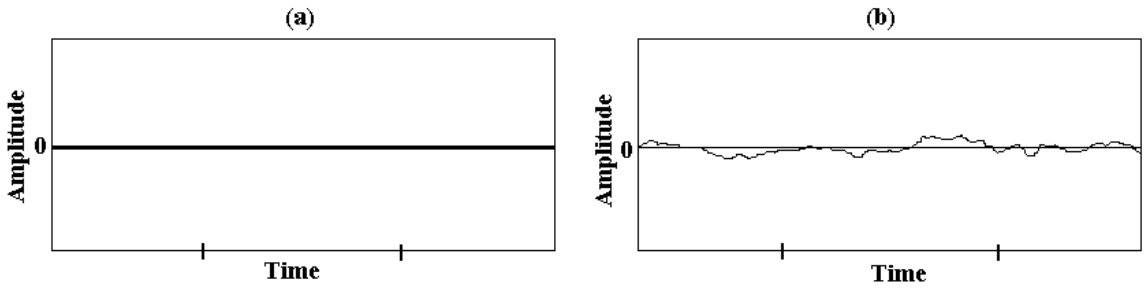

Figure 5.1: The recorded signal from an accelerometer placed on a horizontal surface experiencing no movements: (a) in the absence of measurement error, (b) in the presence of measurement error.

The equipment and setup were calibrated to determine the errors associated with a particular set of test equipment. This was achieved by placing the accelerometer on a solid surface experiencing no movements. In the absence of errors, the recorded vibration signal would be zero throughout (Figure 5.1a). However, since the presence of measurement error is a certainty, the recorded signal can never be zero throughout, and it represents an estimation of the total error associated with the set of equipment (Figure 5.1b). The probability density function (PDF) or cumulative density function (CDF) of these errors could then be estimated (Figure 5.2).

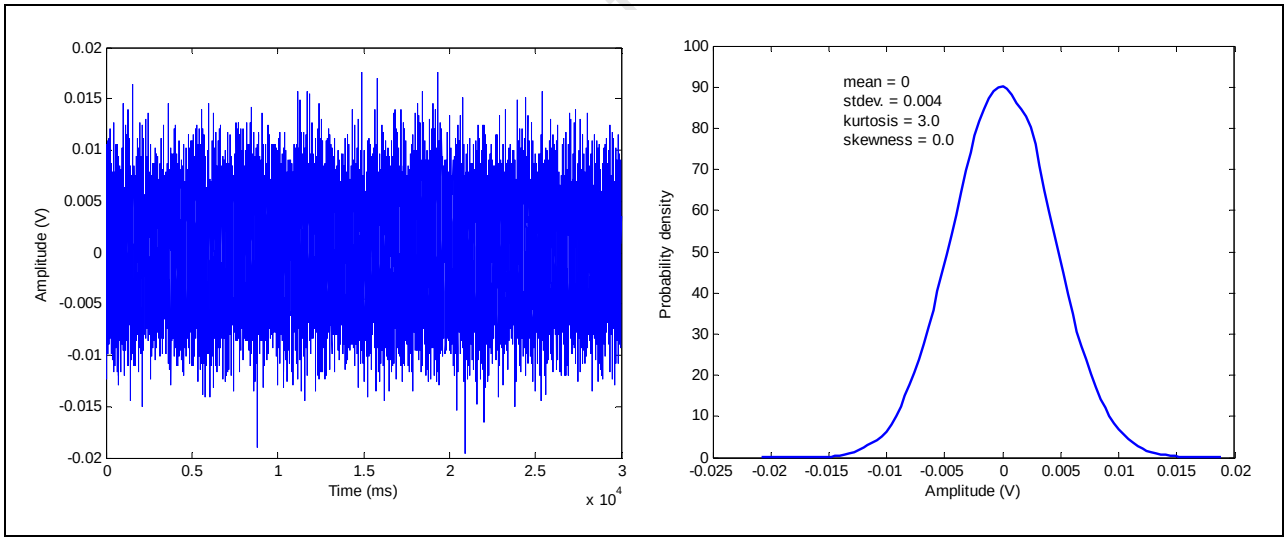

Figure 5.2: Instrumentation errors in an output channel

5.2 ARX feature extraction algorithm

As shown in Section 2.1, particularly equation 2.13, when the vibration response of a structure is modeled using an ARX(2,1), the coefficients of the model are strongly related to the dynamic parameters of the system. A change in the fit of the model indicates a change in the dynamic system, and is likely to be caused by damage. Therefore, an algorithm was developed that compared the residual errors of an ARX(2,1) fitted to a reference dynamic system with the residual errors of the same model fitted to a potentially damaged dynamic system. The model coefficients were computed using the least squares method. The algorithm is summarized as follows.

1. The probability distributions of the instrumentation errors, $f(\boldsymbol{e_u})$ and $f(\boldsymbol{e_x})$, are determined as described in Section 5.1. Adopting Monte Carlo principles to account for instrumentation errors, several possible outcomes of the "true" or "error-free" vibration signals are generated by subtracting possible outcomes of the error signal. The possible outcomes of the error signal are generated in such a way as to have the same probability distributions as the errors in the input signal $\boldsymbol{e_u}$ and the probability distribution of the errors in the output signal $\boldsymbol{e_x}$. In other words, generate a set of vectors $\{\mathbf{e_{u1}}, \boldsymbol{e_{u2}}, \ldots, \boldsymbol{e_{ul}}\}$ and $\{\boldsymbol{e_{x1}}, \boldsymbol{e_{x2}}, \ldots, \boldsymbol{e_{xl}}\}$ such that:

$$\begin{aligned} f(\boldsymbol{e_u}) &\approx f(\boldsymbol{e_{u1}}) = f(\boldsymbol{e_{u2}}) = \ldots = f(\boldsymbol{e_{ul}}) \\ f(\boldsymbol{e_x}) &\approx f(\boldsymbol{e_{x1}}) = f(\boldsymbol{e_{x2}}) = \ldots = f(\boldsymbol{e_{xl}}) \end{aligned} \qquad 5.1$$

   where f denotes the probability density function of the elements in the vector

2. The feature extraction technique is then applied to each outcome of the simulated true vibration signal. Therefore, for the reference (undamaged) state generate n possible outcomes of the "true" signals $\hat{\boldsymbol{u}}$ and $\hat{\boldsymbol{x}}$,

$$\begin{aligned} \hat{\boldsymbol{u}}_j &= \boldsymbol{u}_o - \boldsymbol{e}_{uj} \\ \hat{\boldsymbol{x}}_j &= \boldsymbol{x}_o - \boldsymbol{e}_{xj} \end{aligned} \quad j = 1, 2, \ldots, l \qquad 5.2$$

   where $\boldsymbol{u_o}$ and $\boldsymbol{x_o}$ are the raw input and output signals respectively.

3. Standardize each $\hat{\boldsymbol{u}}_j$ and $\hat{\boldsymbol{x}}_j$ by subtracting the mean and dividing by the standard deviation

$$\bar{\boldsymbol{u}}_j = \frac{\hat{\boldsymbol{u}}_j - mean(\hat{\boldsymbol{u}}_j)}{std(\hat{\boldsymbol{u}}_j)}$$
$$\bar{\boldsymbol{x}}_j = \frac{\hat{\boldsymbol{x}}_j - mean(\hat{\boldsymbol{x}}_j)}{std(\hat{\boldsymbol{x}}_j)} \qquad 5.3$$

4. For long lengths of signal recorded, split each standardized signal into *m* equal sub-signals, $\bar{\boldsymbol{u}}_{jk}$ and $\bar{\boldsymbol{x}}_{jk}$ $(k = 1, 2, \ldots, m)$, to increase the size of the database of extracted features and to improve the "resolution" of the analysis.

5. Steps 1 to 3 are repeated for vibration data $\boldsymbol{u}_\zeta$ and $\boldsymbol{x}_\zeta$, corresponding to the structure in a potentially damaged state. Similarly, this yields $\bar{\boldsymbol{u}}_{\zeta jk}$ and $\bar{\boldsymbol{x}}_{\zeta jk}$.

6. For each pair, $\bar{\boldsymbol{u}}_{jk}$ and $\bar{\boldsymbol{x}}_{jk}$ from the reference data, compute the ARX(2,1)

$$\bar{x}_{i_t} = \alpha_{1_{jk}} \bar{x}_{jk_{t-1}} + \alpha_{2_{jk}} \bar{x}_{jk_{t-2}} + \beta_{jk} \bar{u}_{jk_{t-1}} + \varepsilon_{jk} \quad j=1,2,...,l \; k = 1, 2, ..., m \qquad 5.4$$

where $\alpha_{1_{jk}}$, $\alpha_{2_{jk}}$ and β_{jk} are model coefficients, and $\varepsilon_{x_{i_t}}$ is the residual error in fitting the model to the time domain data. The residual errors for each sampling instant are concatenated to form a residual error vector $\boldsymbol{\varepsilon}_i$. The standard deviation of this error vector is then computed.

$$\sigma_{jk} = std(\boldsymbol{\varepsilon}_{jk}) \qquad 5.5$$

7. For each pair, $\bar{\boldsymbol{u}}_{\zeta jk}$ and $\bar{\boldsymbol{x}}_{\zeta jk}$, from the data corresponding to the structure in a potentially damaged state, fit the ARX(2,1) model structure, using the same coefficients as in equation 5.4

$$\overline{x}_{\zeta jk_t} = \alpha_{1_{jk}} \overline{x}_{\zeta jk_{t-1}} + \alpha_{2_i} \overline{x}_{\zeta jk_{t-2}} + \beta_{jk} \overline{u}_{\zeta jk_{t-1}} + \varepsilon_{\zeta x_{jk}} \quad j=1,2,...,l \; k=1,2,...,m \tag{5.6}$$

Likewise, the residual errors for each sampling instant are concatenated to form a residual error vector $\boldsymbol{\varepsilon}_{\zeta_t}$. The standard deviation of this error vector is then computed.

$$\sigma_{\zeta jk} = std(\boldsymbol{\varepsilon}_{\zeta jk}) \tag{5.7}$$

8. The averages across all the σ_{jk} and $\sigma_{\zeta jk}$ are then computed.

$$\overline{\sigma} = \frac{\sum_{k=1}^{m} \sigma_{jk}}{m}$$
$$\overline{\sigma}_{\zeta} = \frac{\sum_{k=1}^{m} \sigma_{\zeta jk}}{m} \tag{5.8}$$

9. The damage-sensitive feature, *DSF*, was taken as the ratio between the standard deviation of the residual errors for the ARX(2,1) model applied to the reference data and the standard deviation of the residual errors when the same model is fitted to data from an unknown structural state.

$$DSF = \frac{\overline{\sigma}_{\zeta}}{\overline{\sigma}} \tag{5.9}$$

10. Steps 1 through to 7 are repeated for each of the *l* pairs of instrumentation error vectors generated in step 1. This results in *l* values of *DSF*. For large *l*, the probability density function of the *DSF* can be estimated.

11. Statistical models for damage discrimination can then be applied to diagnose the structure.

5.3 Testing of the ARX feature extraction technique on simulated data

As a starting point to identifying effective damage detection techniques, prospective feature extraction techniques must be tested on simulated data. This gives invaluable insight into what data should be collected during vibration tests and what methods should be considered for the analysis of actual vibration test data. The ARX feature extraction technique described in Section 5.2 was investigated.

5.3.1 Generation of the simulated data

The input-output relationship of a single degree-of-freedom vibrating system was used to generate the synthetic data. The response, *x(t)*, of a lumped mass to a harmonic excitation, *u(t)*, was simulated by applying equations 2.16 and 2.17 and combing them as follows.

Given a harmonic excitation u_t at a frequency ω, applied to a single degree-of-freedom dynamic system

$$u_t = U\cos\omega t \tag{5.10}$$

the response at a sampling instance *t* is given by

$$x_t = X\cos(\omega t - \varphi) \tag{5.11}$$

where the amplitude *X* of the response is related to the amplitude *U* of the excitation by

$$X = \frac{U}{\sqrt{k - m\omega^2 + (c\omega)^2}} \tag{5.12}$$

and the difference in phase between the harmonic excitation and the dynamic response is

$$\varphi = \tan^{-1}\left(\frac{c\omega}{k - m\omega^2}\right) \tag{5.13}$$

$$\therefore u_t = \frac{U}{\sqrt{k - m\omega^2 + (c\omega)^2}}\cos\left[\omega t - \tan^{-1}\left(\frac{c\omega}{k - m\omega^2}\right)\right] \tag{5.14}$$

c is the damping of the system, *m* is the mass and *k* is the stiffness.

Structural damage to civil infrastructure results in reductions in stiffness and a corresponding reduction in resonance frequencies. For the purpose of generating data to test the damage detection algorithm, the stiffness, k, of the undamaged system was taken as 100 kN/m. To simulate damage in the system, the stiffness was varied and the response simulated for reduced values of stiffness. The other parameters were fixed at the following values: m = 100 kg, U = 100N, c = 20 kg/s, excitation frequency ω = 32 Hz.

5.3.2 Results of the application of the ARX feature extraction technique to simulated data

The instrumentation errors for an output channel were found to be normally distributed with zero mean and a standard deviation of 0.004. The instrumentation errors for the input channel were found to be normally distributed with zero mean and a standard deviation of $1x10^{-4}$. Input and output signals of length 2s with a sampling interval of 0.001s were generated using equations 5.10 to 5.14. The reference state (100 % stiffness) had a stiffness of $1x10^{5}$. Damage was introduced to the system by reducing the stiffness in decrements of 10 %. Each signal was split into 4 sub-signals. I.e. m = 4 in equations 5.4 to 5.8. One hundred Monte Carlo runs were conducted for each damage state. i.e. l = 100.

Figure 5.3 shows the results of the ARX feature extraction technique. Clear discrimination between the different damage states was achieved for all stiffness losses greater than 10 %.

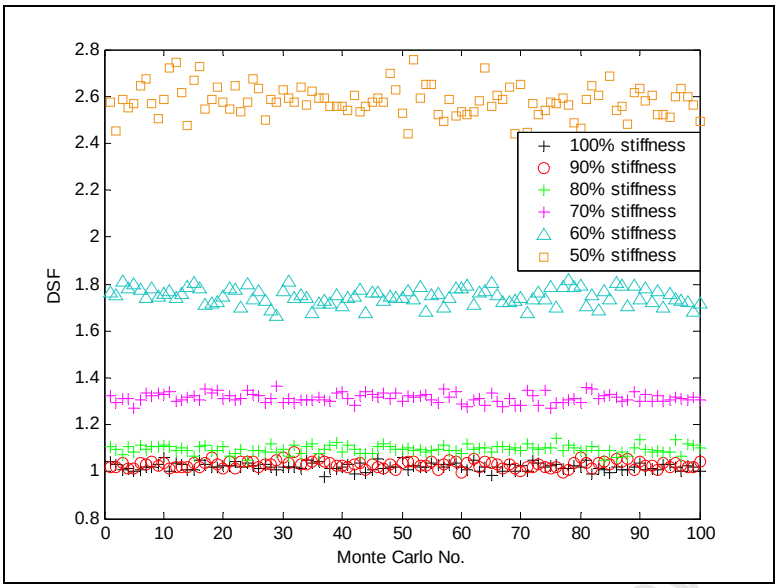

Figure 5.3: An output of the ARX feature extraction technique. The technique is capable of detecting lossess in stiffness.

Feature discrimination was then applied using the probability density based framework and the outlier analysis based framework.

5.3.2.1 Probability density based feature discrimination

The *DSF*s corresponding to 70 %, 60 % and 50 % stiffness clearly indicate damage as they fall well away from the *DSF*s corresponding to 100 % stiffness. However, due to the closeness of the clustering of the damage-sensitive features for the structural states corresponding to 100 %, 90 % and 80 % stiffness, visual inspection of the results may be insufficient. A more objective model for feature discrimination must be employed. The probability distribution of the damage-sensitive features for each structural state can be estimated. This is illustrated using the features from the first three damage states (Figure 5.4).

If a threshold value is established such that any values of *DSF* exceeding this threshold represent a damaged structural state, then the probability that a particular signal represents a damaged structural state is equivalent to the area bounded by a vertical line at the threshold value and the part of the probability distribution curve for values of *DSF* greater than the threshold. Assuming that sufficient data describing the reference structural state has been collected, the threshold can be set based on the probability distribution of the *DSF*s for the reference signal (100 % stiffness).

For example, the threshold can be set at the upper one-sided 99 % confidence interval for the reference data. This implies that 99 % of the time, the *DSF*s for an undamaged structure will be less than this threshold value. In this simulated example, the upper 99 % confidence interval for the *DSF*s of the reference signal is 1.062. Taking this value as the threshold implies that:

- There is 3 % certainty that the signal from the system with 90 % stiffness represents a damaged structure
- There is 90 % certainty that the signal from the system with 80 % stiffness represents a damaged structure

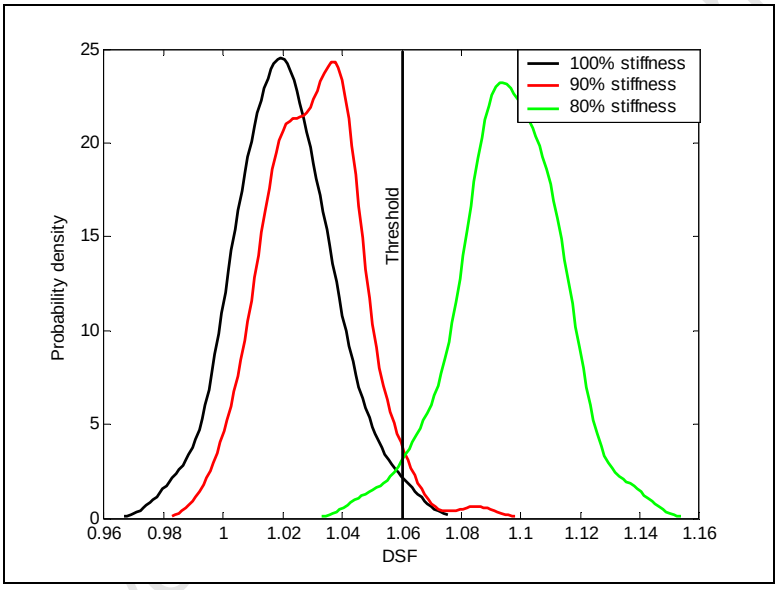

Figure 5.4: The sampled probability distributions of the damage-sensitive features for three different structural states: The threshold was set to the upper one-sided 99 % confidence interval of the DSFs for the reference signal (100 % stiffness).

5.3.2.2 Outlier analysis based feature discrimination

Quantitative feature discrimination was achieved by applying the outlier analysis based feature discrimination framework. The discordancy measure corresponding to a 5 % significance level was chosen from the reference data. Figure 5.5 shows the discrimination of the *DSF*s from three different structural states of the simulated structure. The *DSF*s from the simulated structure at 80 % stiffness clearly represent a damaged structure as 98 % of the discordancy measures exceed the threshold.

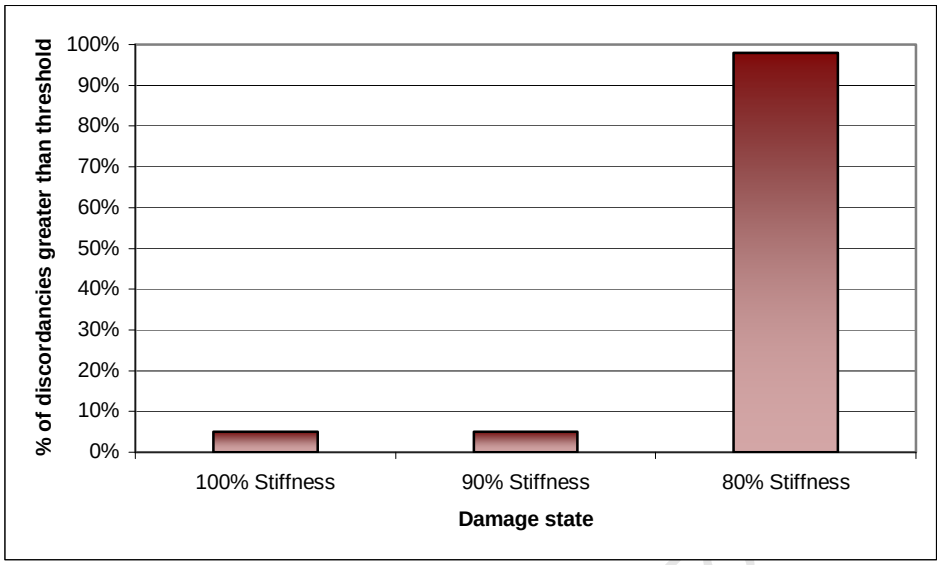

Figure 5.5: Outlier analysis based feature discrimination applied to the *DSF*s of the simulated structure at different structural states. A 5 % discordancy threshold was adopted.

5.3.3 Discussion of the results of the application of the ARX feature extraction technique to simulated data

It was found that the damage-sensitive features of the ARX feature extraction technique were sensitive to changes in the simulated structure due to purely stiffness loss. However, it was hoped that, in addition to changes in stiffness, the effects of corrosion degradation in steel-reinforced concrete structures would result in other changes in the vibration behaviour of the structure and would result in changes in the damage-sensitive features of the ARX feature extraction technique. This highlights an advantage of adopting non-model-based damage detection approaches based on statistical pattern recognition, over model-based parameter estimation approaches. Non-model-based damage detection techniques may detect non-parametric changes that may not be directly measurable.

By combining feature extraction with statistical models for feature discrimination, the ARX technique was upgraded from being merely a feature extraction technique to being a *damage detection technique*, capable of quantifying the uncertainty in its diagnoses.

5.4 Laboratory experiments to assess the ARX damage detection technique

As mentioned in Chapter 1, non-model-based damage detection algorithms have been successfully applied to mechanical infrastructure. This thesis and the experiments described here aim to assess the applicability of these damage detection algorithms to civil infrastructure. A typical problem associated with civil infrastructure is their gradual, and sometimes subtle, deterioration over time. For this reason, experiments were setup to detect the damage caused by steel reinforcement corrosion in concrete beams. The algorithm to be validated by the experiments took into account uncertainties due to instrumentation errors and changes in environmental conditions. For the purpose of this study, only temperature was considered as a variable environmental condition. The main aims of the experiments were:

- to assess whether the damage detection algorithm could, under constant environmental and operational conditions, discriminate between a reference state and a new state of damage
- to assess whether, at a particular state of damage, the damage detection algorithm discriminated between data from one environmental condition to another. In other words, the algorithms were tested for false-positive diagnoses as a result of variable environmental conditions.

The damage detection algorithms were then deemed to be effective or ineffective based on the following criteria:

Data discrimination must occur across different damage states, but must not occur across environmental conditions. In other words, an effective damage detection algorithm would result in statistically significant variation in damage indicators from one damage state to another, but no statistically significant variation from one environmental condition to another.

5.4.1 Experimental procedure

The experimental procedure entailed damaging concrete beams gradually and conducting vibration tests at intervals, thereby creating a database of vibration data at various states of damage in the test beams. The test specimens consisted of four reinforced concrete beams, each with dimensions 2200 x 120 x 100 mm. Two beams served as controls. Steel reinforcement consisted of two Y10 bars as shown in Figure 5.6. The beams were made from concrete with a

target strength of 20 MPa. Such low strength concrete is of relatively low durability, and it allowed for rapid deterioration of the beams during the controlled damage by accelerated corrosion. Details of the controlled damage are described in Section 5.4.2. In preparation for the controlled damage of the beams, insulated copper wire was attached to the steel reinforcement before casting. To ensure that the support conditions remained relatively constant, a knife-edge support was fixed to either end of each beam, to provide a simply supported span of 2m. Small plates, onto which the accelerometers could be fixed, were glued onto the beams.

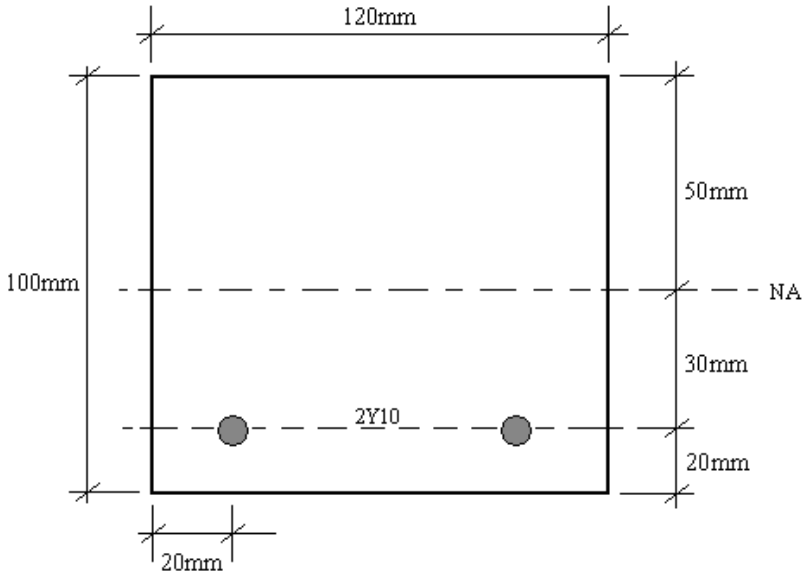

Figure 5.6: Cross-section through the test specimens

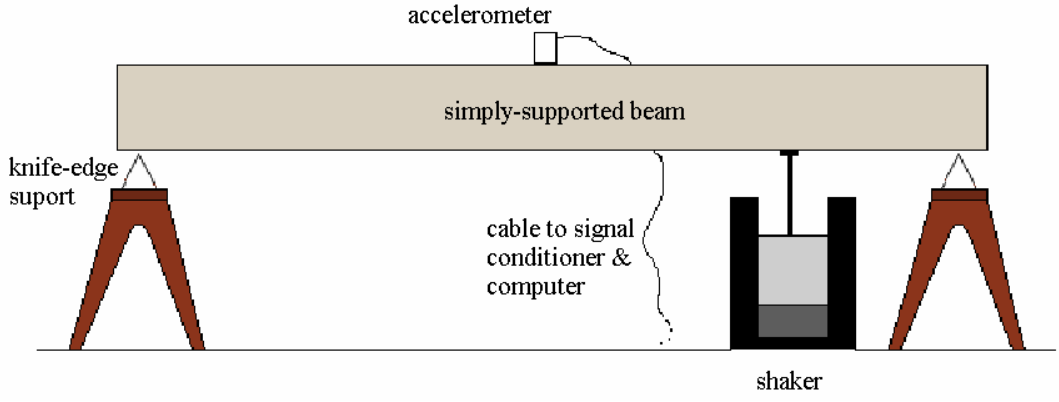

Figure 5.7: The vibration test setup

A schematic of the vibration test setup is shown in Figure 5.7. The two main variables under investigation were damage state (degree of corrosion), and environmental condition (temperature). The temperature was measured during the test session using a thermocouple sensor imbedded in the concrete (Figure 5.8).

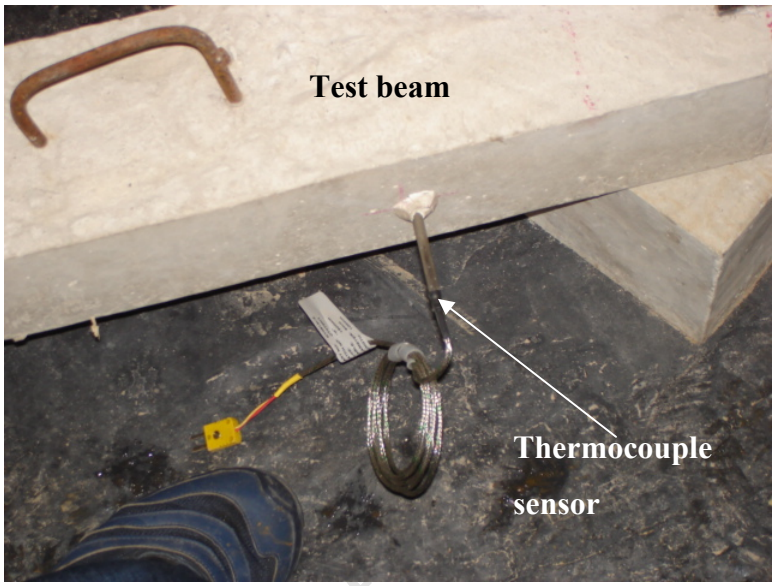

Figure 5.8: Thermocouples were imbedded in the concrete for temperature measurement during vibration tests.

Two beams, C1 and C2, were assigned as controls, and were therefore not subjected to any damage. The remaining two beams, B1 and B2 were subjected to gradual damage due to accelerated corrosion of their steel reinforcement. beams B1 and C1 were located in a fairly constant environment with a relative humidity of 60 % ± 2 % and a temperature of 27°C ± 1°C . This procedure made it possible to assess

- whether the damage indicator for control beam C1 changed over time when no change in damage state or environmental condition occurred. This served as a test for false-positive detections of damage.
- whether the damage detection algorithm was capable of discriminating between damage states in the simple case of constant environmental conditions.

The second pair, consisting of beam B2 and control beam C2, was subjected to changing temperatures, and tests were conducted on these beams at temperatures ranging from 13°C to 33°C. The highest temperature was attained by leaving the beams in the sun, while the lowest was attained by leaving the beams in a 10°C temperature-controlled room. This procedure made it possible to assess whether, at any particular state of damage of the beams, the damage indicator varied with changes in environmental condition. This served as a test for false-positive diagnoses due to both instrumentation errors and changing environmental conditions.

The equipment calibration procedure described in Section 5.1 was conducted after every test session. Each probability distribution was estimated from 30 000 samples. The set of equipment was connected in the same way for each test session. For this reason clear labelling of equipment was necessary in order to aid repeatability. Furthermore, because the probability distributions of the instrumentation errors were determined under the same environmental conditions that the vibration data was collected, it made it possible to use the instrumentation errors in the damage detection algorithms without the need to determine the relationship between the environmental condition and the form of the probability distribution of the instrumentation errors.

Because the damage detection algorithms are based on pattern recognition, consistency of the testing procedure was of the utmost importance. Errors such as those due to sensor placement introduce uncertainty into the outputs of the algorithms. In order to eliminate sensor placement errors in practice, accelerometers can be embedded in the structure or screwed onto fixed locations at every test session. In this experiment, the accelerometers were fitted with magnetic bases and attached to steel plates glued onto the beams. For repeatability of placement, the positions of the accelerometers were marked on the plates. For the purpose of this study it could then be assumed that errors due to inconsistency of sensor placement were negligible.

5.4.2 Controlled damage of the test specimens

Steel corrosion is a slow process. Harsh marine environments increase the rate of corrosion of steel reinforcement in concrete structures due to an increased concentration of chloride ions. Even under such conditions, the corrosion process may take years before its effects, such as cracking and spalling, become apparent. Therefore, it was necessary to accelerate the corrosion process for practical reasons. The corrosion of the concrete beams was to be restricted to a 50 cm

long section of the tension steel reinforcement bars at midspan. An electric current was used to accelerate the corrosion. A circuit was created in which the tension steel reinforcement bars were the anode. A solution containing 5 % sodium chloride was used as the electrolyte. A PVC pond, as shown in Figure 5.9, was attached to the soffit of the beam at midspan using silicon adhesive. The pond was filled with electrolyte and a reference electrode (cathode) was placed in the pond. Figure 5.9 illustrates the setup of the localized corrosion circuit.

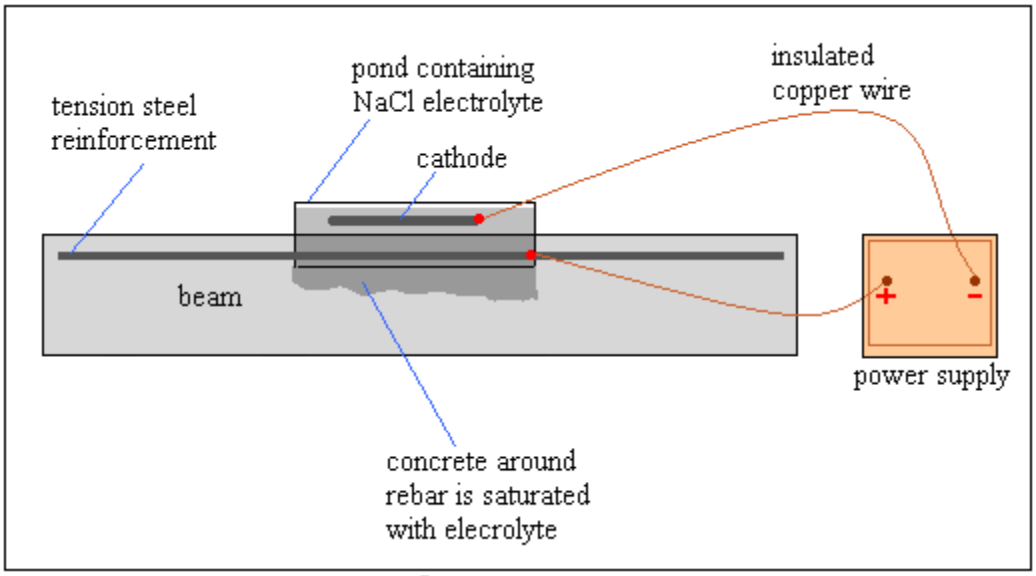

Figure 5.9: Accelerated corrosion of the test specimens

According to Faraday's Law, the degree of corrosion of steel is proportional to the magnitude of the applied current and the duration of the application of the current. The governing equation is as follows:

$$Q = 5.32 \times 10^4 \frac{I \cdot t}{\pi D^2 L} \qquad 5.15$$

where Q is the degree of corrosion as the percentage of the steel mass lost to the process, I is the current applied in units of Ampere, t is the duration of the application of the current in units of hours, D is the diameter of the uncorroded steel bar in units of mm, L is the length of the corroding bar in units of mm. Faraday's law was used to estimate the degree of corrosion in beams B1 and B2 at each test session. Table 2 summarises the estimated degrees of corrosion of the steel in the test specimens at each test session.

Table 2: The estimated degree of corrosion in each steel bar as a percentage of the original steel mass in the middle 50 cm of each beam.

Test session/ Damage state	Beam				Observations
	B1	B2	C1	C2	
Baseline	0	0	0	0	All beams undamaged
Damage1	3	3	0	0	Reddish-brown rust stains in the localised corrosion region of beams B1 &B2
Damage2	6	6	0	0	Fine longitudinal cracks on tension face of beams B1 & B2
Damage3	12	10	0	0	An increase in width of longitudinal cracks on tension face of beams B1 & B2 (Figure 5.10)
Damage4*	12	10	0	0	Fine transverse crack on tension face of all beams
Damage5*	15	13	0	0	No visible change from Damage4 for all beams

* Damage4 and Damage5 tests were conducted after loading the beams

Figure 5.10: Longitudinal cracks due to corrosion of the steel reinforcement

Structural members in civil infrastructure are constantly subjected to in-service loading. The loads result in transverse cracks in the tension zone that terminate at the level of the tension steel reinforcement. The dynamic loads imposed on the test beams during vibration testing were incapable of inducing such cracks. To investigate the effects of static loading on the detection of corrosion damage, static loading was incorporated into the test procedure. After the third spell of accelerated corrosion, each beam (control beams included) was subjected to a static point-load of

1.3 kN at midspan, for an arbitrary duration of 2 hours. This was repeated again after the 4th spell of corrosion. The magnitude of the static load was calculated as the minimum load required to induce a stress equivalent to the tensile strength of the concrete, at the level of the tensile reinforcement. The tensile strength of the concrete was taken as 2 MPa.

5.4.3 Elastic modulus tests

Environmental conditions such as temperature affect the material properties of structures. For example, the elastic modulus of concrete is expected to decrease with an increase in temperature. This poses a problem for damage detection techniques, as stiffness reduction due to an increase in temperature may be incorrectly attributed to structural damage. In order to investigate the effects of temperature on the test beams, elastic modulus tests were conducted on concrete samples that had been cast from the same batch of concrete as the test beams. The exercise was not intended as part of the damage detection procedure, since one reason for departing from model-based damage detection techniques was the difficulty associated with accurately determining material properties and modal parameters such as stiffness. However, it provided, for the sake of this study, insight into the magnitude of variation to be expected as a result of changes in temperature. The samples consisted of cylinders with a diameter of 100 mm and a length of 200 mm. Figure 5.11 describes the test apparatus and setup.

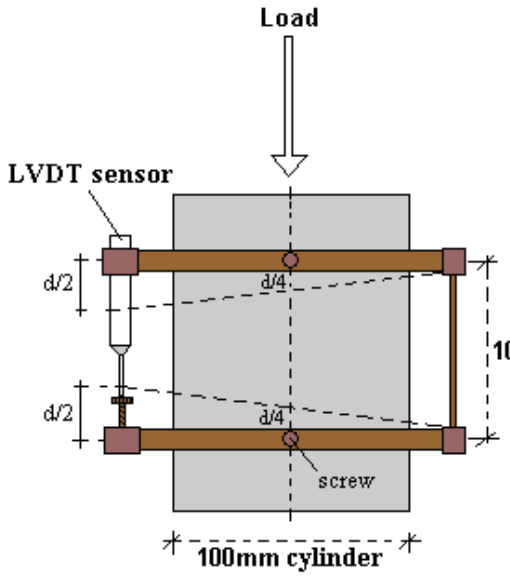

Measured deflection	= 2 x d/2 = d
Deflection required for strain calculations	= 2 x d/4 = d/2
Strain	= (d/2)/gauge length
Stress	= load/C.S. area
Elastic modulus	= gradient (stress vs strain)

Figure 5.11: Elastic modulus test setup.. A load cell was used to measure applied loads and an LVDT measured deflections.

The samples were loaded axially, while a load cell at the base of the cylinder measured the applied load. A linear variable displacement transducer (LVDT) was used to measure the resulting deflection. A graph of stress versus strain was plotted for each cylinder and the gradient of the best fit straight line was taken as the elastic modulus. Each sample was tested at two different temperatures. The samples were left overnight to "acclimatize" in a 10°C temperature-controlled room before testing. They were then allowed to reach room temperature before being placed in a 40°C oven and left overnight to acclimatize before testing again. The results are summarized in Table 3.

5.5 Results of the experiments to assess the ARX damage detection technique

The ARX feature extraction algorithm described in Section 5.2 was applied to the vibration data collected from the 4 test beams B1, C1, B2 and C2. The vibration tests were conducted at the stages of induced damage described in Table 2. Excitation of the beams was achieved using a 32 Hz sinusoidal forcing signal. The sampling rate for the data acquisition was 1 kHz and a filter of 1 kHz was applied. Figure 5.12 shows a typical response signal for beam B1. Vibration signals of length 10 000 were used for each analysis, and these were split into smaller sub-signals of length 1 000 (Section 5.2). One hundred Monte Carlo runs were conducted for each application of the algorithm.

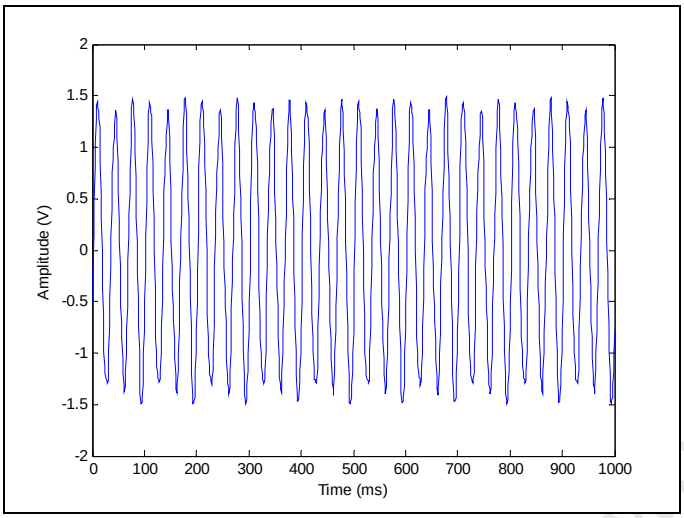

Figure 5.12: A typical vibration response for beam B1. Only the first 1000 samples are shown.

As mentioned in Section 5.4.1, the experiments involved two main investigations. Firstly the sensitivity of the ARX damage detection technique to changes in the core temperature of the beams was investigated. At their Baseline or undamaged state, beams B2 and C2 were each tested for damage using vibration data collected from the beams at core temperatures of 13°C, 16°C, 18°C, 20°C, 27°C, and 33°C ± 1°C to assess the damage detection algorithm for false diagnoses due to changing temperature. The results of the elastic modulus tests (Section 5.4.3) on samples of the same concrete used in the test beams are also presented. Next, the ability of the technique to detect corrosion damage in the concrete beams was investigated by applying the technique to vibration data collected from the six damage states described in Table 2.

5.5.1 Results of the elastic modulus tests

Table 3 summarizes the results of the elastic modulus tests. A reduction in elastic modulus of no more than about 10 % was realized for an increase in temperature of about 30°C.

Table 3: Elastic modulus of the test specimens at two different temperatures. Four samples were cast per beam. Measurements are in GPa.

Beam	Elastic Modulus (GPa)		Difference in Modulus (GPa)	% Difference in Modulus
	Cold Sample (~10°C)	Hot Sample (~40°C)		
B1	24.9	24.7	0.2	0.8
	25.4	22.9	2.5	9.8
	24.2	22.6	1.6	6.6
	23.0	23.6	-0.6	-2.6
mean	**24.4**	**23.5**	**1**	**3.8**
C1	25.5	23.5	2.0	7.8
	25.7	23.5	2.2	8.6
	23.9	21.3	2.6	10.9
	24.4	21.3	3.1	12.7
mean	**24.9**	**22.4**	**2**	**9.9**
B2	21.0	18.4	2.6	12.4
	22.3	21.4	0.9	4.0
	26.0	21.6	4.4	16.9
	20.9	19.7	1.2	5.7
mean	**22.6**	**20.3**	**2**	**10.1**
C2	23.1	22.4	0.7	3.0
	23.9	22.9	1.0	4.2
	18.4	19.5	-1.1	-6.0
	20.3	18.6	1.7	8.4
mean	**21.4**	**20.9**	**1**	**2.7**
Overall Mean	**23**	**21**	**2**	**6.7**

This result had implications for the ARX damage detection algorithm described in Section 5.2. Inspection of the results of the ARX feature extraction technique, applied to simulated data (Section 5.3.2), revealed that a reduction in stiffness of less than 10 % was barely detectable by the damage detection algorithm. Consequently variations in temperature, over the range investigated in the experiments, were expected not to cause significant changes in the damage-sensitive features, unless significant changes in damping occur. However, the disadvantage is that sensitivity to damage has been compromised in favour of *insensitivity* to environmental variability. Therefore, considering instrumentation errors and temperature variability, the ARX damage detection technique described here cannot be expected to detect reductions in stiffness of less than 10 %. Other, not necessarily measurable, changes in the structure brought about by steel reinforcement corrosion would have to contribute towards changes in the damage-sensitive features of the chosen feature extraction technique.

5.5.2 Results of the application of the ARX damage detection technique at various temperatures

Figure 5.13 shows the features extracted from the Baseline data for beams B2 and C2. In each case, the vibration signal for the beams at 13°C ± 1°C was taken as the reference data and was used to develop the ARX. No visual feature discrimination was evident from the plot of the damage-sensitive features.

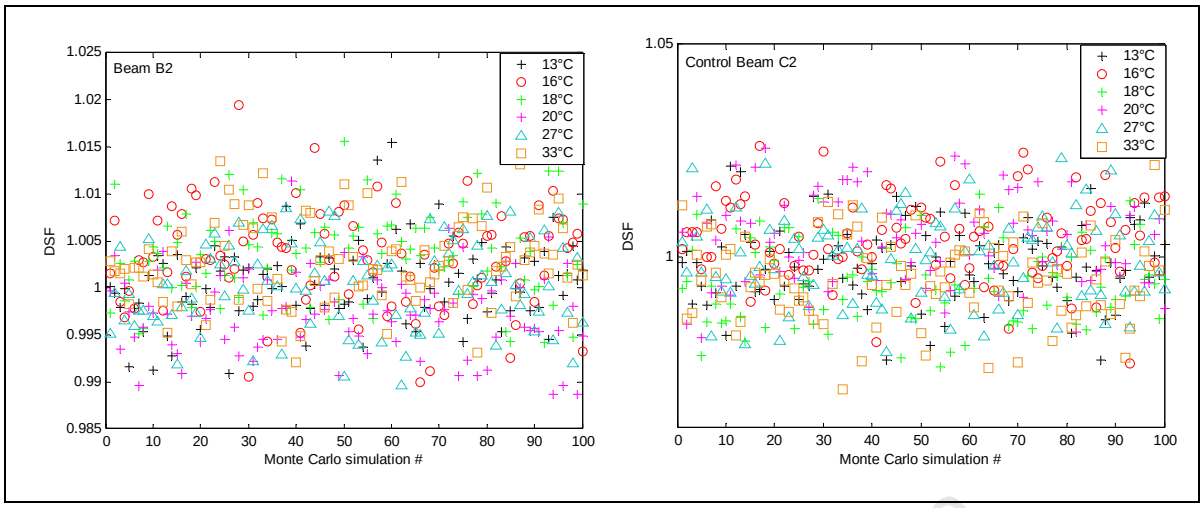

Figure 5.13: The damage-sensitive features for the Baseline state of beam B2 and beam C2, at different temperatures. There was no visible discrimination between the DSFs corresponding to the different temperatures.

For quantitative feature discrimination, the two frameworks described in Chapter 4, namely probability density based feature discrimination and outlier analysis based feature discrimination, were applied to the same set of damage-sensitive features.

5.5.2.1 Probability density based feature discrimination

As demonstrated in Section 5.3.2, quantitative feature discrimination can be achieved by estimating the sampled probability distribution of the damage-sensitive features for each temperature of the test specimen (Figure 5.14).

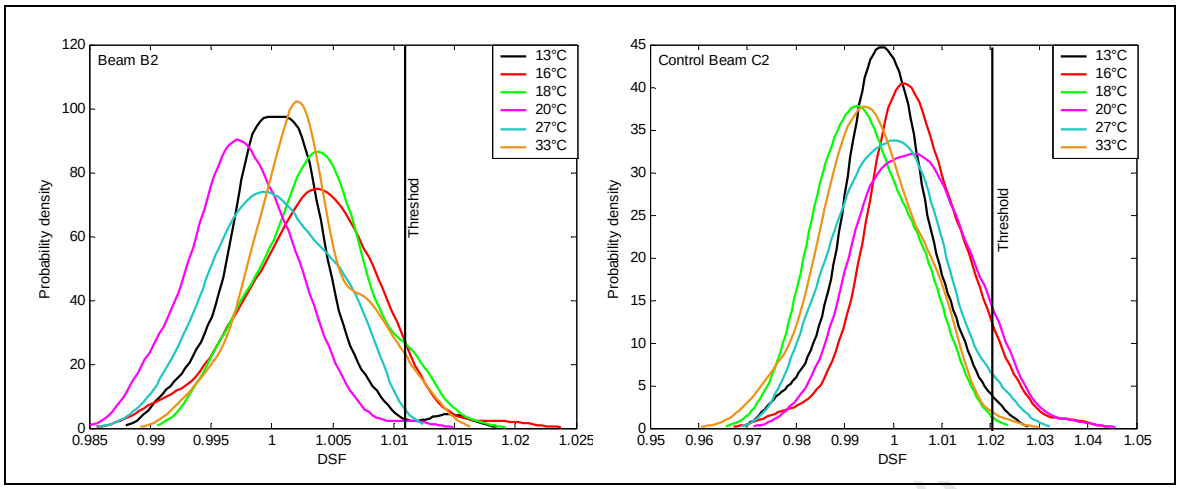

Figure 5.14: The sampled probability distributions of the damage-sensitive features (DSF) for beam B2 and beam C2, at varying temperatures.

The upper one-sided 99 % confidence interval for the damage-sensitive features of the reference data was chosen as a threshold. With this threshold, the probability that the beams were damaged was low for all temperatures investigated (Figure 5.15).

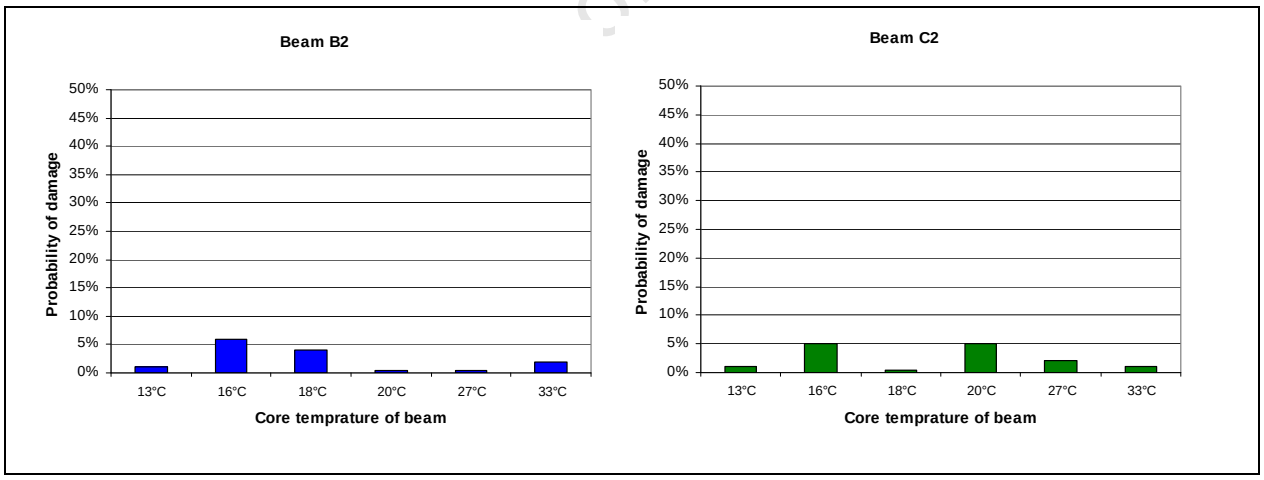

Figure 5.15: The probability of damage in beams B2 and C2 at different temperatures of the beams

5.5.2.2 Outlier analysis based feature discrimination

The outlier analysis based feature discrimination was applied to the *DSF*s of beams B2 and C2 at different temperatures. Because the Mahalanobis discordancy calculation assumes that the reference data set is normally distributed, it was necessary to test for normality. Normally

distributed data has a kurtosis of three and a skewness of zero. The kurtosis and skewness of the 13°C-data for both beams B2 and C2 were shown to be close to these values (Table 4).

Table 4: Kurtosis and skewness of the 13°C-data for beams B2 and C2

	Kurtosis	Skewness
Beam B2	4.0	0.5
Beam C2	3.1	-0.00

Normal probability plots of the 13°C data for the two beams are also shown in Figure 5.16. A linear scatter of the data on a normal probability plot indicates a normally distributed data set. Therefore, there is sufficient evidence to assume that the distributions of both data sets are near normal.

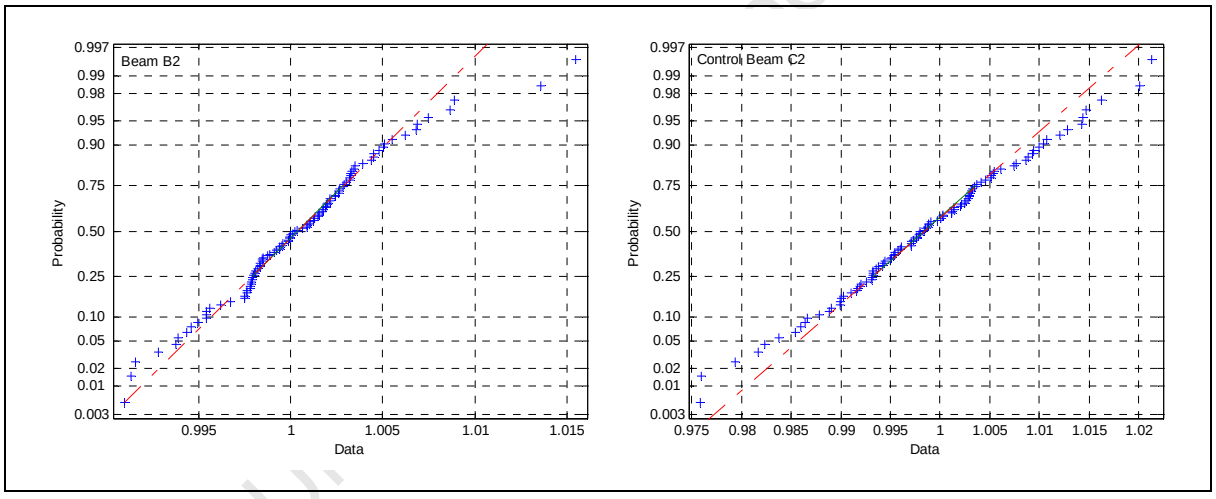

Figure 5.16: Normal probability plots for the 13°C data sets for beams B2 and C2.

A 5 % discordancy threshold was adopted for the outlier analysis. For each beam, the percentage of discordancy measures that exceeded the threshold was low, indicating that the damage-sensitive features extracted using the ARX feature extraction technique were insensitive to changes in temperature over the range investigated (Figure 5.17).

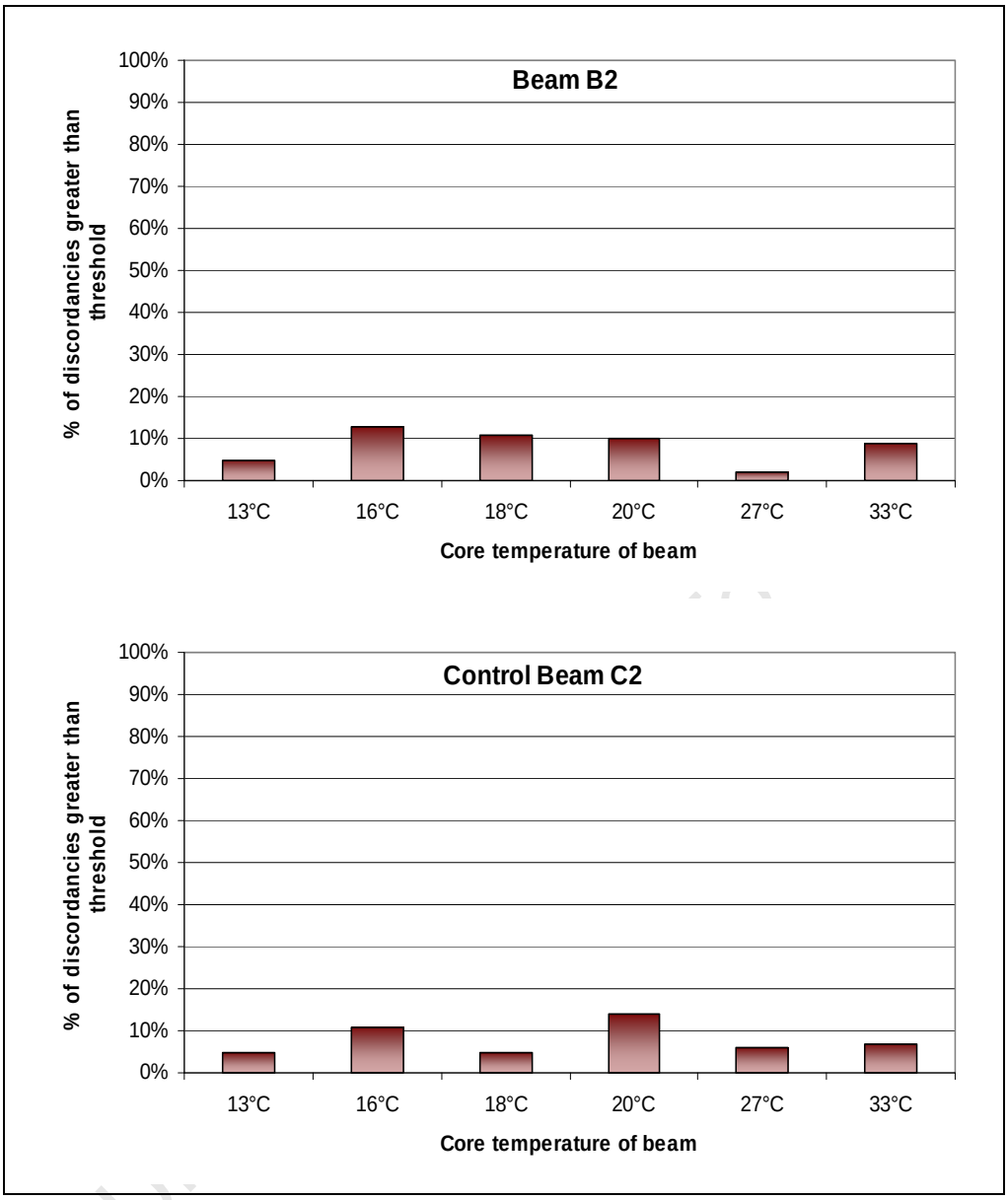

Figure 5.17: Outlier analysis based feature discrimination applied to the DSFs of beams B2 and C2 at different temperatures. A 5 % discordancy threshold was adopted

5.5.3 Results of the application of the ARX damage detection technique to the beams at various states of damage

In order to test the damage detection capabilities of the ARX feature extraction, the technique was applied to the vibration data from each of the damage states described in Table 2. Vibration data collected from the beams at a core temperature of 27°C ± 1°C was used for comparison between damage states. Figure 5.18 shows the resulting plots of the damage-sensitive features. For quantitative feature discrimination, the two frameworks described in Chapter 4, namely

probability density based feature discrimination and outlier analysis based feature discrimination, were applied to the same set of damage-sensitive features.

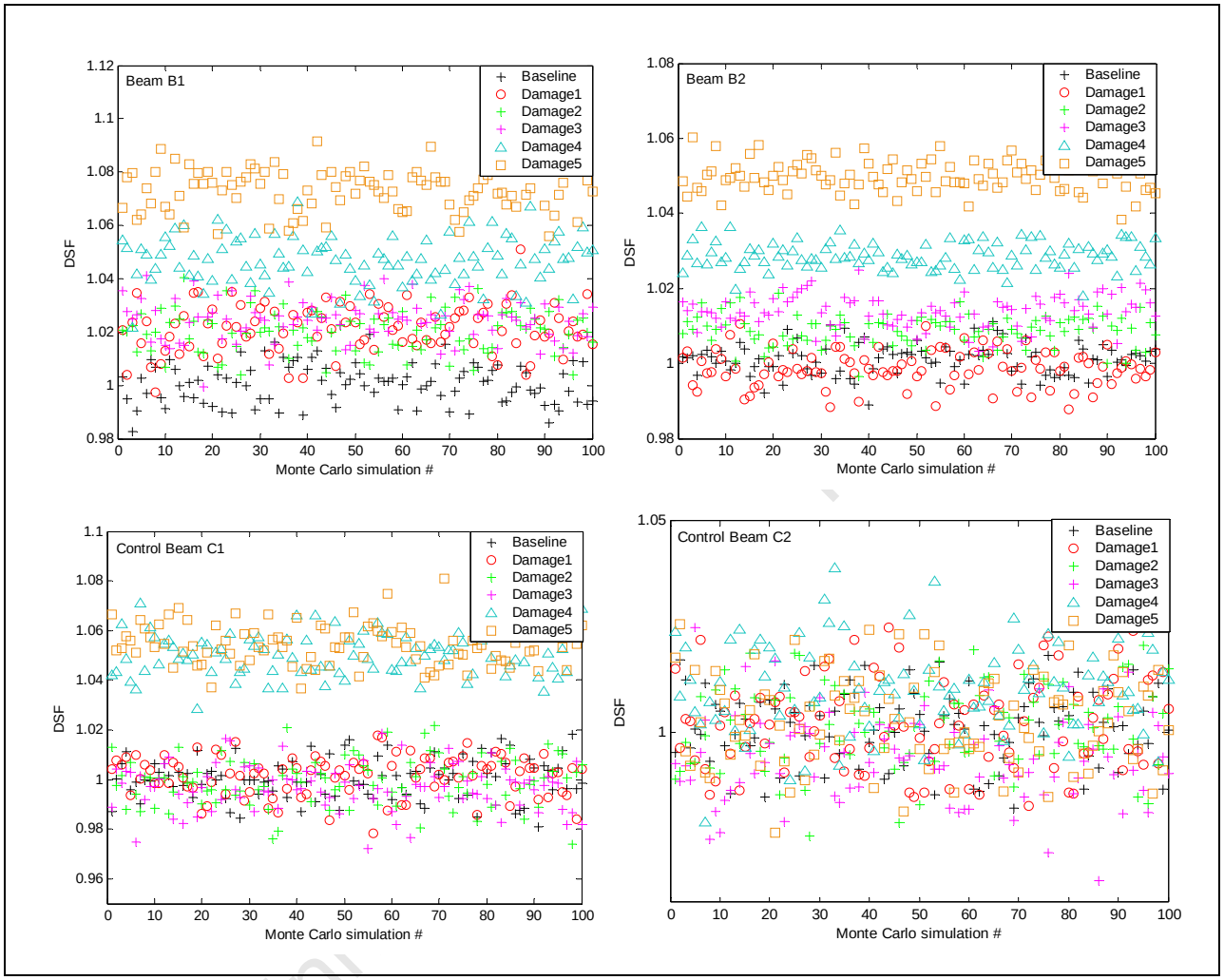

Figure 5.18: Plots of the damage-sensitive features from the test beams at various states of damage.

5.5.3.1 Probability density based feature discrimination

Figure 5.19 shows the sampled probability distributions of the damage-sensitive features of beam B1 at the various damage states. A threshold value was chosen as the upper one-sided 99 % confidence interval on the damage-sensitive features of the Baseline data. Damage-sensitive features above this threshold value were considered to represent a damaged beam.

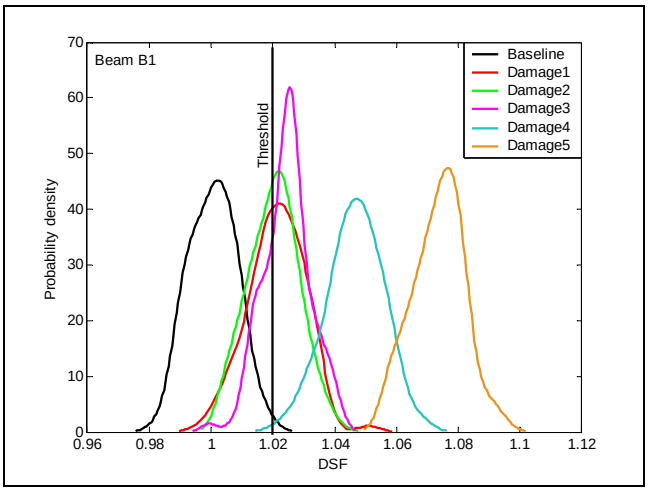

Figure 5.19: The sampled probability distributions of the damage-sensitive features of beam B1 at the various damage states.

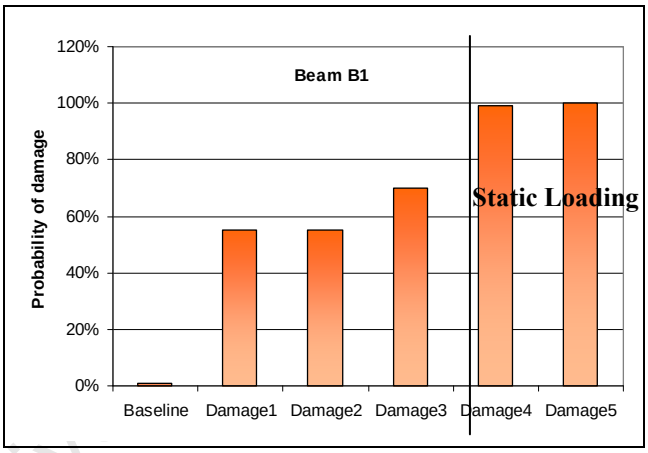

Figure 5.20: The probability of damage in beam B1 at different test sessions.

Figure 5.20 shows the probability of damage in beam B1 at the different test sessions, based on the areas below the probability density plots of the damage-sensitive features in Figure 5.19. For example, for the damage-sensitive features corresponding to Damage3, 70 % of the area below the probability density curve fell to the right of the threshold value. Therefore, it can be said that, at the time of testing, the probability that beam B1 was damaged was 70 %. Similarly, based on the selected threshold, it can be said that there is a 100 % probability that beam B1 was damaged at the state of damage represented by Damage5. The ARX technique appears to have detected a general increase in the probability of damage from one test session to another.

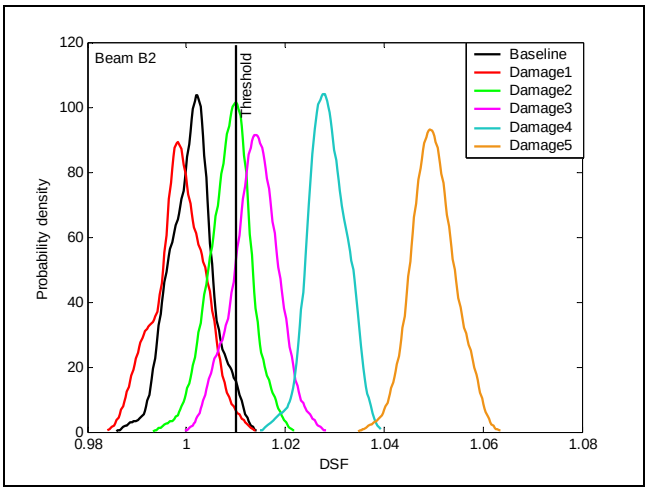

Figure 5.21: The sampled probability distributions of the damage-sensitive features of beam B2 at the various states of damage.

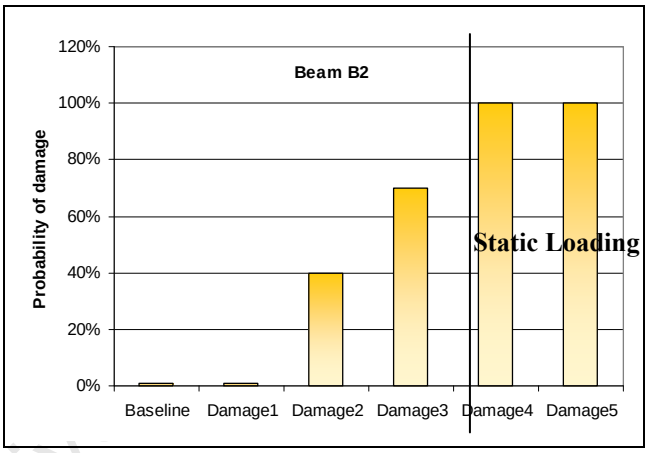

Figure 5.22: The probability of damage in beam B2 at different test sessions.

For damage detection in beam B2, the threshold was again set at the upper one-sided 99 % confidence interval on the damage-sensitive features of the Baseline data. Figure 5.22 shows the probabilities of damage in beam B2 based on the areas below the probability density curves of the damage-sensitive features and to the right of the threshold value. The ARX technique appears to have detected a general increase in the probability of damage from one test session to another.

It must be noted that the controls, beam C1 and beam C2, were not subjected to accelerated corrosion. They were, however, both subjected to the same static loading regime that was applied

to beams B1 and B2 at Damage4 and Damage5 (Section 5.4.2). Figure 5.23 and Figure 5.24 show that, for control beam C1, the first four damage states represent low probabilities of the presence of damage. Indeed, with the threshold set at the upper one-sided 99 % confidence interval on the damage-sensitive features of the Baseline data, the maximum probability of damage for the first four damage states was 2 %, corresponding to Damage2.

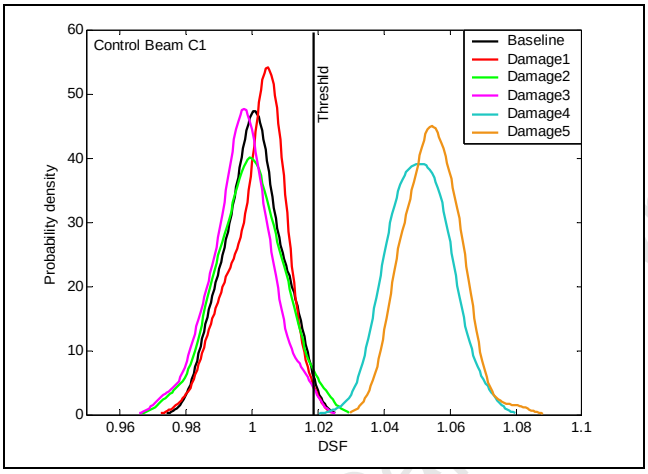

Figure 5.23: The sampled probability distributions of the damage-sensitive features of control beam C1 at the various states of damage.

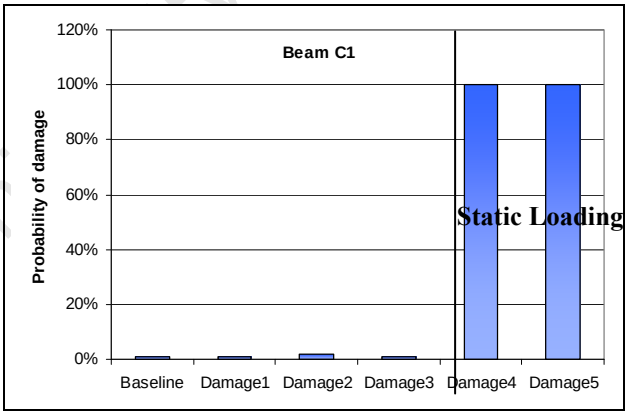

Figure 5.24: The probability of damage in control beam C1 at different test sessions.

As with control beam C1, the first four damage states in the control beam C2 were characterized by low probabilities of damage when assessed using the ARX damage detection technique (Figure 5.25 and Figure 5.26). With the threshold set at the upper one-sided 99 % confidence interval on the damage-sensitive features of the Baseline data, the highest probability of damage

for the first four damage states was 5 %, corresponding to Damage2. Again, a marked increase in the probability of damage was evident in the last two damage states, with a probability of damage of 20 % for Damage4 and 18 % for Damage5 (Figure 5.26).

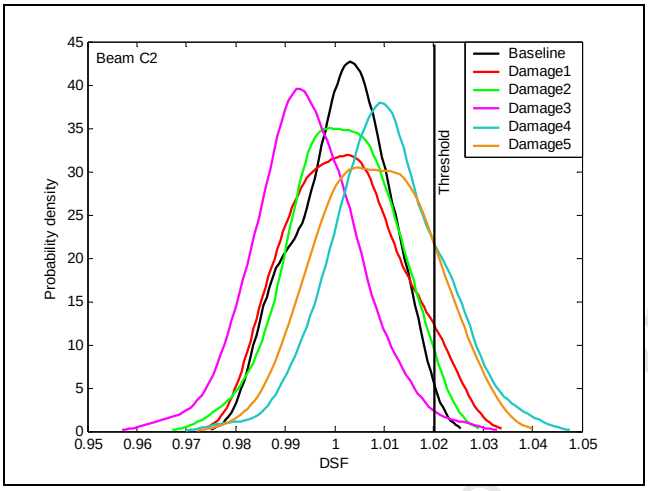

Figure 5.25: The sampled probability distributions of the damage-sensitive features at the various states of damage for control beam C2.

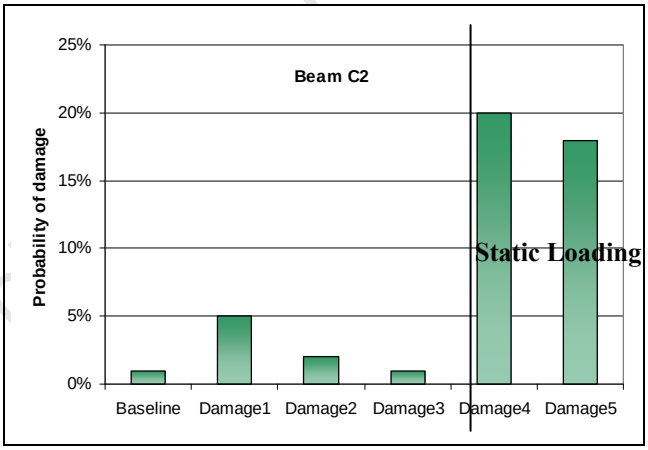

Figure 5.26: The probability of damage in control beam C2 at different test sessions.

The results of the application of the ARX damage detection technique to experimental data using the probability density based feature discrimination framework are summarised in Figure 5.27 and Figure 5.28.

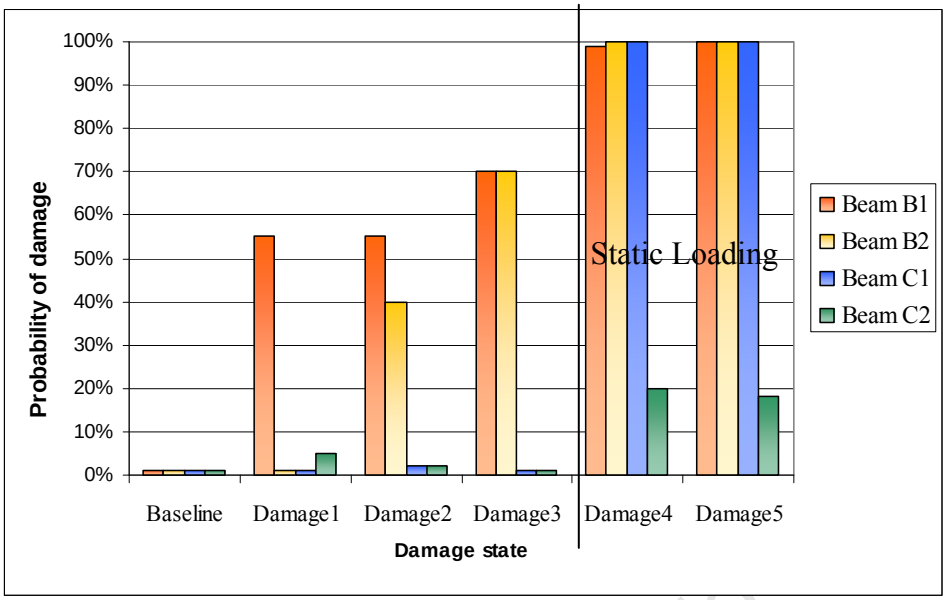

Figure 5.27: Summary of the damage discrimination achieved by applying the ARX feature extraction technique and the probability density based feature discrimination. Damage4 and Damage5 incorporated equal static loading for all beams.

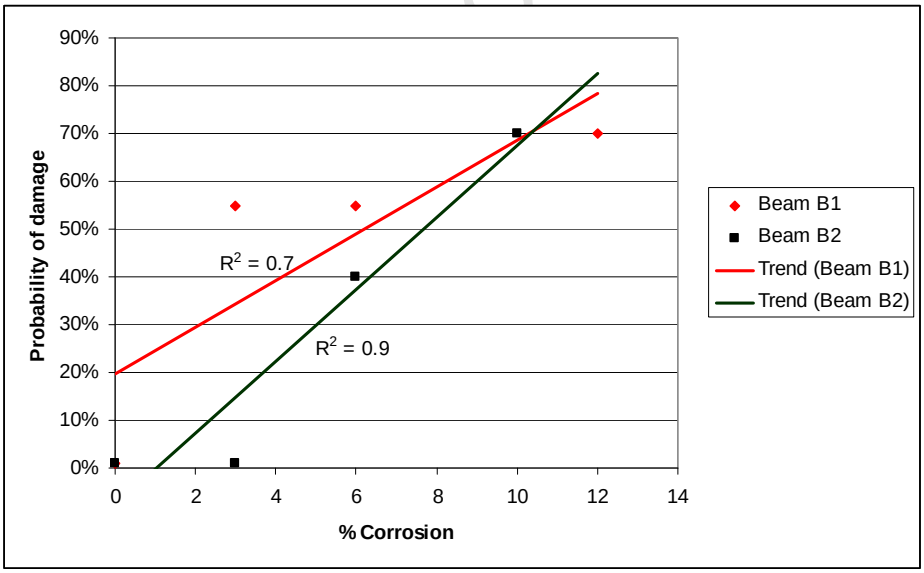

Figure 5.28: The correlation between the percentage of corrosion and the probability of damage for beams B1 and B2. The results for the beams after static loading are not included.

5.5.3.2 Outlier analysis based feature discrimination

The outlier analysis based feature discrimination framework was applied to the *DSF*s of the beams at different damage states (Figure 5.18). Because the Mahalanobis discordancy calculation assumes that the reference data set is normally distributed, it was necessary to test for normality. Normally distributed data has a kurtosis of three and a skewness of zero. The kurtosis and skewness of the Baseline data for all four beams were shown to be close to these values (Table 5).

Table 5: Kurtosis and skewness of the baseline data for each test beam.

	Kurtosis	Skewness
Beam B1	2.4	0.03
Beam B2	3.2	-0.03
Beam C1	2.5	-0.02
Beam C2	2.3	-0.2

Normal probability plots of the baseline data for each beam are also shown in Figure 5.29. A linear scatter of the data on a normal probability plot indicates a normally distributed data set. Therefore there is sufficient evidence to assume that the distributions of the data sets are near normal.

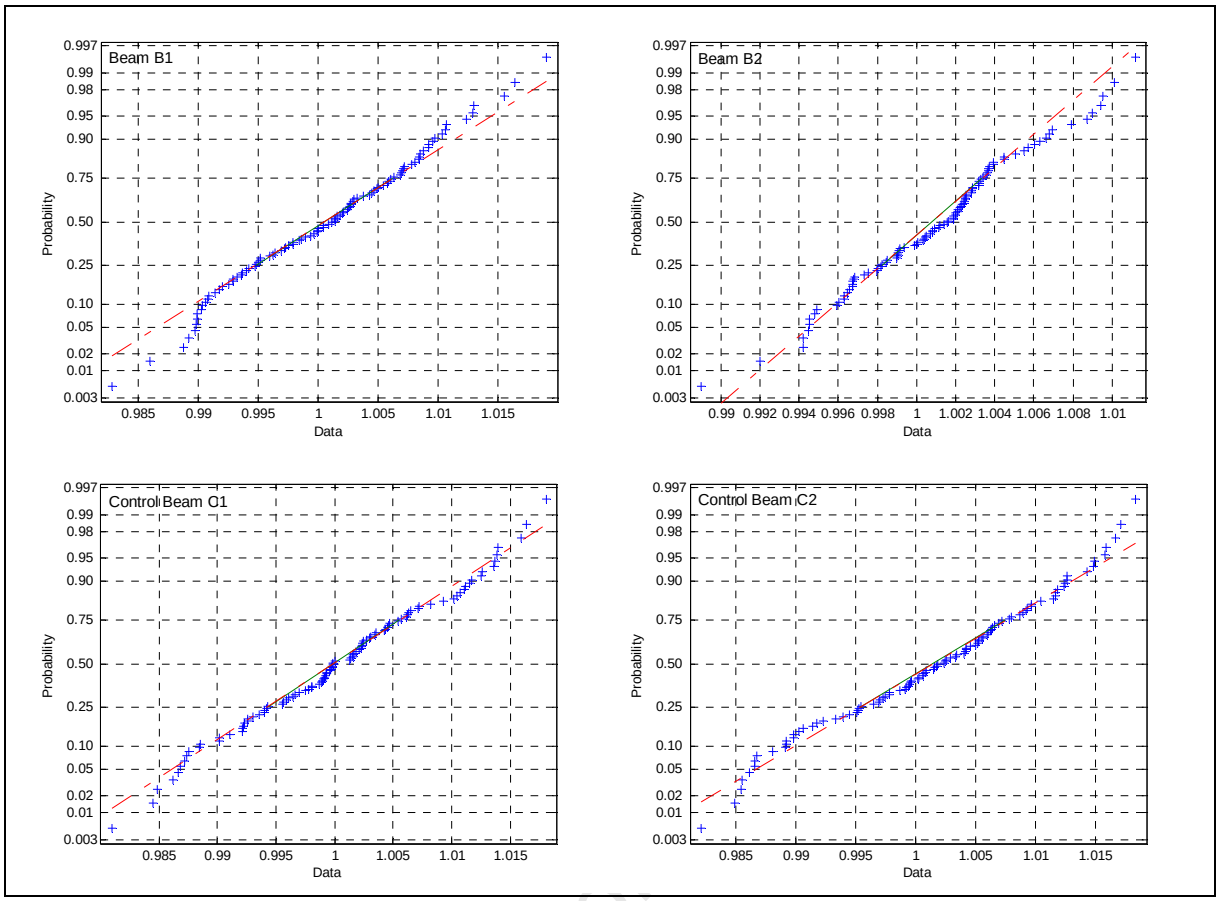

Figure 5.29: Normal probability plots for the Baseline *DSF*s of each test beam

A 5 % discordancy threshold was adopted for the outlier analysis. The percentage of discordancy measures that exceeded the threshold generally increased from one damage state to another for both beams B1 and B2 (Figure 5.30). The ARX technique appears to have detected a general increase in the probability of damage from one test session to another in beams B1 and B2. The control beams C1 and C2 had low probabilities of the presence of damage for the first four damage states but showed an increase in the percentage of discordancy measures exceeding the threshold value after the inclusion of static loading in the test procedure (Figure 5.31).

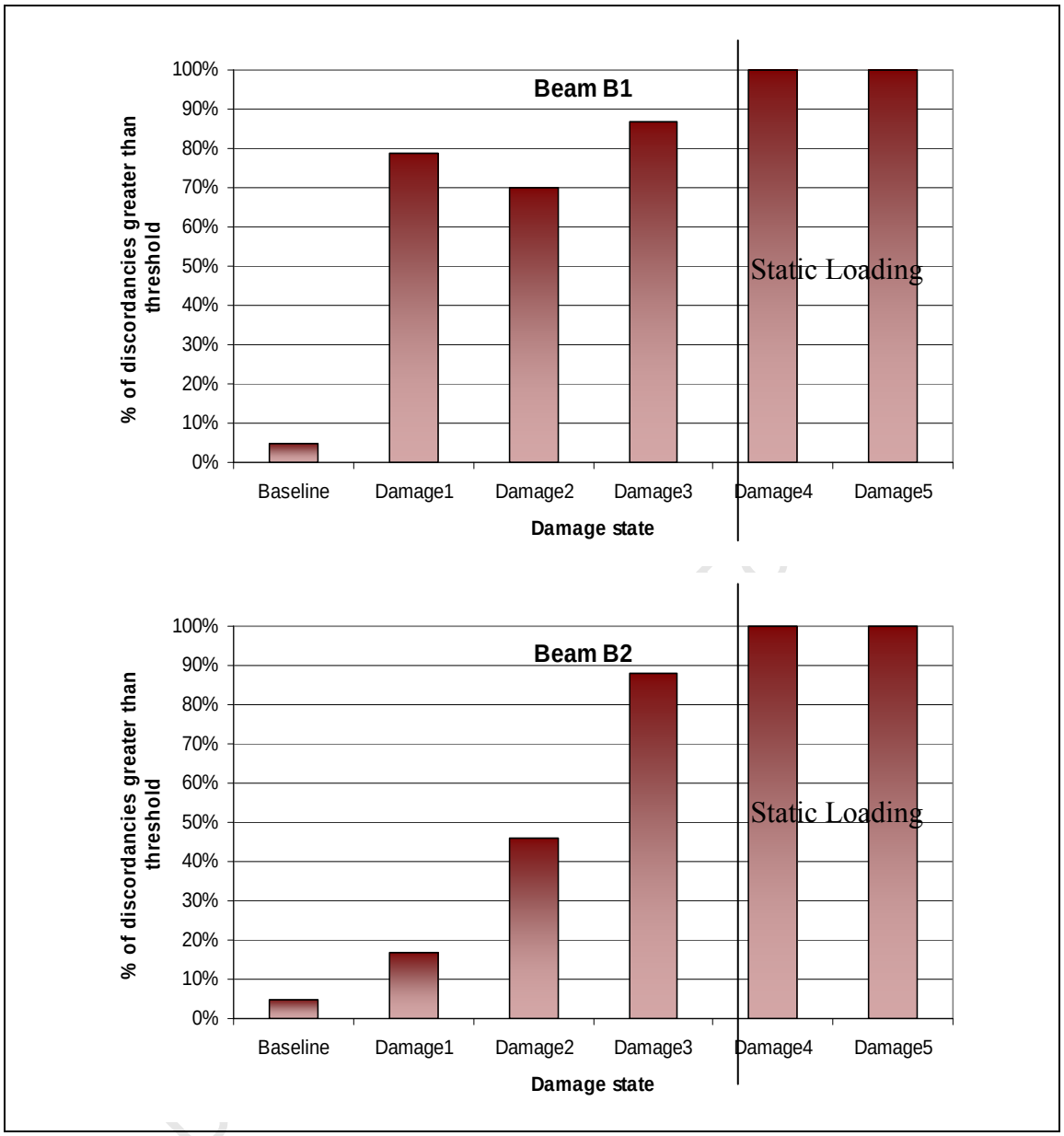

Figure 5.30: Outlier analysis based feature discrimination applied to the DSFs of beams B1 and B2 at different temperatures. A 5 % discordancy threshold was adopted

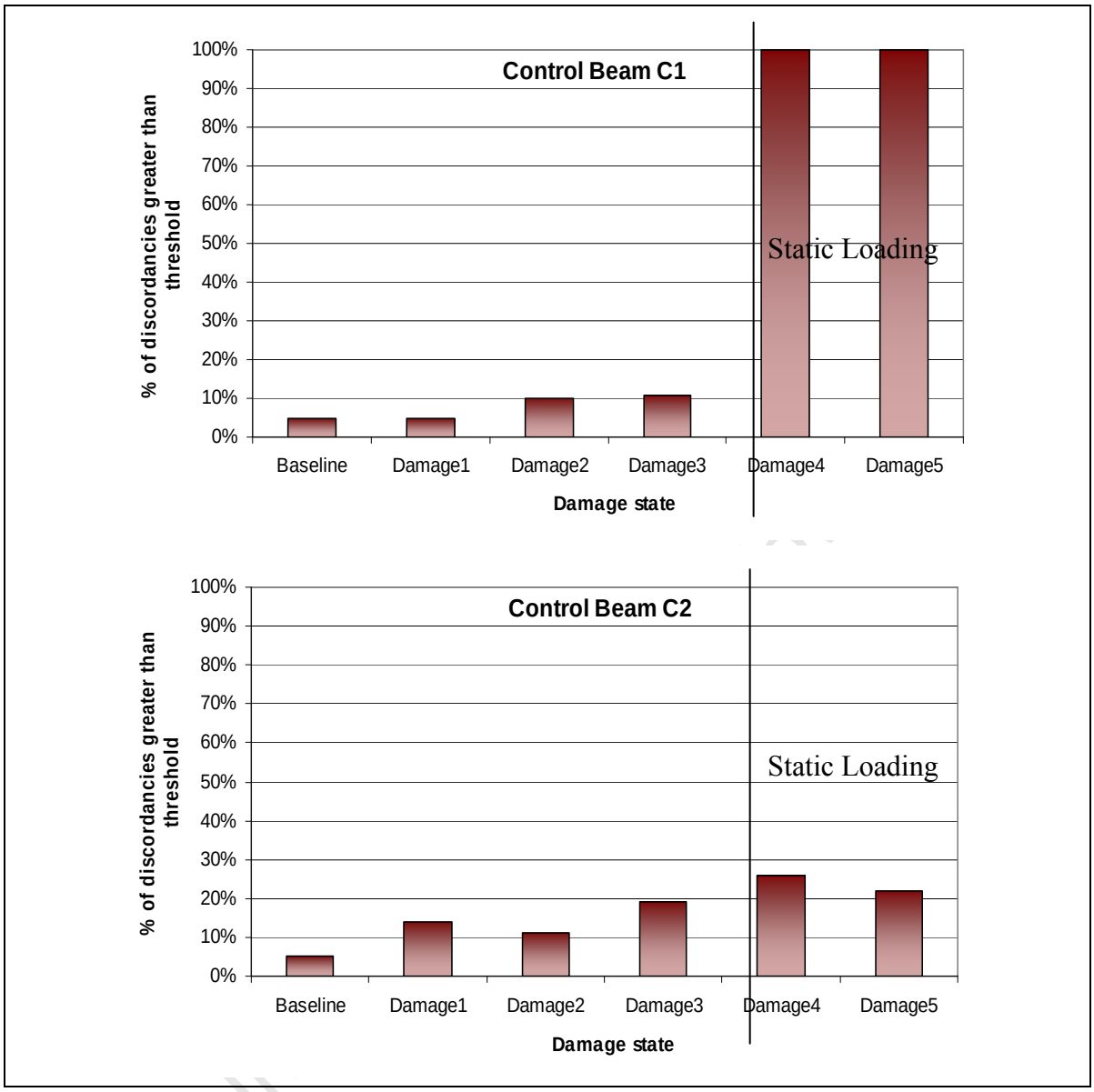

Figure 5.31: Outlier analysis based feature discrimination applied to the DSFs of beams C1 and C2 at different temperatures. A 5 % discordancy threshold was adopted.

The results of the application of the ARX damage detection technique to experimental data using the probability density based feature discrimination framework are summarised in Figure 5.32 and Figure 5.33).

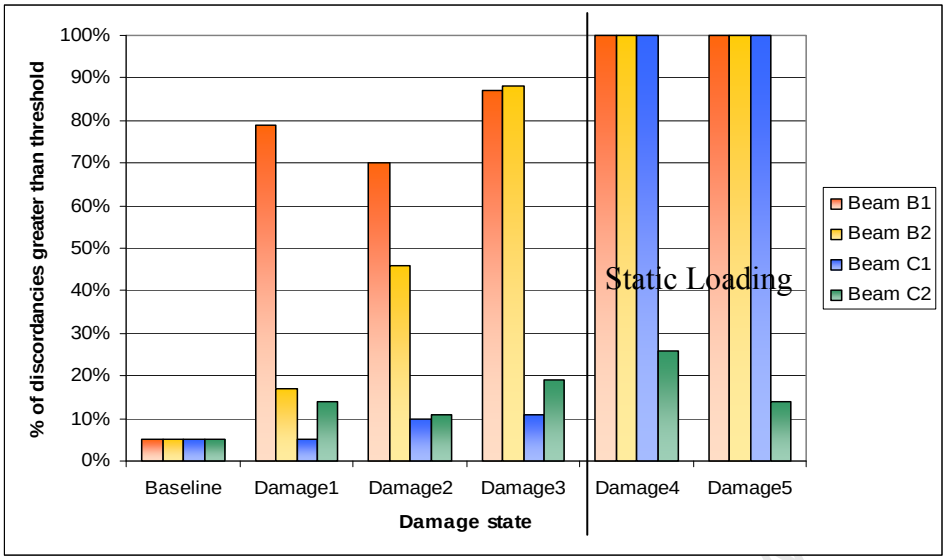

Figure 5.32: Summary of the damage discrimination achieved by applying the ARX feature extraction technique and the outlier analysis based feature discrimination. Damage4 and Damage5 incorporated equal static loading for all beams.

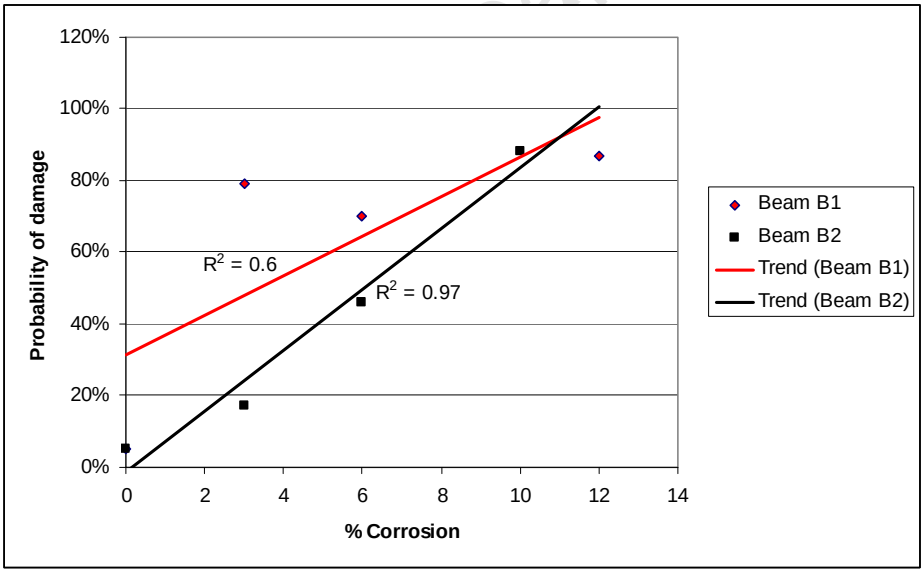

Figure 5.33: The correlation between the percentage of corrosion and the probability of damage for beams B1 and B2. The results for the beams after static loading are not included.

5.6 Discussion of the results of experiments to assess the ARX damage detection technique

This section comments on the issues highlighted by the results of the experiments and provides explanations for certain observations.

5.6.1 Detection of corrosion damage

Inspection of Figure 5.27 and Figure 5.32 reveals that the damage detection algorithm was capable of detecting damage due to corrosion of the steel reinforcement. Furthermore, the trend lines in Figure 5.28 and Figure 5.33 with fairly high correlation coefficients (R^2 values) demonstrate a positive correlation between the degree of corrosion in the steel reinforcement and the probability that damage is detected. Since the control beams C1 and C2 experienced no accelerated steel corrosion, low probabilities of damage were observed in these beams, as expected. This provided evidence that the higher probabilities of damage observed in beams B1 and B2 were due to the effects of the accelerated corrosion of their reinforcement.

Corrosion of steel reinforcement results in the reduction of the steel diameter and cross-sectional area. Figure 5.34 shows that very high degrees of corrosion would be required to significantly reduce the steel diameter and the cross-sectional area. For example, at 6 % corrosion each reinforcement bar would have a diameter of 9.7 mm and the total cross sectional area in the beam section would reduce by less than 10 mm^2. Despite the subtle changes in the steel itself, 6 % corrosion resulted in about 60 % probability of damage in beam B1 and 40 % probability of damage in beam B2 when assessed using the ARX damage detection technique.

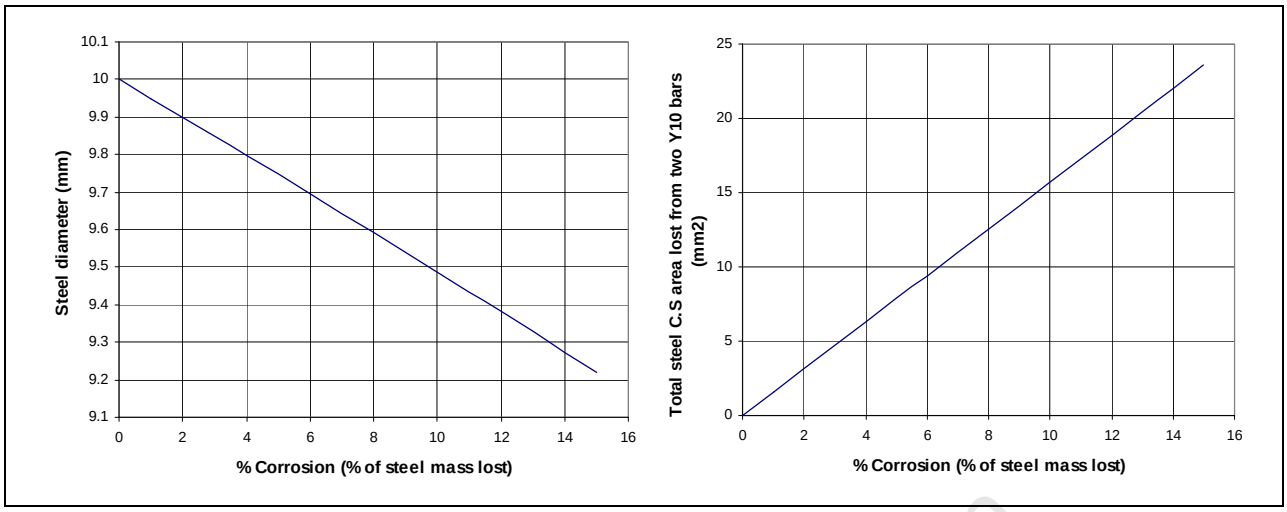

Figure 5.34: The theoretical relationship between the degree of corrosion and the diameter of the steel reinforcement for a Y10 bar.

This observed sensitivity of the damage sensitive features to steel corrosion in concrete can be attributed to the contributions of other effects of steel reinforcement corrosion. For example, the corrosion of longitudinal steel reinforcement in a concrete beam induces longitudinal cracks. Indeed, at about 6 % corrosion, fine longitudinal cracks were visible on the tension face of beams B1 and B2 (Table 2). While cracks that are parallel to the plane of bending may not affect the bending stiffness of the beam (Figure 7.1), they may change the dynamic behaviour of the beam in the vicinity of the cracks. Friction between adjacent surfaces in the crack may change properties such as damping.

5.6.2 The effects of in-service loading

The damage detection technique proposed here was shown to be sensitive to static loading. Figure 5.27 and Figure 5.32 showed marked increases in the probability of damage in all beams (including the control beams C1 and C2) after static loading. This can be attributed to transverse cracks forming in the tension zone of the beams (Figure 5.35). Transverse cracks reduce the effective area of a beam, thereby reducing the bending stiffness. Structures in service are subjected to static loading and their concrete members are expected to crack in the tension zone. In order to isolate the effects of normal service loading from the effects of corrosion damage, the reference data must be collected from the loaded (cracked) structure. This would prevent false-

positive diagnoses of damage due to the formation of transverse cracks in the tension zone of reinforced concrete members.

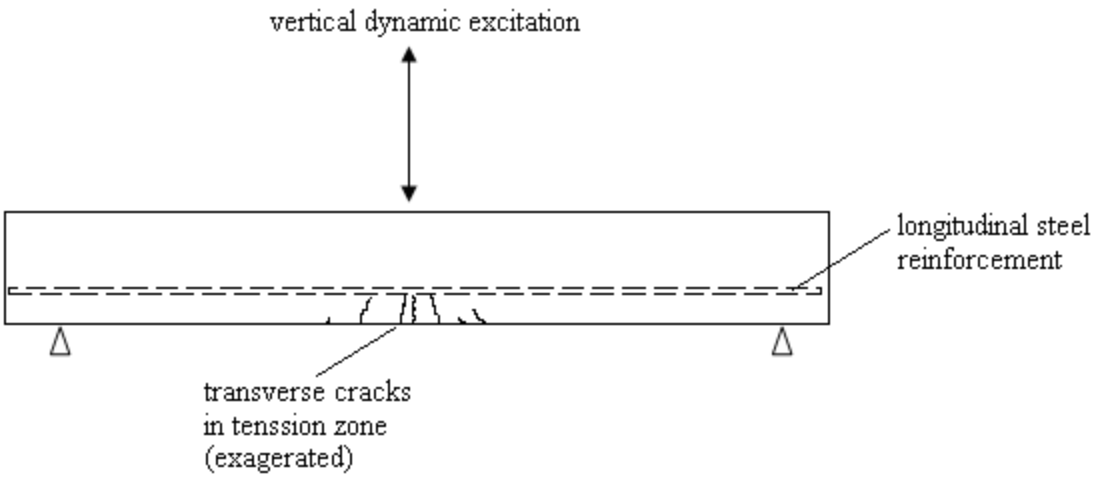

Figure 5.35: Vibration tests were carried out on the beams after inducing transverse cracks using static loads.

The same static loading regime was applied at test session Damage4 as at test session Damage5. An estimated increase of 3 % in the degree of corrosion was introduced in beams B1 and B2 between the two test sessions. It is clear from Figure 5.19 and Figure 5.21 that there is a separation of damage sensitive features between Damage4 and Damage5 in beams B1 and B2. Possible reasons for this are proposed:

1. If the static loading at Damage4 was just sufficient to cause transverse cracks that terminated at the level of the steel reinforcement, further application of the same loading regime at Damage5 would not cause further cracking in the beams. Therefore the two distinct damage states observed between Damage4 and Damage5 resulted from an increase in the degree of corrosion between Damage4 and Damage5.
2. The added energy provided by the static load at Damage5 exacerbated the loss of bond between the steel and concrete.
3. The static loads applied at Damage4 may have been insufficient to cause cracks terminating at the level of the steel reinforcement. Due to experimental errors (such as slightly different rates of loading, durations of loading, magnitudes of loading or locations of loading) the effects of the static loads applied at Damage5 may have differed

from the effects of the static loads applied at Damage4. The static loading at Damage5 could have caused the transverse cracks to propagate further, reducing the effective cross-sectional area of the beams at Damage5. This would result in two distinct damage states of the beams.

5.6.3 The choice of feature extraction technique

As no two structures are identical, the dynamic responses of all structures differ from each other. This is especially so when dealing with a composite material such as concrete, which has an inhomogeneous microstructure. It is possible that a feature extraction technique that yields features that are extremely sensitive to damage in one structure may yield features that are insensitive to damage in another structure. An example of this is the greater sensitivity of he ARX features to the early stages of corrosion in beam B1 than in beam B2. Therefore a damage detection technique applies to a specific structure and may not necessarily be directly applicable to another structure.

5.7 Summary

The following constitute the main points of the chapter:

- Laboratory experiments were conducted to assess whether the damage detection frameworks, incorporating uncertainty quantification, could successfully diagnose the damage state of test structures in the presence of instrumentation errors and changing environmental conditions.
- The adopted feature extraction technique consisted of an algorithm that compared the residual errors of an ARX(2,1) model fitted to a reference dynamic system with the residual errors of the same model fitted to a potentially damaged dynamic system. The damage-sensitive feature was chosen as the ratio between the standard deviation of the residual errors for the ARX(2,1) model applied to the reference data and the standard deviation of the residual errors when the same model is fitted to data from an unknown structural state. Both the probability density feature discrimination technique and the outlier analysis feature discrimination technique were investigated on experimental data.

- To account for instrumentation errors, the equipment and setup were calibrated to determine the errors associated with a particular set of test equipment. The probability density function (PDF) of these errors could then be estimated and the resulting uncertainty accounted for using Monte Carlo simulations.
- The test structures were steel-reinforced concrete beams. Damage was gradually introduced into the beams by the accelerated corrosion of their steel reinforcement, and vibration tests were conducted on the beams at various degrees of corrosion and different core temperatures of the beams. Control beams, which were not subjected to any corrosion damage, were included to test for false-positive damage diagnoses.
- The results of the application of the proposed damage detection frameworks to the test data revealed a high correlation between the degree of corrosion and the probability that the structure was damaged. The chosen damage-sensitive feature proved to be insensitive to changes in the core temperature of the beams. It, however, showed some sensitivity to static loading, highlighting the importance of the collection of reference data after typical service loading of the structure.
- It is possible that a feature extraction technique that yields features that are extremely sensitive to damage in one structure may yield features that are insensitive to damage in another structure. Therefore, a damage detection technique should be developed for application to a specific structure.

Chapter 6

6 Conclusions

The aim of the research was to investigate the application of non-model-based vibration-based damage detection techniques to the detection of reinforcement corrosion damage in concrete structures, and to develop a practical framework that quantifies the uncertainty in the damage detection techniques in the presence of changing environmental and operational conditions. The objectives of the research were met, and the conclusions drawn are summarized below.

6.1 Detection of damage

It was concluded that the ARX damage detection technique was capable of detecting the damage brought about by corrosion of the longitudinal steel reinforcement in concrete beams. Similar frameworks for damage detection can be applied to civil structures. The results of the experiments conducted in this research demonstrated that the adopted feature extraction technique must be specific to the structure being monitored because a feature extraction technique that yields features that are extremely sensitive to damage in one structure may yield features that are insensitive to damage in another structure. Factors to consider when developing the damage detection technique include the nature of in-service loading and the environmental and operational effects that affect the chosen damage-sensitive features.

6.2 Quantification of uncertainty

The need for the detection of subtle damage leads to problems associated with the sensitivity of the damage detection techniques to uncertainties. The frameworks proposed in this thesis accounted for instrumentation errors and errors due to changes in temperature. These frameworks can however be generalised to account for other environmental and operational effects by developing a comprehensive reference database of the adopted damage sensitive features. Because of the uncertainty quantification included in the damage detection frameworks, it was possible to show that the ARX damage detection technique was insensitive to

experimental errors resulting from temperature changes, for the particular structure under investigation. The damage detection frameworks proposed here were able to output quantitative measures of the certainty in their diagnoses. For the management of civil infrastructure, a diagnosis accompanied by a quantitative measure of confidence in that diagnosis would allow for informed, less subjective decision making and risk assessments.

6.3 Applicability of the damage detection frameworks to civil infrastructure

The frameworks developed in this thesis have been categorized as vibration-based damage detection techniques. Such techniques were shown to be desirable for their non-destructive nature, their potential for global system monitoring and their potential for full automation. More specifically, *non-model-based* vibration-based damage detection techniques are preferred to model-based techniques due to the difficulty and computational expense of accurately modelling complex structures and their support conditions.

Civil infrastructure suffers from subtle and complex forms of damage, such as the deterioration brought about by steel reinforcement corrosion in concrete structures and due to the problems brought about by uncontrollable environmental and operational conditions. The frameworks developed in this thesis for the detection of damage address these complexities and are therefore applicable to the structural health monitoring of civil infrastructure.

Chapter 7

7 Recommendations for future research

Based on the findings of this thesis, the following recommendations are made for future research into corrosion damage detection in civil infrastructure.

7.1 The direction of dynamic excitation

Since one of the characteristics of steel reinforcement corrosion is the formation of cracks parallel to the corroding steel, it would be desirable to make the damage detection technique more sensitive to longitudinal cracks, which are caused by corrosion, than to transverse cracks, which may be caused by normal service loading. It is likely that an alternative arrangement for the dynamic excitation and measurement during vibration tests would yield data that is more sensitive to longitudinal cracks. This point can be illustrated with the aid of Figure 7.1:

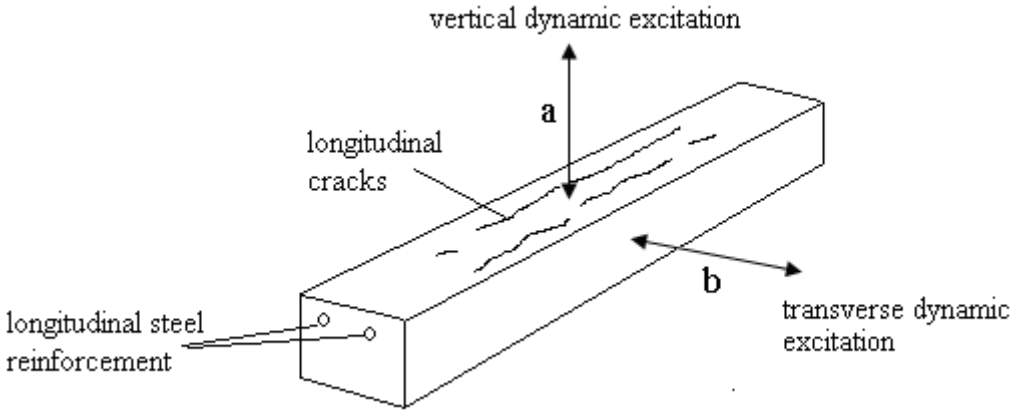

Figure 7.1: Alternative directions for dynamic excitation for the detection of corrosion damage. Direction (a) was adopted in this thesis. Direction (b) is proposed for future research.

Cyclic loading in the direction ‘a’ in Figure 7.1 was adopted in this thesis. Vibration in the direction ‘a’ is controlled by stiffness about a bending axis parallel to direction ‘b’ and, conversely, vibration in the direction ‘b’ is controlled by stiffness about a bending axis parallel to direction ‘a’. Therefore, cracks parallel to the reinforcing steel bars do not affect the flexural

stiffness of the beam bending about an axis parallel to direction ‘b’. The longitudinal cracks have very little effect on the position of the neutral axis and will not affect stiffness unless either: they are wide enough to significantly reduce the bond between the steel and concrete, the de-bonded area is so long that there is insufficient anchorage for the steel bars, or the applied cyclic load is large enough to cause flexural cracks in the beam (Cairns *et al.* 1993).

For the stiffness about a bending axis parallel to direction ‘a’ the longitudinal cracks can be viewed as having divided the beam into three sections of smaller depth, similar to delamination. Therefore, it is likely that applying an excitation in direction ‘b’, and recording the vibrations in the same direction, will yield data that is more sensitive to the type of damage caused by corrosion of longitudinal steel reinforcement in concrete beams.

7.2 The method of inducing controlled damage

In-service infrastructure is continuously subjected to static loads. Therefore, any laboratory experiments aimed at developing damage detection techniques, and conducted on physical models, should attempt to simulate service loading. The reference vibration data and all subsequent data must be collected from the test structure while subjected to service loads. The use of control specimens would confirm whether only deliberate damage due to induced corrosion of steel reinforcement has been detected.

7.3 Non-linear behaviour of cracked concrete

When a dynamic excitation is applied to a cracked concrete beam, the cracks open and close as the beam vibrates. The amplitude of the excitation force affects how wide the cracks open. As a result, the dynamic response, particularly the natural frequency of the beam, is affected by the amplitude of the excitation. This has obvious implications for damage detection in concrete structures, as non-linear behaviour may result in false diagnoses if excitation levels vary from one test session to another. While excitation levels in the experiments conducted in this study were kept essentially the same from one test session to another, damage detection techniques need to be assessed for the effects of the non-linear behaviour of cracked concrete.

7.4 Management of reference databases of damage-sensitive features

Since the detection of outliers is dependent on the probability distribution of the damage-sensitive features in the reference database, care must be taken that in attempting to represent a wide range of environmental and operational conditions in the database, there is no distortion of the probability distribution of the damage-sensitive features. This could arise, for example, by including data from less likely environmental conditions in similar proportions to data from more prevalent environmental conditions. A possible solution to this problem is to identify the environmental and operational conditions that affect the damage-sensitive features, and then develop separate reference databases that correspond to particular periods in time when these conditions prevail. The different categories of reference data could, for example, correspond to different seasons of the year and different times of the day. New data can then be compared with the database category that matches the season and time of day that it was collected. The procedure would be equally applicable to both the probability density based feature discrimination framework and the outlier analysis based feature discrimination framework proposed in this thesis. Barring extreme and unusual conditions, effective management of reference databases could ensure that direct measurements of environmental and operational conditions are not required for non-model-based vibration-based damage detection techniques.

References

1. Bae, H. 2004. *Uncertainty quantification and optimization of structural response using evidence theory.* Ph.D. dissertation, Wright State University, U.S.A.
2. Bae, H., Grandhi, R., Canfield, R. 2004. *Epistemic uncertainty quantification techniques including evidence theory for large-scale structures.* Computers and Structures 82 (2004) 1101-1112. Elsevier.
3. Barnett, V., Lewis, T. 1994. "Outliers in statistical data". Third Edition. Chichester. John Wiley Sons Ltd.
4. Basu, B. 2005. *Identification of stiffness degradation in structures using wavelet analysis.* Construction and Building Materials 19 (2005) 713–721. Elsevier.
5. Berleant, D., Ferson, S., Kreinovich, V., Lodwick, W. 2005. *Combining interval and probabilistic uncertainty: Foundations, algorithms, challenges – An overview*. 4th International Symposium on Imprecise Probabilities and Their Applications, Pittsburgh, Pennsylvania.
6. Box, G., Jenkins, G., Reinsel G. 1994. "Time Series Analysis: Forecasting & Control". Third Edition. New Jersey: Prentice-Hall Inc.
7. Brown, R., Geoghegan, M., Baker, M. 1983. *Corrosion of reinforcement in concrete construction.* A.P. Crane, London. ch. 13.
8. Cairns, J. 1993, *Behaviour of concrete beams with exposed reinforcement.* In Proceedings of the institution of civil engineers, structures and buildings. Vol 99. pg. 141-154
9. Castrup, H. 1992. *Practical Methods for Analysis of Uncertainty Propagation*. In Proceedings of the 38th Annual ISA Instrumentation Symposium, Las Vegas.
10. Castrup, H. 2004. *Estimating and Combining Uncertainties.* In 8th Annual ITEA Instrumentation Workshop, Lancaster, California.
11. Cattarius, J., Inman, D. 1996. *Time domain analysis for damage detection in smart structures.* Mechanical Systems and Signal Processing (1997) 11 (3), 409-423. Academic press limited.
12. De Vos Theron, G. 1994. *Effects of reinforcement corrosion on the structural performance of reinforced concrete beams.* MSc. Thesis. University of Cape Town. South Africa.

13. Doebling, S. W. and Hemez, F. M. 2001. *Overview of Uncertainty Assessment for Structural Health Monitoring*. In Proceedings of the 3rd International Workshop on Structural Health Monitoring, Stanford University, Stanford, California
14. Donders, S., Vandepitte, D., Van de Peer, J., Desmet, W. 2005. *Assessment of uncertainty on structural dynamic responses with the short transformation method.* Journal of Sound and Vibration 288 (2005) 523–549. Elsevier.
15. Dong, C., Zhang, P., Feng, W., Huanng, T. 1994. *The sensitivity study of the modal parameters of a cracked beam*. Proceedings of the 12th IMAC, 98-105, Honolulu.
16. Elsener, B. 2001. *Half-cell potential mapping to assess repair work on RC structures.* Construction and Building Materials 15 (2001) 133-139. Elsevier.
17. Fassois, S., Sakellariou, J. 2006. *Time series methods for fault detection and identifcation in vibrating structures.* Proceedings of the Royal Society: Mathematical, Physical and Engineering Sciences (London, UK).
18. Ferson, S., Ginzburg, L. 1996. *Different methods are needed to propagate ignorance and variability. Reliability Engineering and System Safety* 54 (1996) 133-144. Elsevier Science Limited
19. Fonseca, J., Friswell, M., Mottershead, J., Lees, A. 2005. *Uncertainty identification by the maximum likelihood method*. Journal of Sound and Vibration 288 (2005) 587–599. Elsevier.
20. Fugate, M., Sohn, H., Farrar, C. 2001. *Vibration-based damage detection using statistical process control*. Mechanical Systems and Signal Processing 15(4) (2001) 707-721
21. Ha-Won Song, Saraswathy, V. 2007. *Corrosion monitoring of reinforced concrete structures*. International Journal of Electrochemical Science 2 (2007) 1-28.
22. Johnson, T. 2002. *Analysis of dynamic transmissibility as a feature for structural damage detection*. Masters dissertation, Purdue University, Purdue.
23. Keller, G., Warrack, B. 2000. "Statistics for management and economics." Fifth Edition. Duxbury Thomson Learning. London.
24. Kim, H., Melhem, H. 2003. *Damage detection of structures by wavelet analysis.* Engineering Structures 26 (2004) 347–362. Elsevier.
25. Knorr, E., Ng, R., Tucacov, V. 2000. *Distance-based outliers: algorithms and applications*. The VLDB Journal (2000) 8: 237–253. J Widon.

26. Knorr, E. Ng, R. 2001. *A unified approach for mining outliers*. University of British Columbia.
27. Korn, G., Korn, T. 1968. "Mathematical Hanbook of Scientists and Engineers". McGraw-Hill, New York.
28. Kottegoda, N., Rosso, R. 1998. "Statistics, Probability, and Reliability for Civil and Environmental Engineers". McGraw-Hill, International.
29. Kullaa, J. 2002. *Elimination of environment influences from damage-sensitive features in a structural health monitoring system*. In: Proceedings of the 1st European Workshop on Structural Health Monitoring, pp. 742–749.
30. Lu, Y, Gao, F. 2004. *A novel time-domain auto-regressive model for structural damage diagnosis.* Journal of Sound and Vibration 283 (2005) 1031–1049.
31. Marshal, A. 1990. "Marine Concrete". Blackie, London. pp. 291-301.
32. Melchers, R. 1999. "Structural Reliability Analysis and Prediction", second ed., Wiley, New York.
33. Morgan, M., Henrion, M. 2004. "Uncertainty: A Guide to Dealing with Uncertainty in Quantitative Risk and Policy Analysis". Cambridge University Press, Cambridge, NY.
34. Nair, K., Kiremidjian A, Law K. 2005. *Time series-based damage detection and localization algorithm with application to the ASCE benchmark structure*. Journal of Sound and Vibration 291 (2006) 349-368
35. Oberkampf, W. 2005. *Uncertainty quantification using evidence theory*. Presentation for: Advanced Simulation & Computing Workshop Error Estimation, Uncertainty Quantification, and Reliability in Numerical Simulations. Stanford University.
36. Owen, J. S., Pearson, R. 2004. *The use of vibration data for the structural health monitoring of bridges.* United Kingdom
37. Park, J. 2005. *Transer function methods to measure the dynamic mechanical properties of complex structures.* Journal of Sound and Vibration 288 (2005) 57-79.
38. Peeters, B., De Roeck, G. 2000. *One year monitoring of the z24-bridge: environmental influences versus damage events*. In Proceedings of IMAC-XVIII, San Antonio, Texas, USA, February, 2000, pp. 1570–1576
39. Polder, R. 2001. *Test methods for on site measurement of resistivity of concrete – a RILEM TC-154 technical recommendation*. Construction and Building Materials 15 (2001) 125-131. Elsevier.

40. Regan, H., Ferson, S., Berleant, D. 2006 "Equivalence of methods for uncertainty propagation of real-valued random variables". San Diego State University. U.S.A.
41. Rizos, P., Apragathos, N. 1990. *Identification of crack location and magnitude in a cantilevered beam from the vibration modes*. Journal of Sound and Vibration. 138 (1990) 381-388.
42. Smith, L., 2002. *A tutorial on principal components Analysis*. Unpublished.
43. Sohn, H., Farrar, C., Hunter, N., Worden, K. 2001. *Applying the LANL Statistical Pattern Recognition Paradigm for Structural Health Monitoring to Data from a Surface-effect Fast Patrol Boat*. California: Los Alamos National Laboratory.
44. Sohn, H., Farrar, C., Hemez, F., Shunk, D., Stinemates, D., Nadler, B. 2003. *A review of structural health monitoring literature: 1996-2001.* Los Alamos National Laboratory.
45. Sohn, 2003. *Application of extreme value statistics for structural health monitoring.* Los Alamos Laboratory.
46. Taha, M., Lucero, J. 2005. *Damage identification for structural health monitoring using fuzzy pattern recognition*. Engineering Structures 27 (2005) 1774–1783. Elsevier
47. Vanlanduit, S., Parloo, E., Cauberghe, B., Guillaume, P., Verboven, P. 2004. *A robust singular value decomposition for damage detection under changing operating conditions and structural uncertainties*. Journal of Sound and Vibration 284 (2005) 1033–1050. Elsevier.
48. Worden, K., Manson, G., Lord, T., Friswell, M. 2005. *Some observations on uncertainty propagation through a simple non-linear system*. Journal of Sound and Vibration 288 (2005) 601-621. Elsevier.
49. Worden, K., Manson, G., Fiella, N. 1999. *Damage detection using outlier analysis.* Journal of Sound and vibration (2000) 229(3), 647-667. IdealLibrary.com.
50. Worden, K., Tomlinson, G. 2001. "Non-Linearity in Structural Dynamics. Detection, Identification and Modelling." IOP Publishing Ltd. pp. 231
51. Yan, A., Kerschen, G., De Boe, P., Golinval, J. 2005. *Structural damage diagnosis under varying environmental conditions — Part I: A linear analysis.* Mechanical Systems and Signal Processing 19 (2005) 847–864. Elsevier
52. Yan, B.,Miyamoto, A., Bruhwiler, E. 2005. *Wavelet transform-based modal parameter identification considering uncertainty.* Journal of Sound and Vibration 291 (2006) 285-301. Elsevier

53. http://www.wavemetrics.com/products/igorpro/dataanalysis/signalprocessing.htm
54. http://www.bently.com/articles/apnotes/an002.asp
55. http://www.iotech.com/handbook/chapt_2.html

Appendices

Appendices

List of Figures in Appendices

A Matlab Scripts for the ARX damage detection algorithm

A.1 Main scripts

```
function d=tp(a,u,xa,xu,ad,ud,xad,xud,n,nn)
%implements the ARX feature extraction algorithm incorporating Monte Carlo simulations for uncertainty propagation. It returns, for each signal acquired, a row vector of several damage sensitive features

% a is the raw output vibration signal from one channel
% u is the raw input vibraion signal
% xa is the vector of sensor errors obtained from callibration of the output sensor
% xu is the vector of sensor errors obtained from callibration of the input sensor
% n is the number of runs of the monte carlo simulation for propagating the sensor errors through the damage detection algorithm nn is the length of the subsignals that the raw signal is to be split into

starttime
mu=0;
s=std(xa);
m=length(a);
gg=[];
y=ones(m,n);
b=[];
mui=0;
si=std(xu);
mi=length(u);
ggi=[];
bi=[];
muxad=0;
sxad=std(xad);
muxud=0;
sxud=std(xud);
```

```
bxad=[];
bxud=[];

% generate n error vectors
for i=1:n
    kk=normrnd(mu,s,m,1).*y(:,i);
    b=[b kk];
    kki=normrnd(mui,si,mi,1).*y(:,i);
    bi=[bi kki];
    kkxad=normrnd(muxad,sxad,m,1).*y(:,i);
    bxad=[bxad kkxad];
    kkxud=normrnd(muxud,sxud,m,1).*y(:,i);
    bxud=[bxud kkxud];
end

% subtract error vectors
aa=repmat(a,1,n)-b;
uu=repmat(u,1,n)-bi;
aad=repmat(ad,1,n)-bxad;
uud=repmat(ud,1,n)-bxud;

% standardize corrected signals
br=monte_preproc(aa);
bri=monte_preproc(uu);
brad=monte_preproc(aad);
brud=monte_preproc(uud);
g=[];

% split each corrected signal into nn subsignals
for i=1:n;
   oo=br(:,i);
   c=split(oo,nn);
   ooi=bri(:,i);
```

```
    ci=split(ooi,nn);
    ooad=brad(:,i);
    ooud=brud(:,i);
    cad=split(ooad,nn);
    cud=split(ooud,nn);

 % Apply ARX and calculate ratio of standard deviation of residual errors (damaged/baseline)
    ddd=arxresiduals(c,ci,cad,cud);
    g=[g;ddd];       % matrix where each row is many instances of the dmage sensitive feature
end

d=g;

endtime
```

A.2 Sub-scripts

A.2.1 "starttime"

```
function starttime
% Records the start time of the calculation

start_time=DATESTR(NOW)
```

A.2.2 "monte_preproc"

```
function clean=monte_preproc(a)
%  Preprocesses by subtracting the mean then dividing by standard deviation
%  Designed for the matrix "a" being an fxn matrix
b=mean(a);
c=std(a);
d=[];
[f,n]=size(a);

for i=1:n;
   aa=a(:,i);
   bb=b(1,i);
   cc=c(1,i);
   dd=(aa-bb)/cc;
   d=[d dd];
end

clean=d;
```

A.2.3 "split"

```
function j=split(a,k)
%simply splits (with no overlap) a column vector of length p into smaller column vectors each of length
%k and returns them as a matrix.

p=length(a);
h=p/k-1;
j=[];

for i=0:h;
    q=1+i*k;
    r=k+i*k;
    u=a(q:r,1);
    j=[j u];
end
```

A.2.4 "arxresiduals"

```
function ss=arxresiduals(j,u,jd,ud)
% Computes the damage sensitive features

% j is a matrix where each column is a possible outcome of the vibration output signal at the reference (baseline) damage state

% u is a matrix where each column is a possible outcome of the vibration input signal at the reference (baseline) damage state

% jd is a matrix where each column is a possible outcome of the vibration output signal at an unknown (potentially damaged) damage state

% ud is a matrix where each column is a possible outcome of the vibration input signal at an unknown (potentially damaged) damage state

%computes an ARX model of order (2,1) for each pair of columns: the ith column of the output matrix j and the ith column of the input matrix u. It computes the standard deviation of the residual errors and then calculates the mean value of (standard dev damaged residuals)/(standard dev baseline residuals)

[f,v]=size(j);
d=[];
dd=[];
orders=[2 1 0];

for i=1:v;
   a=j(:,i);
   ai=u(:,i);
   ajd=jd(:,i);
   aud=ud(:,i);

   m=arx([a ai],orders);
```

```
    eo=resid(m,[a ai]);
    sigeo=std(eo);
    ed=resid(m,[ajd aud]);
    siged=std(ed);
    d=[d sigeo];
    dd=[dd siged];
end

tr=mean(d);
trd=mean(dd);
ss=trd/tr;
```

A.2.5 "endtime"

```
function endtime
% Records the time at which the calculation ends

end_time=DATESTR(NOW)
```

B Vibration data

B.1 Vibration data at different temperatures

B.1.1 Beam B2

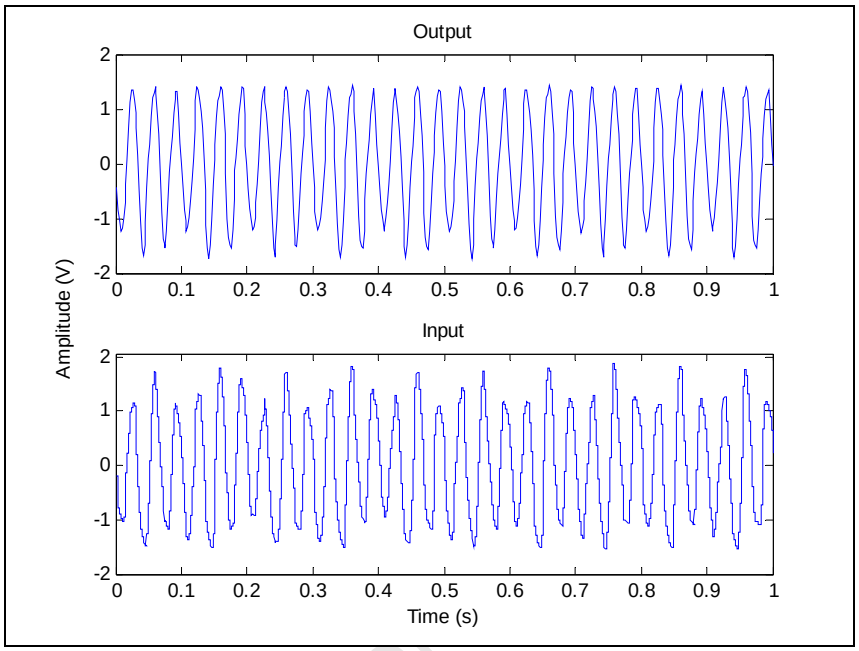

Figure B.1: Beam B2 - 13°C

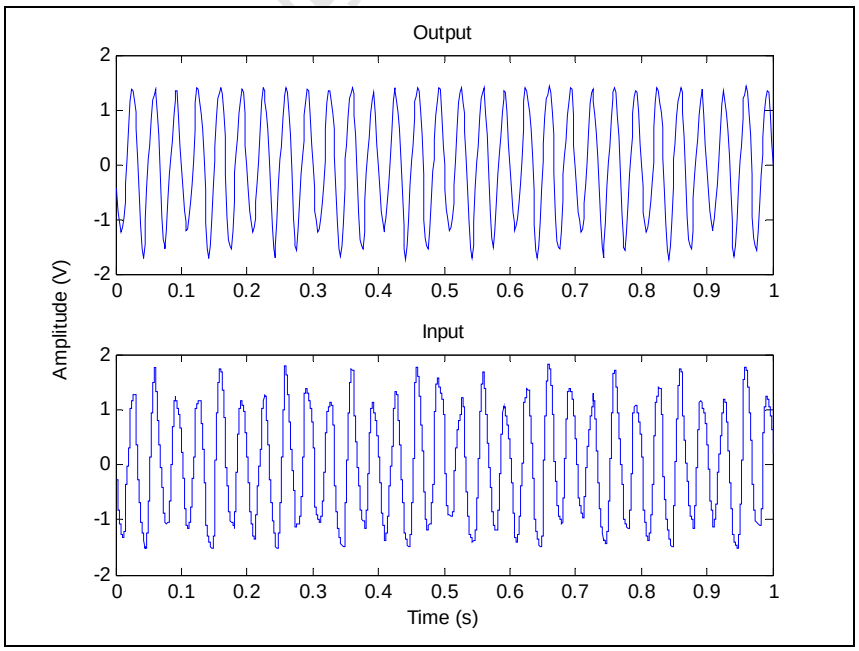

Figure B.2: Beam B2 - 16°C

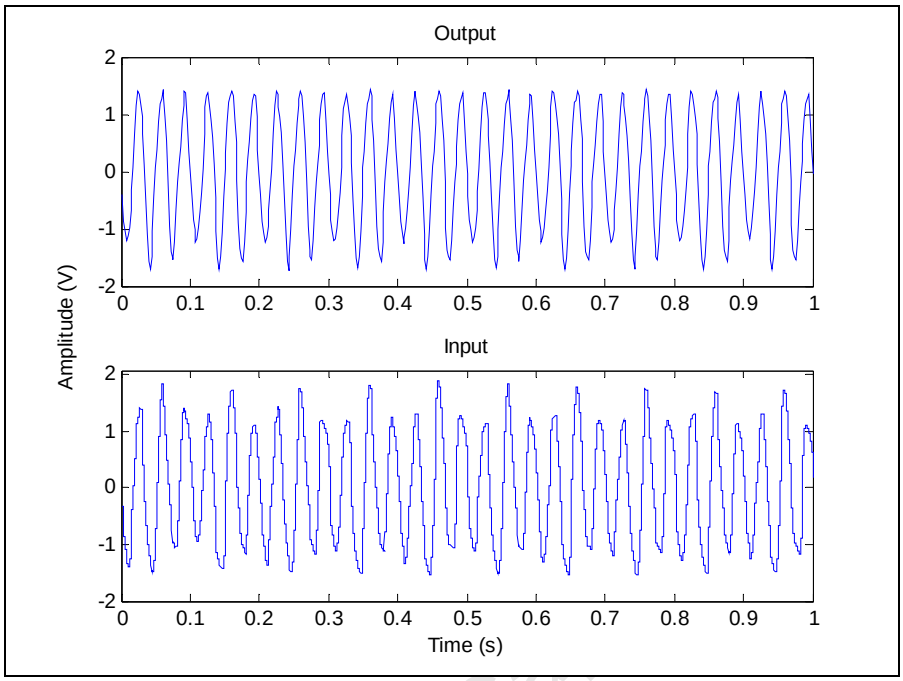

Figure B.3: Beam B2 - 18°C

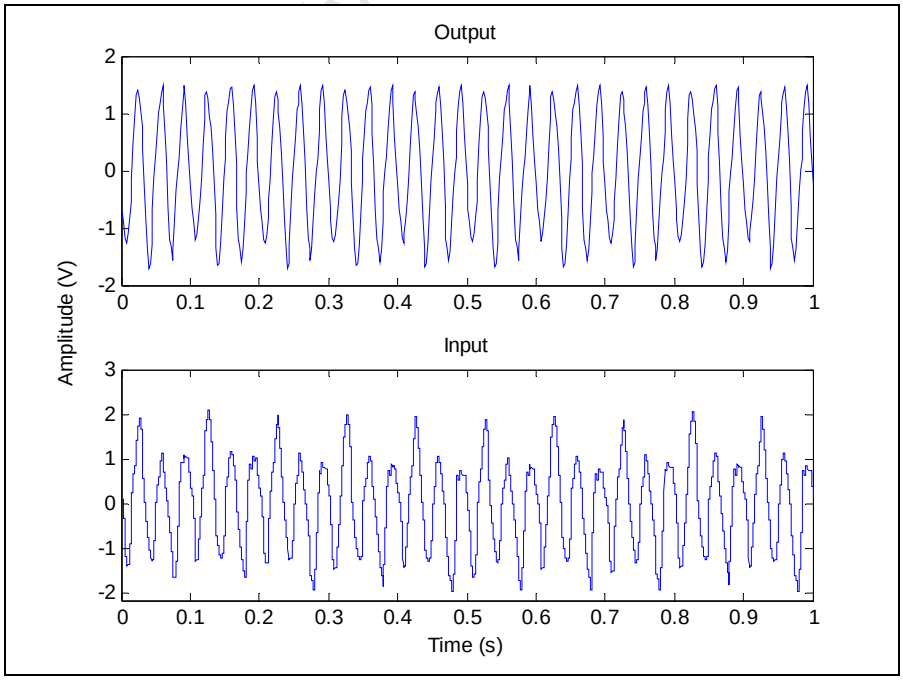

Figure B.4: Beam B2 - 20°C

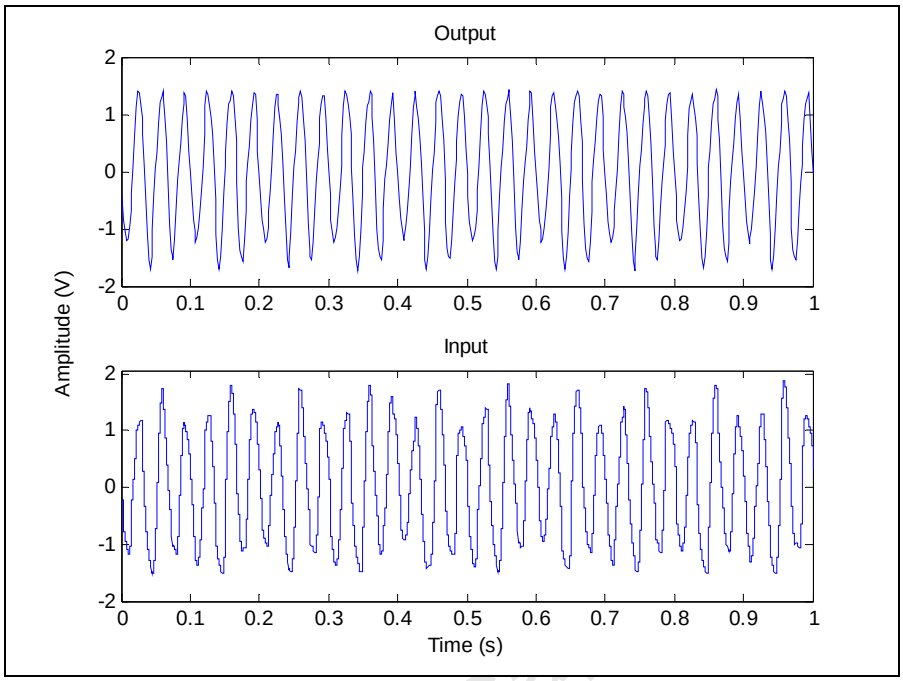

Figure B.5: Beam B2 - 27°C

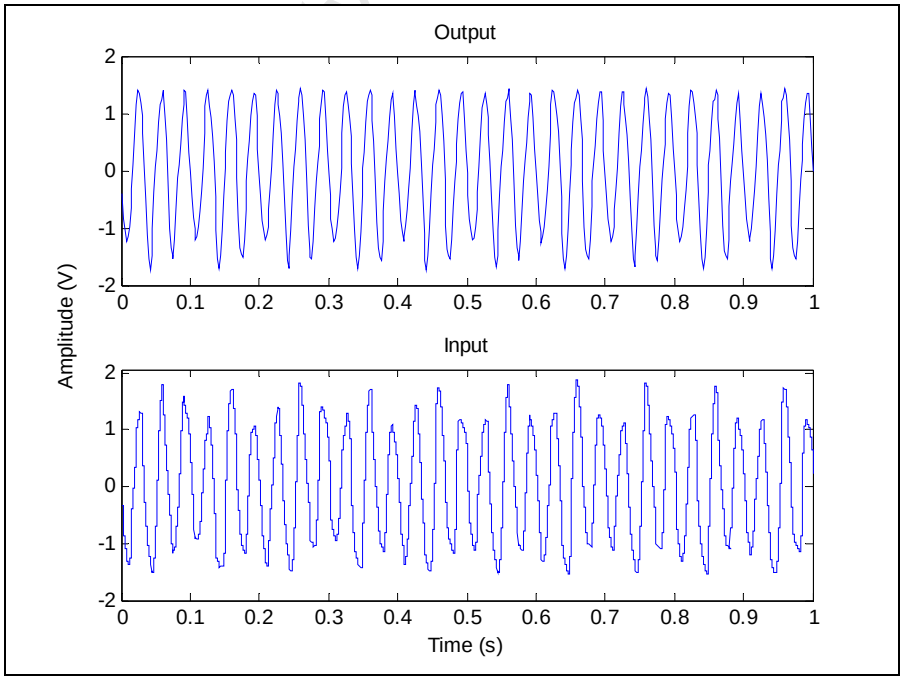

Figure B.6: Beam B2 - 33°C

B.1.2 Beam C2

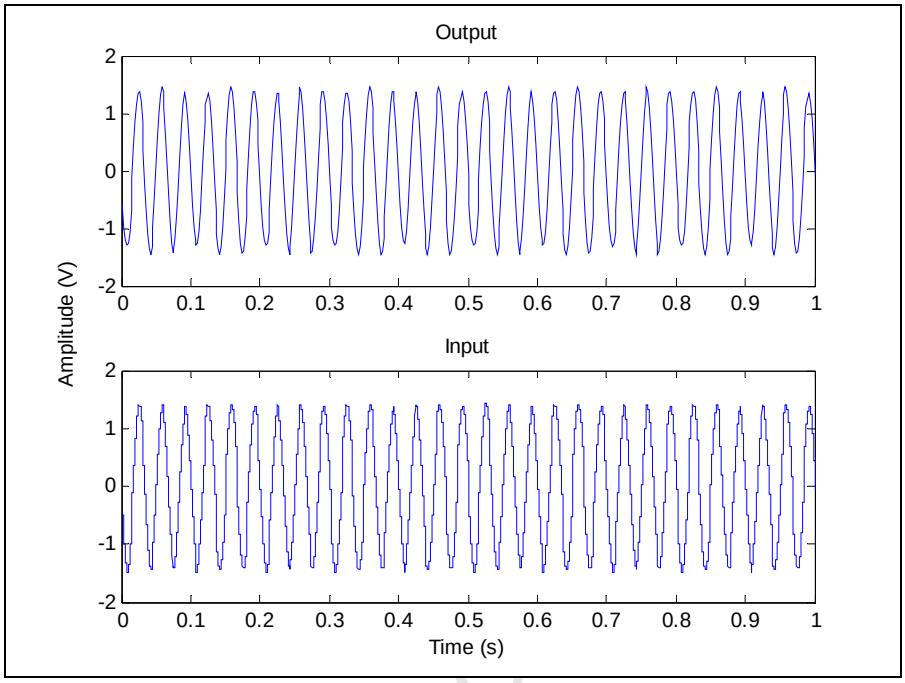

Figure B.7: Beam C2 - 13°C

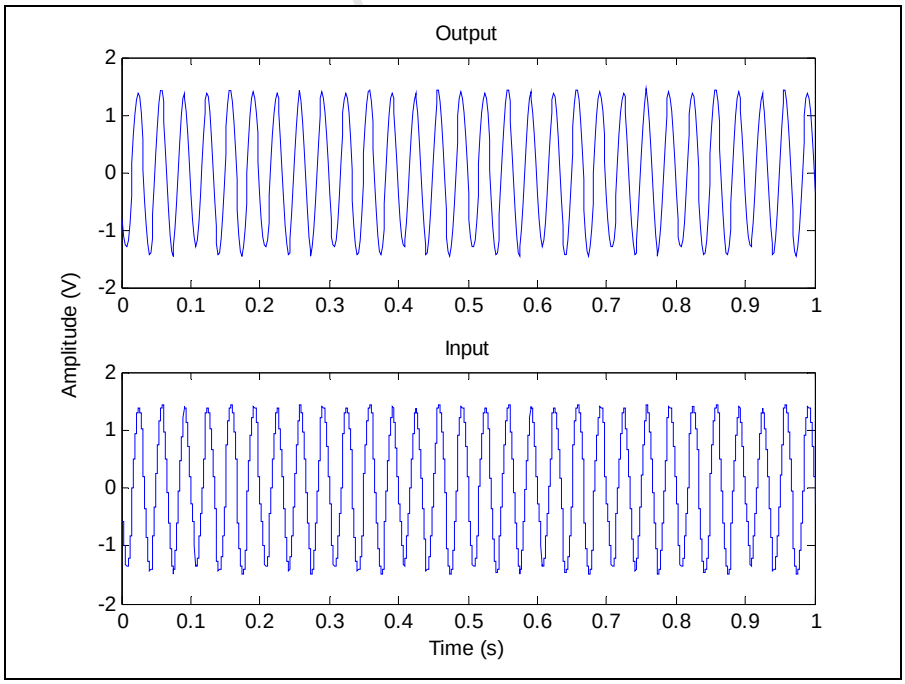

Figure B.8: Beam C2 - 16°C

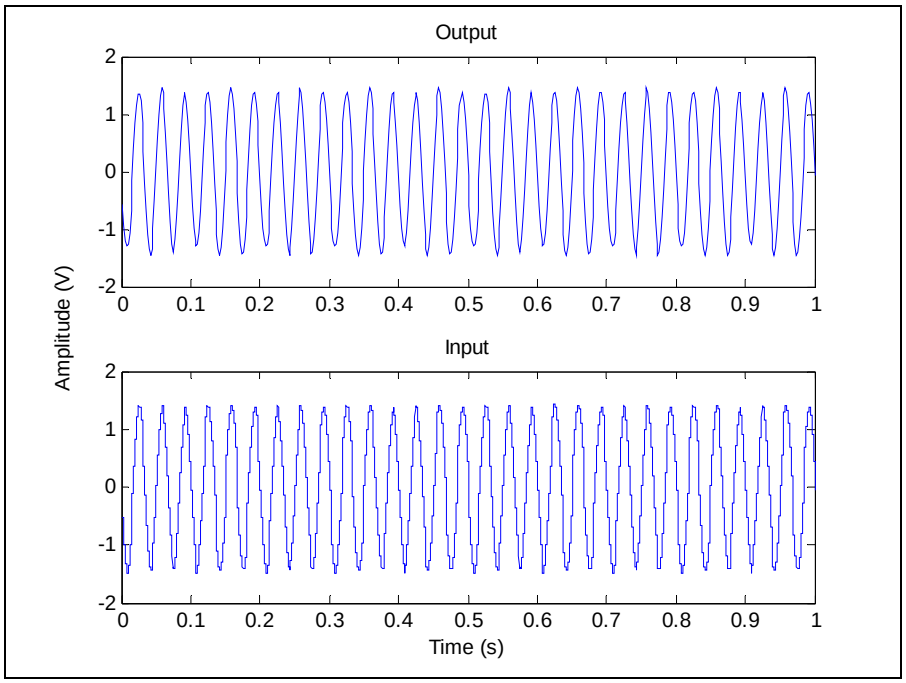

Figure B.9: Beam C2 - 18°C

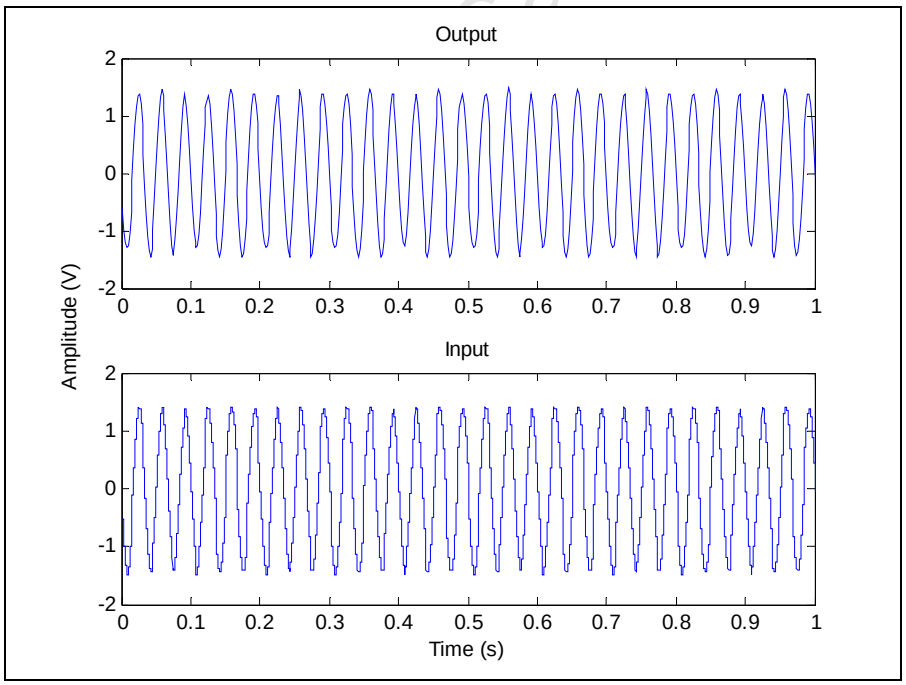

Figure B.10: Beam C2 - 20°C

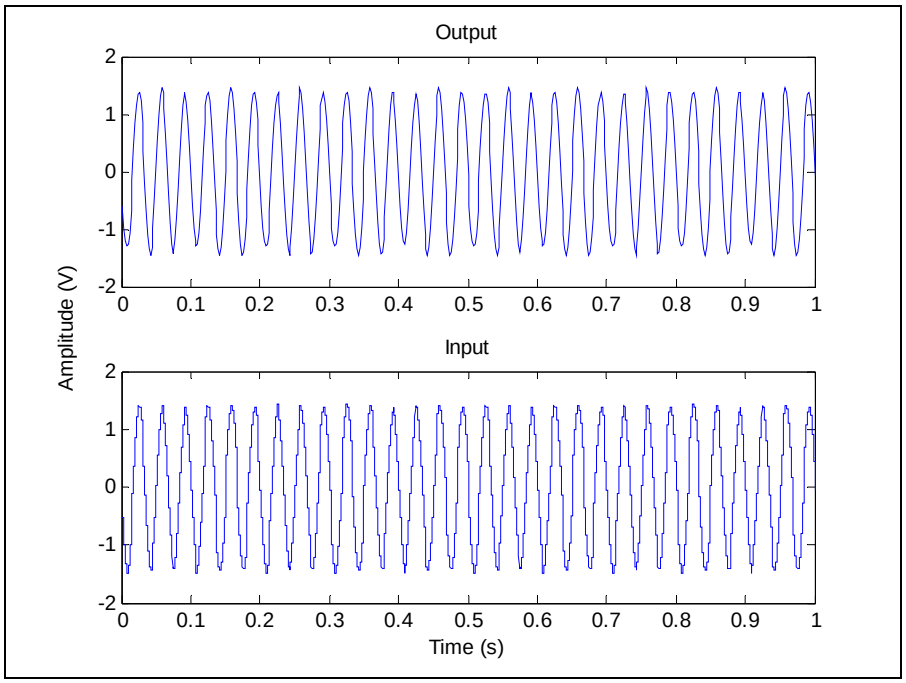

Figure B.11: Beam C2 - 27°C

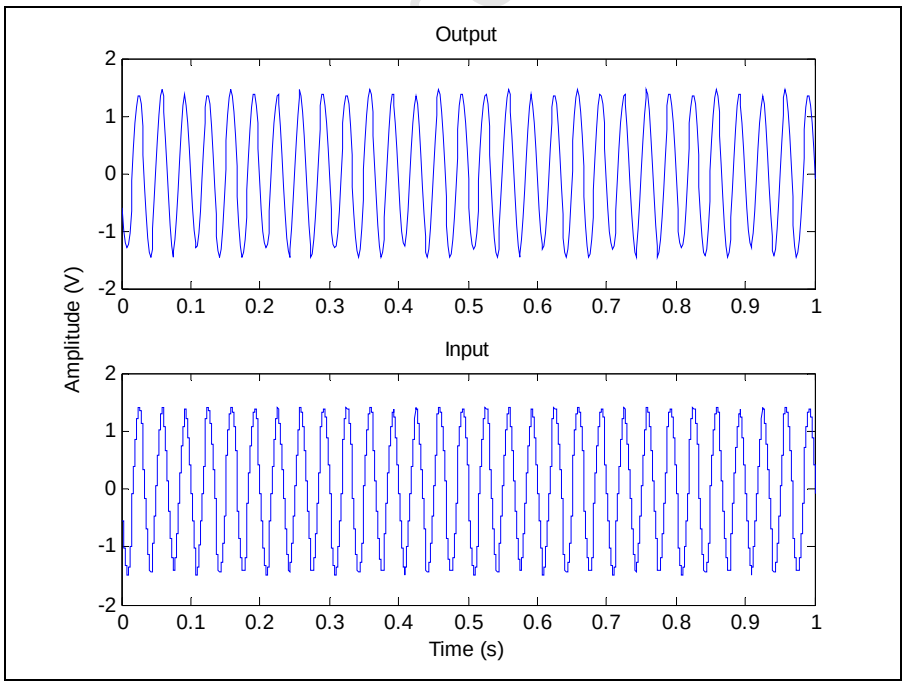

Figure B.12: Beam C2 - 33°C

B.2 Vibration data at different damage states

B.2.1 Beam B1

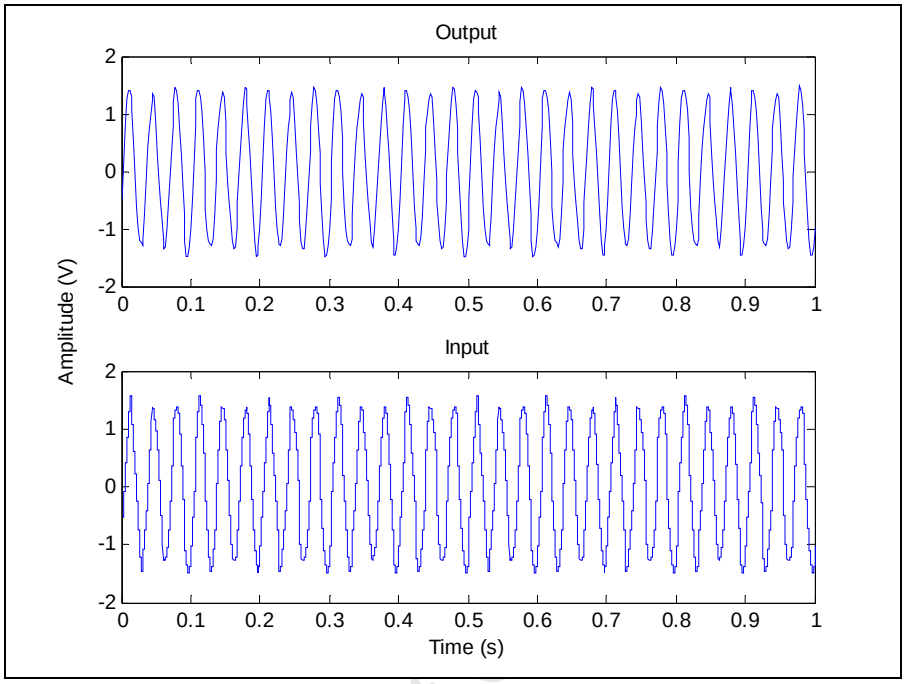

Figure B.13: Beam B1 - Baseline

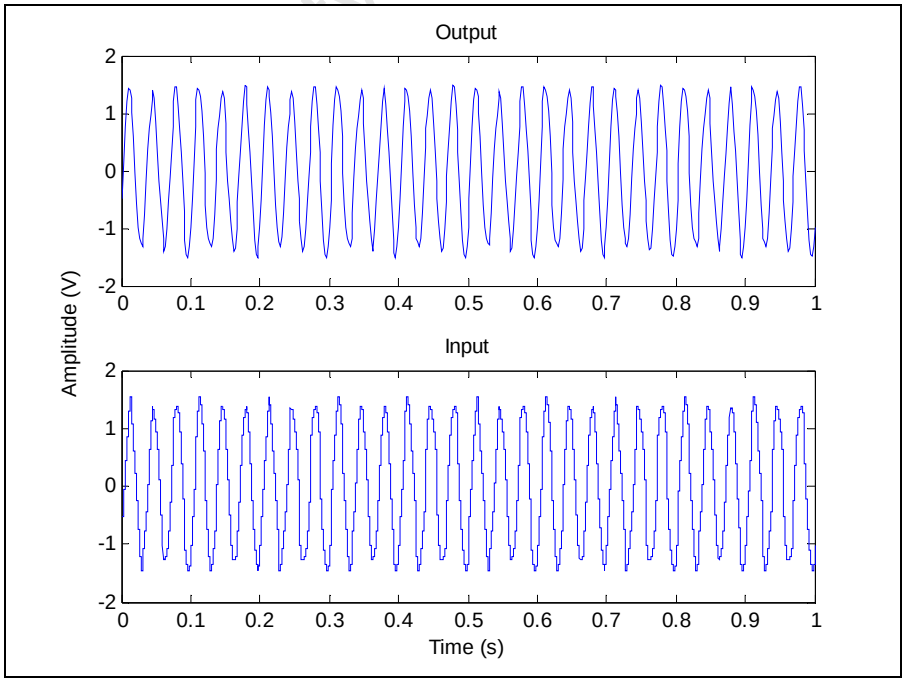

Figure B.14: Beam B1 - Damage1

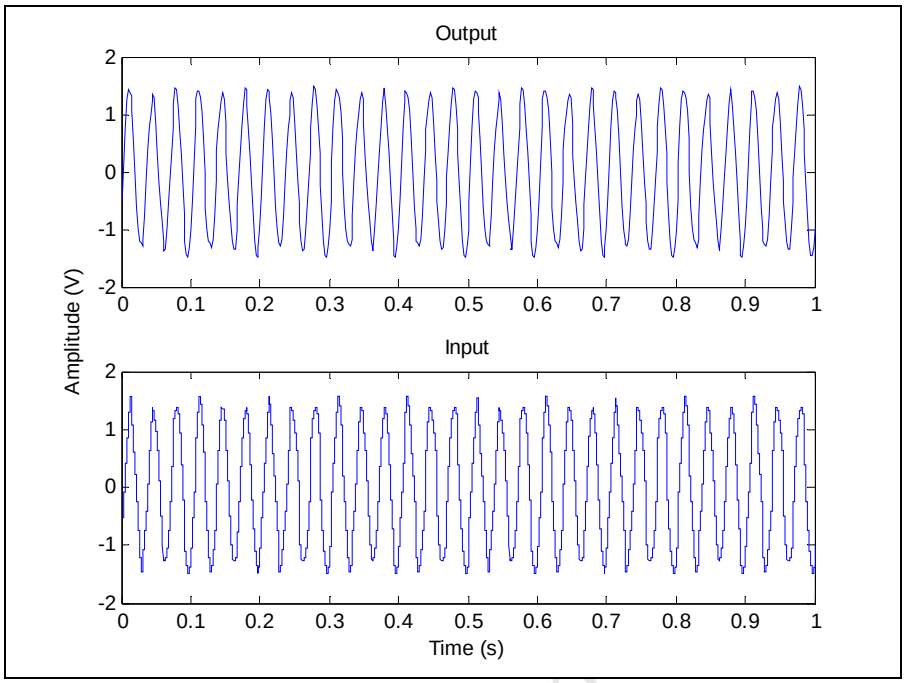

Figure B.15: Beam B1 - Damage2

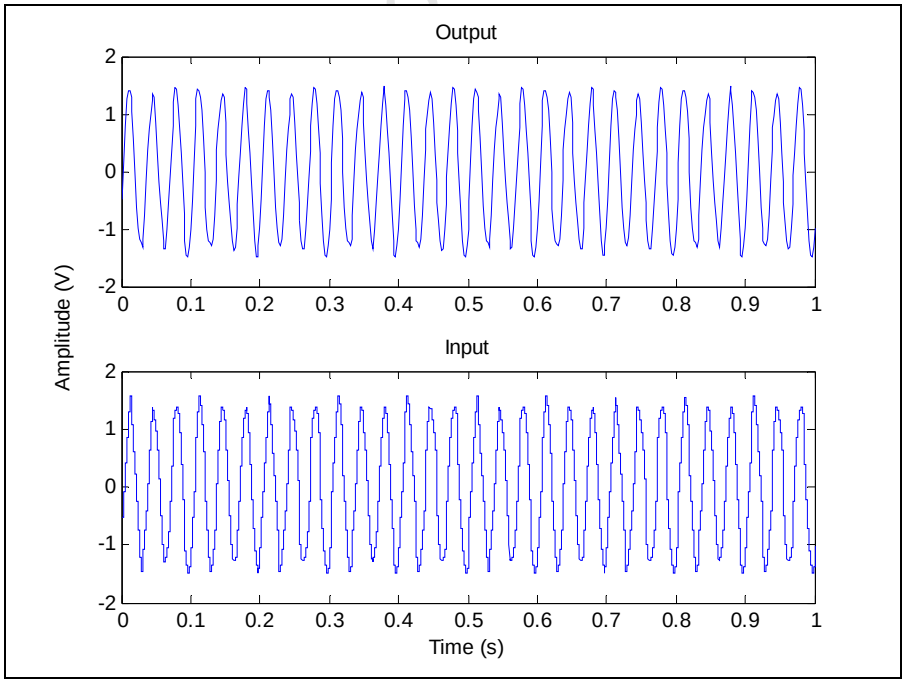

Figure B.16: Beam B1 - Damage3

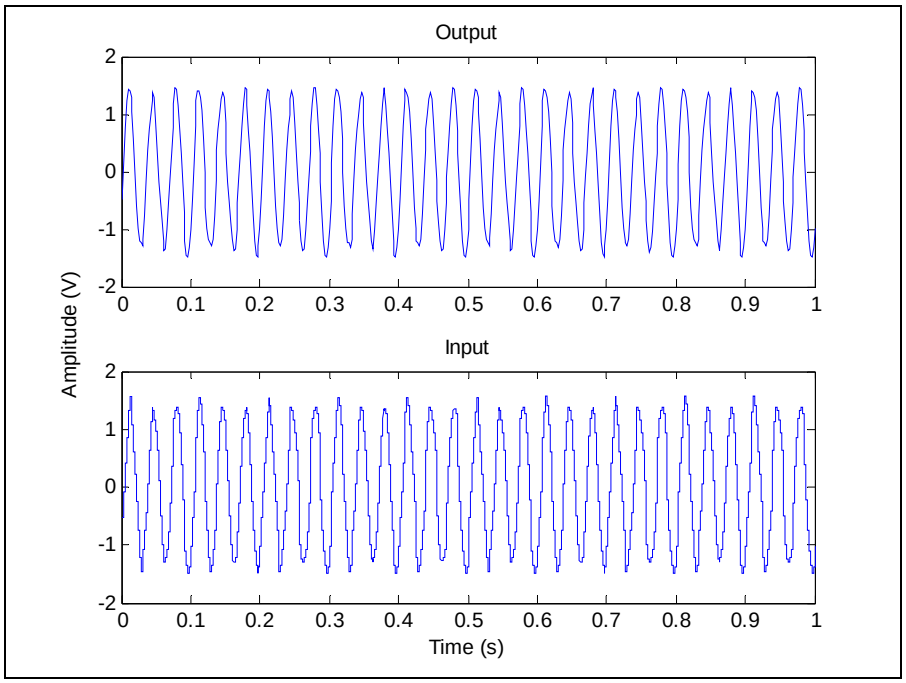

Figure B.17: Beam B1 - Damage4

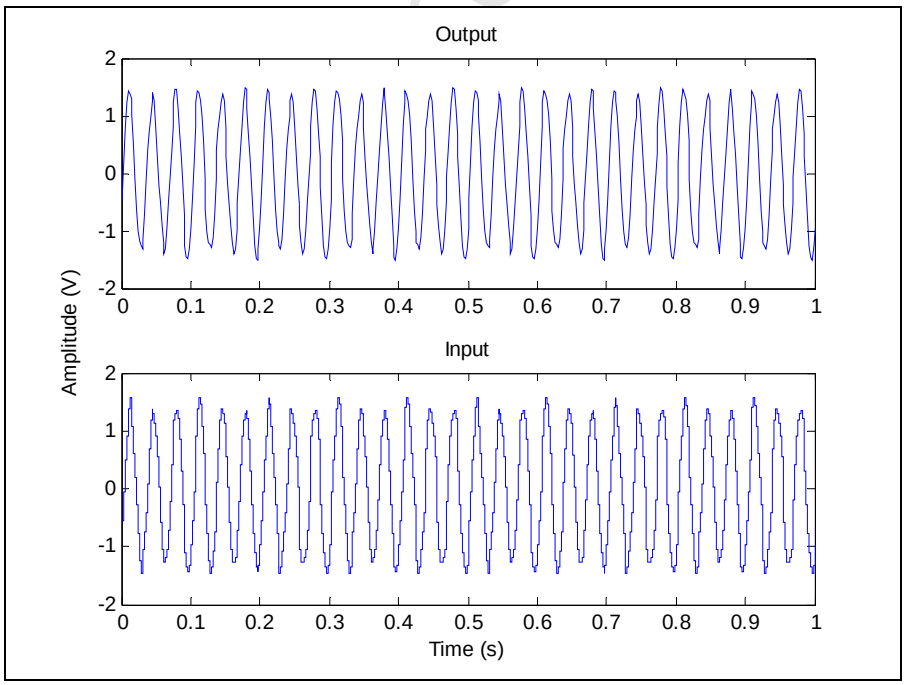

Figure B.18: Beam B1 - Damage5

B.2.2 Beam B2

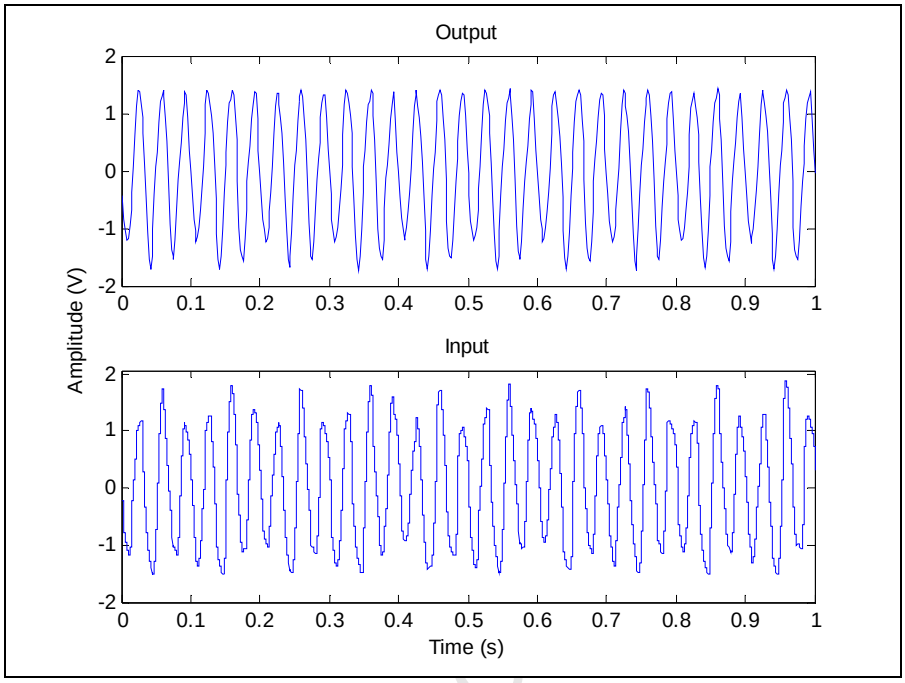

Figure B.19: Beam B2 – Baseline

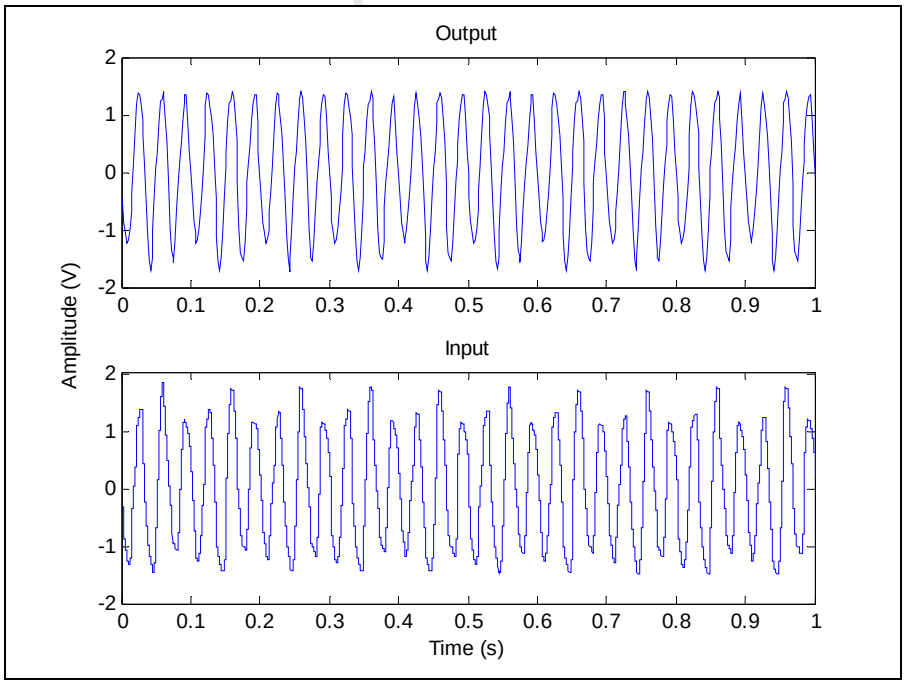

Figure B.20: Beam B2 – Damage1

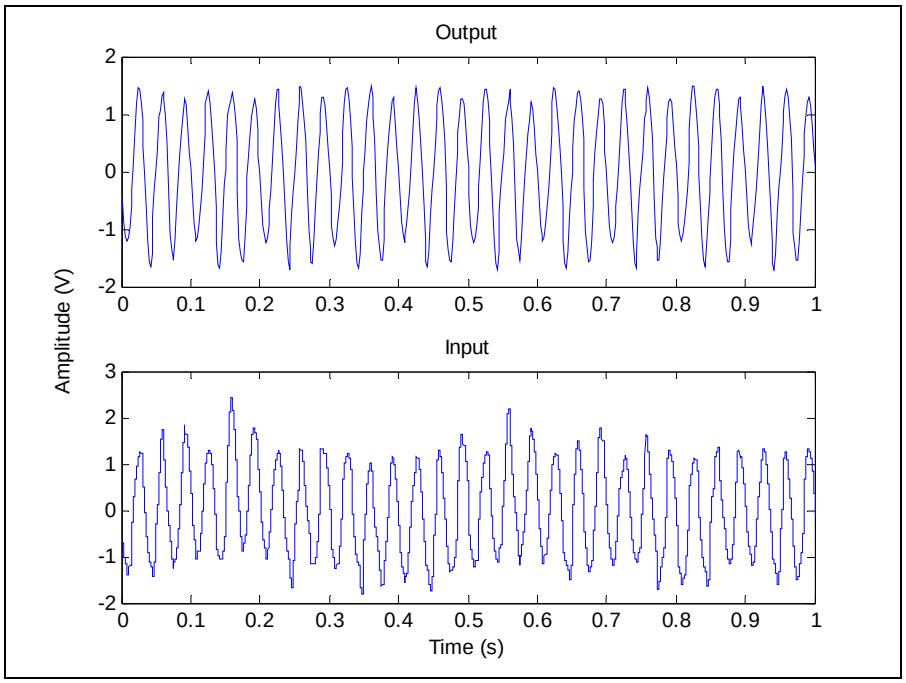

Figure B.21: Beam B2 – Damage2

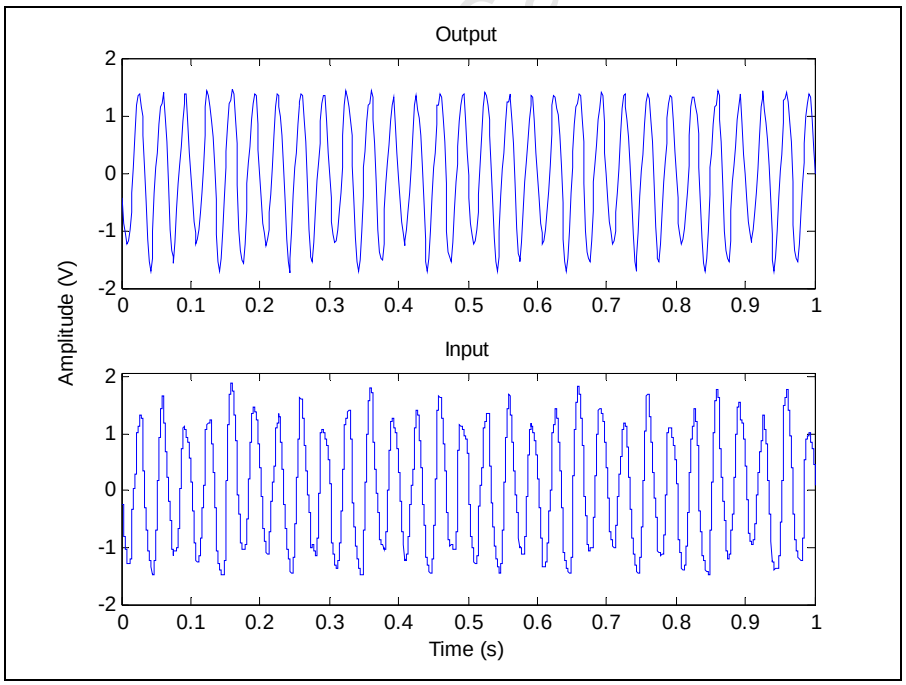

Figure B.22: Beam B2 – Damage3

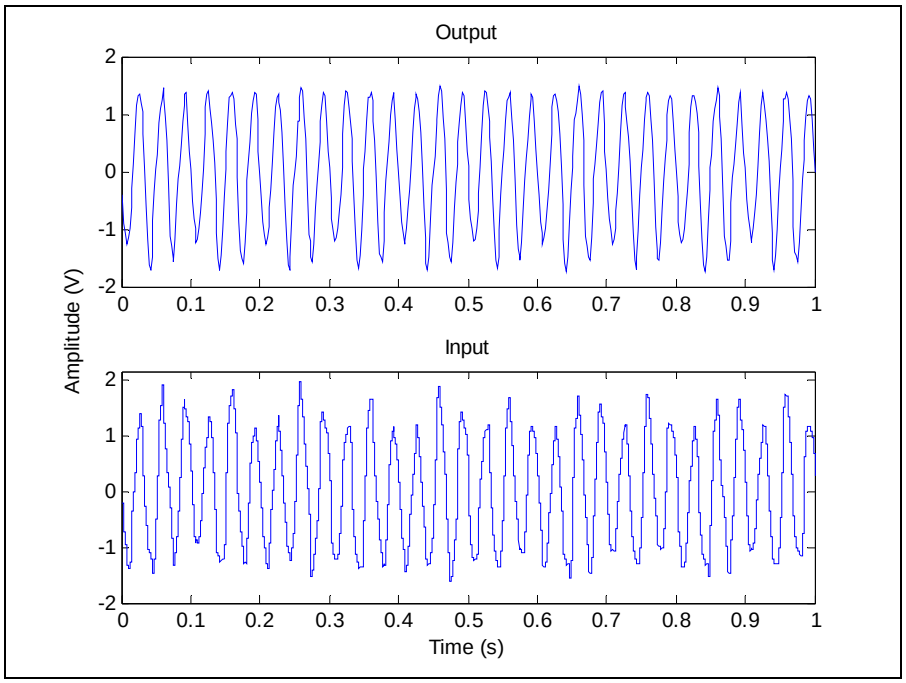

Figure B.23: Beam B2 – Damage4

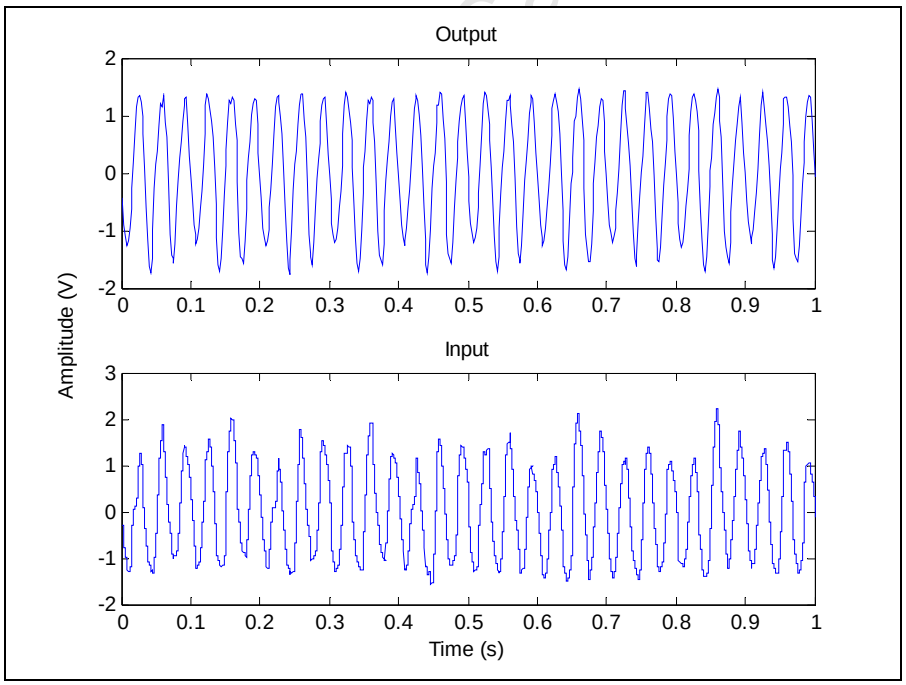

Figure B.24: Beam B2 – Damage5

B.2.3 Beam C1

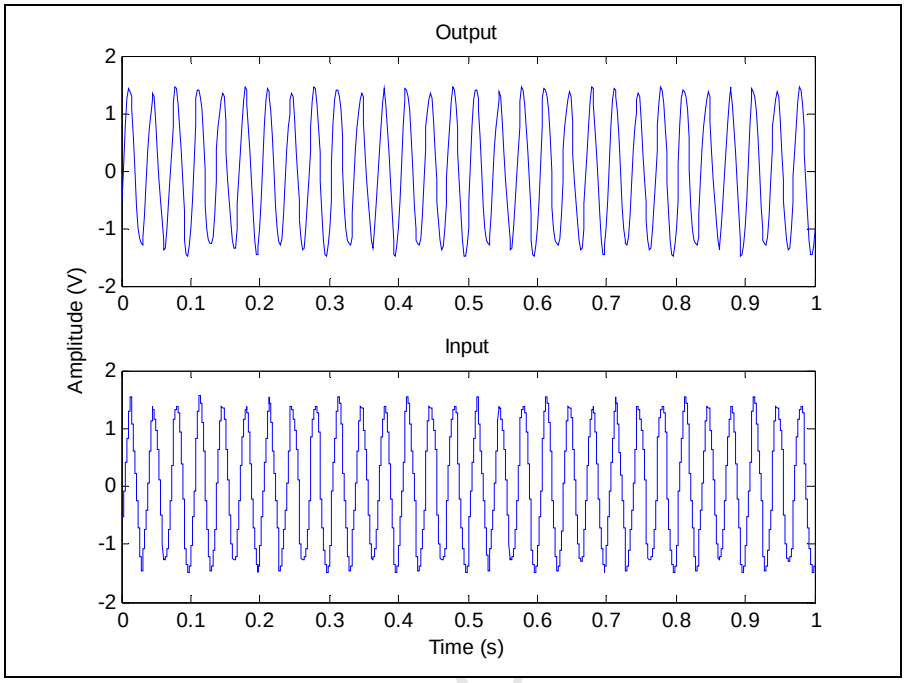

Figure B.25: Beam C1 - Baseline

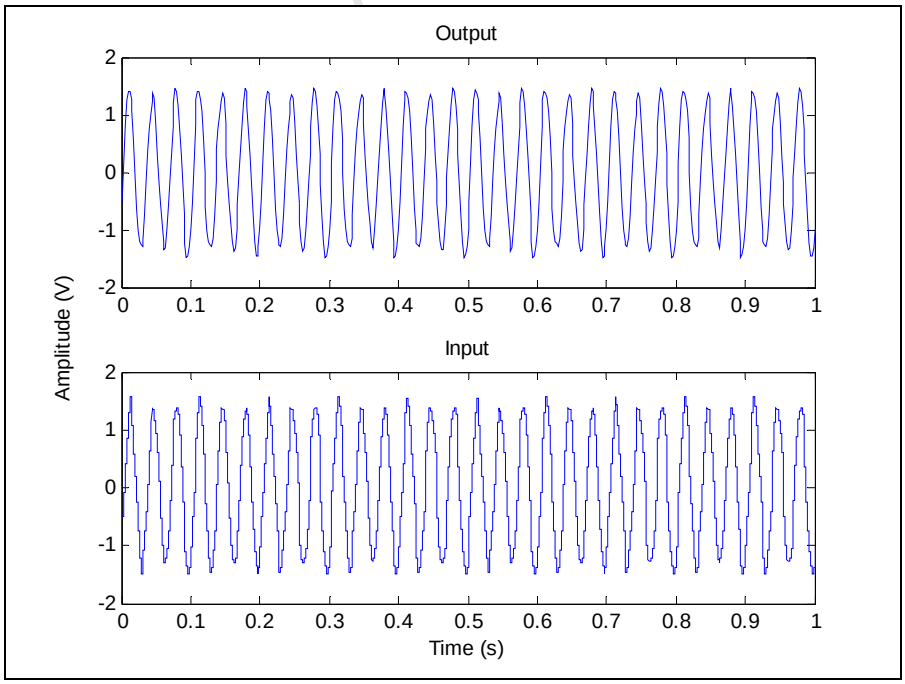

Figure B.26: Beam C1 – Damage1

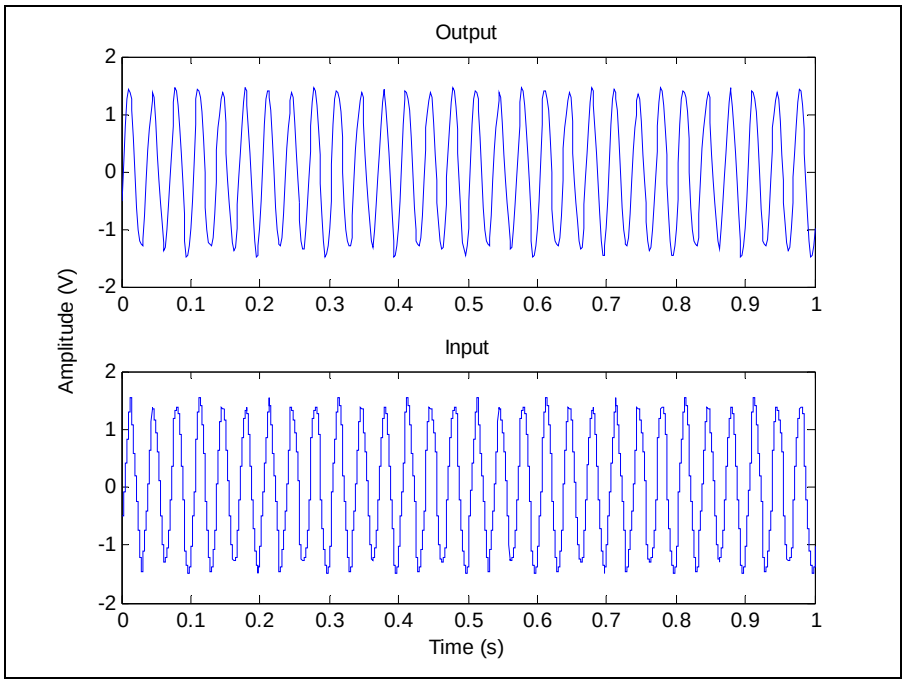

Figure B.27: Beam C1 – Damage2

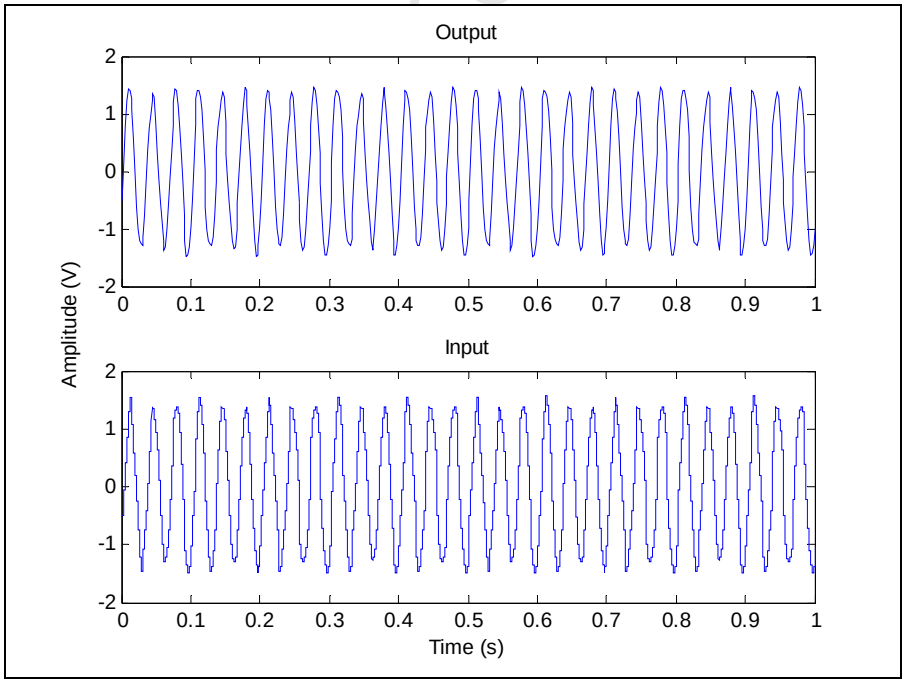

Figure B.28: Beam C1 – Damage3

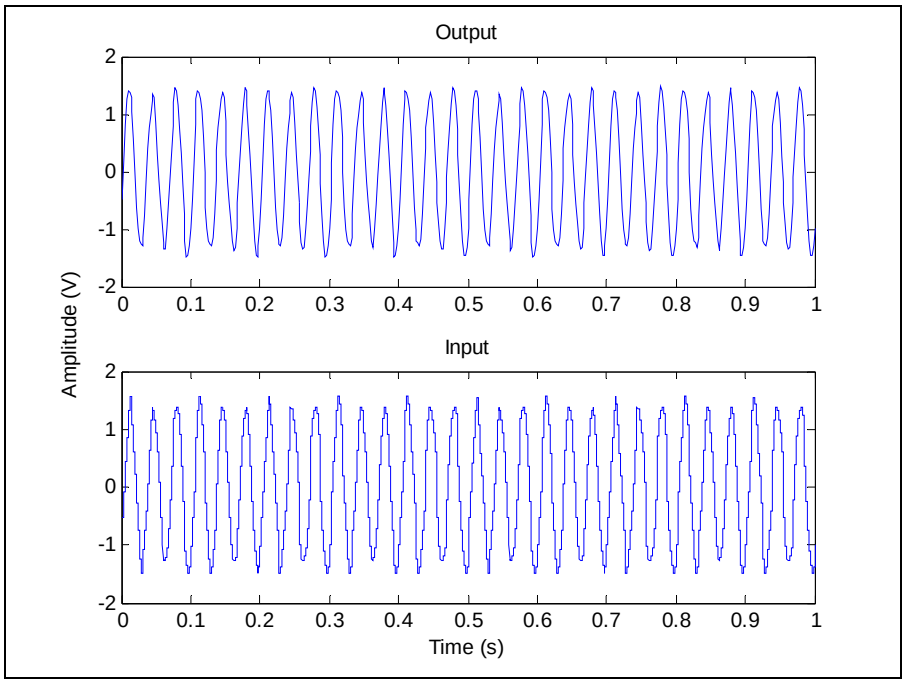

Figure B.29: Beam C1 – Damage4

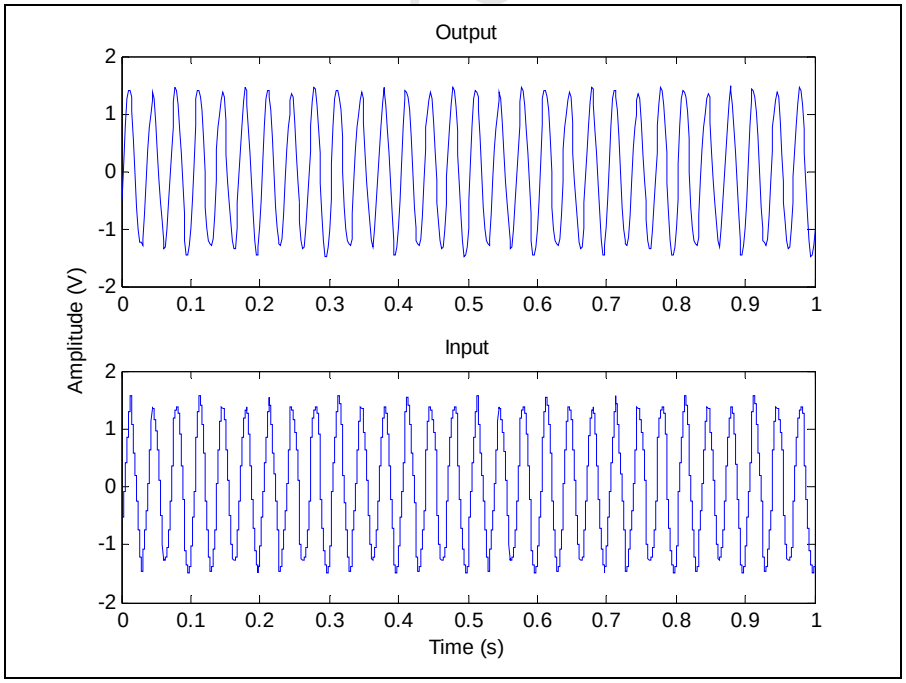

Figure B.30: Beam C1 – Damage5

B.2.4 Beam C2

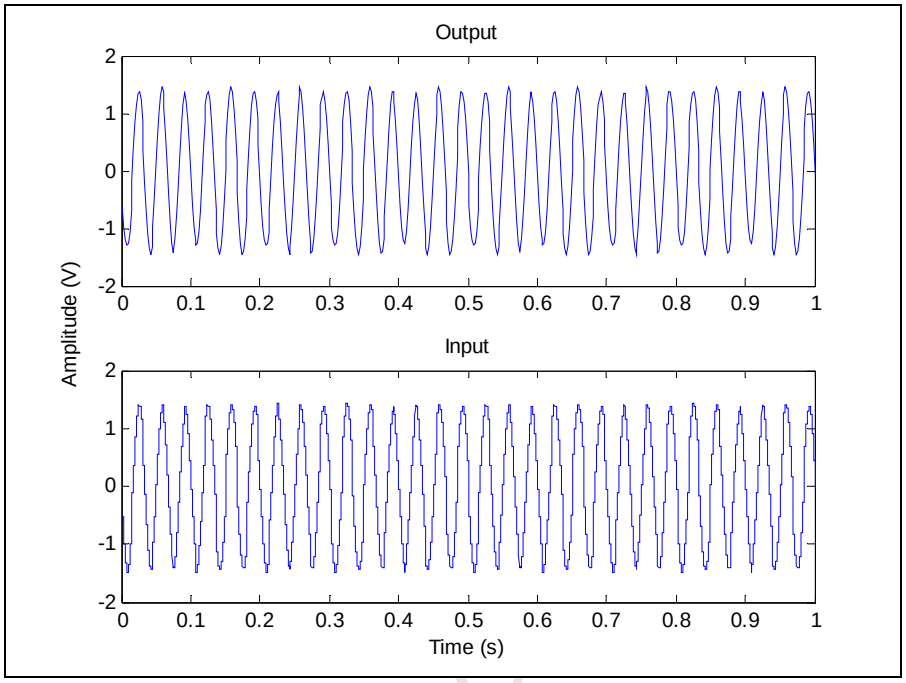

Figure B.31: Beam C2 - Baseline

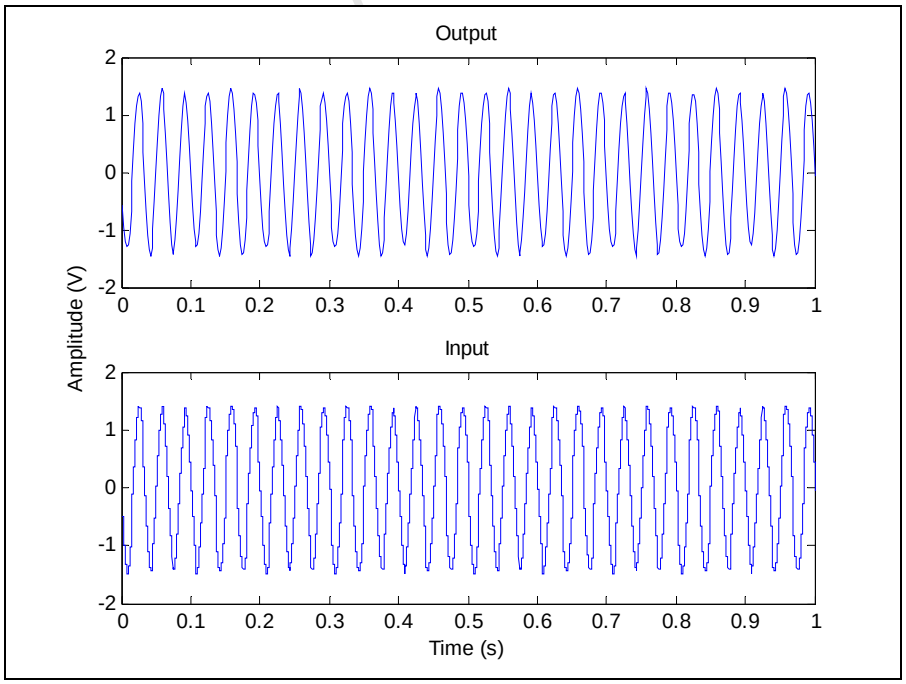

Figure B.32: Beam C2 – Damage1

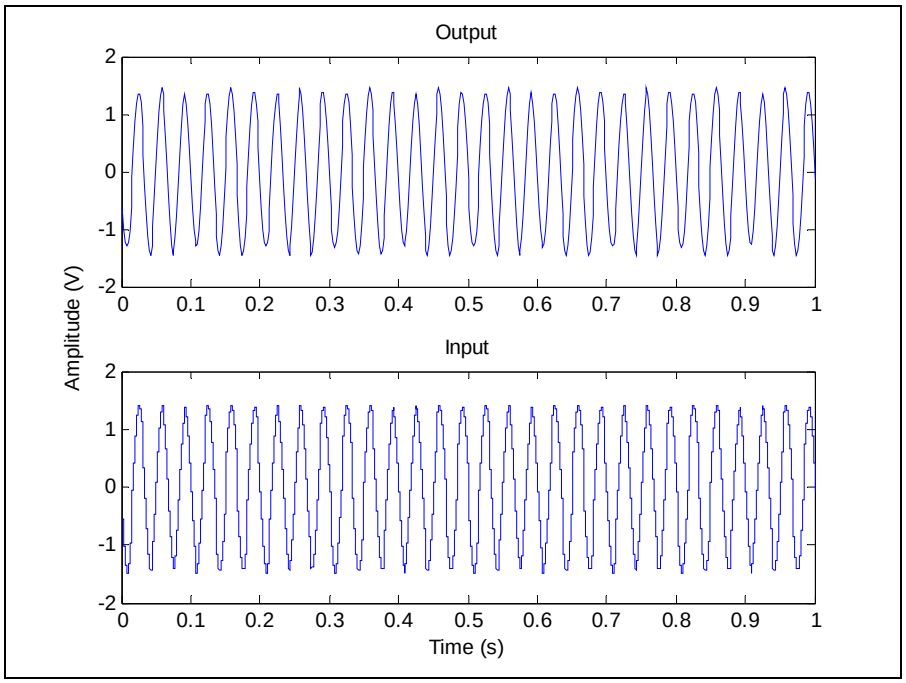

Figure B.33: Beam C2 – Damage2

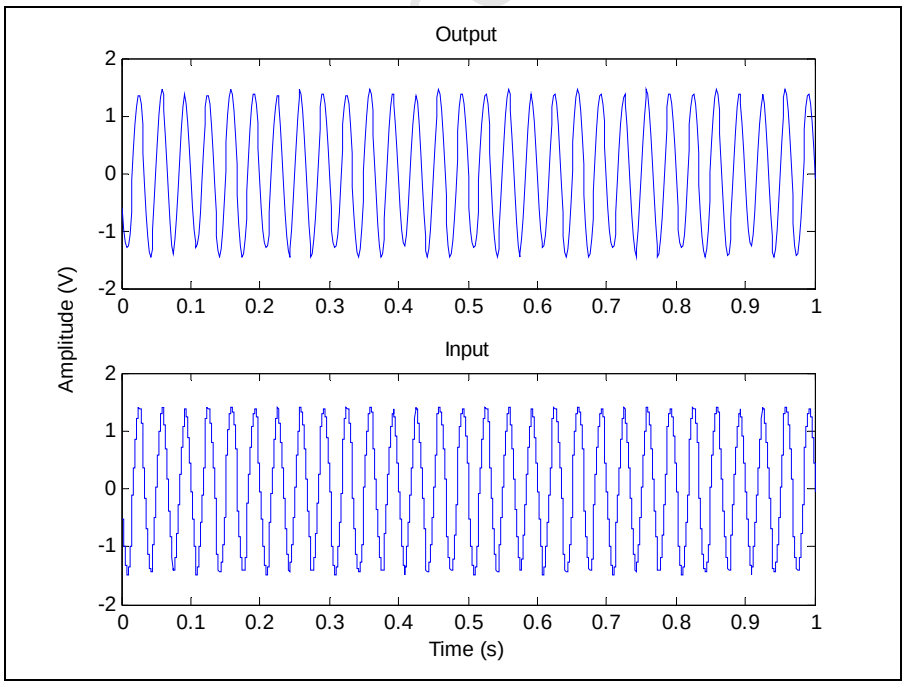

Figure B.34: Beam C2 – Damage3

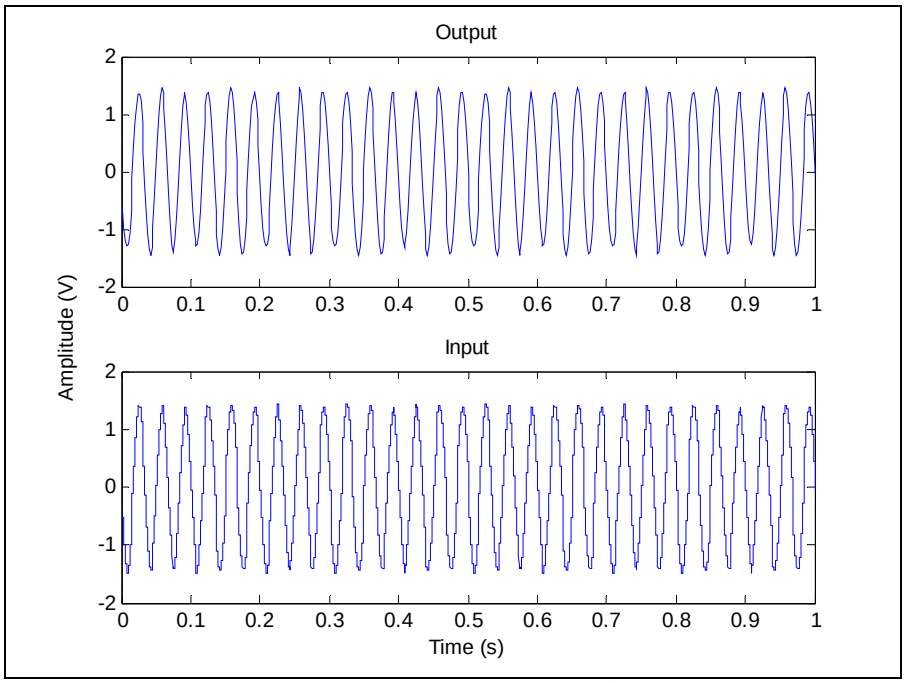

Figure B.35: Beam C2 – Damage4

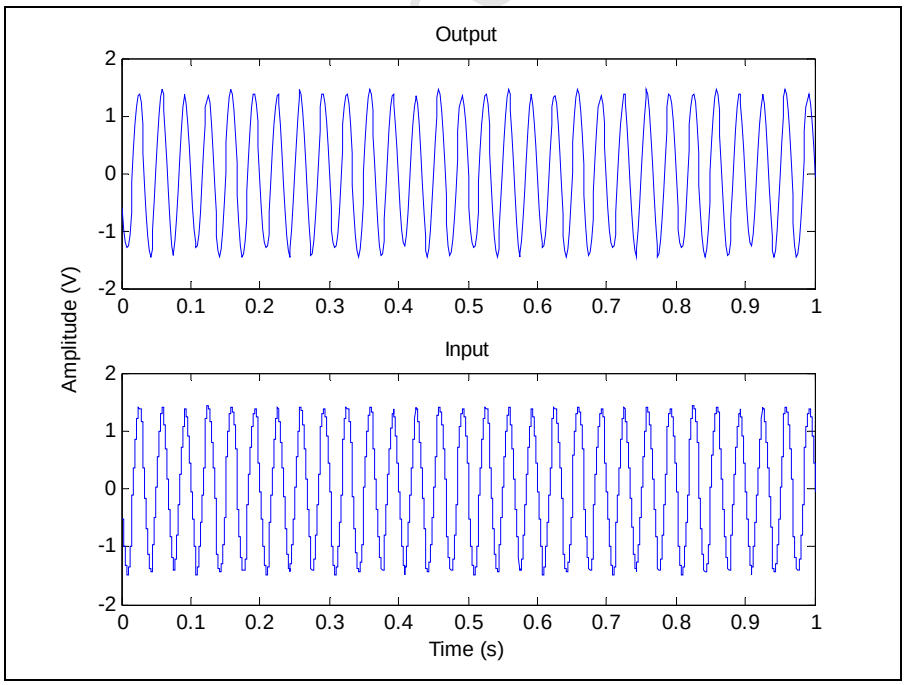

Figure B.36: Beam C2 – Damage5